Clemens Ebner

Polyesters as Bioresorbable Materials for Orthopedic Surgery

PhD Thesis

Dissertation

Zur Erlangung des akademischen Grades eines
Doktors der Naturwissenschaften
eingereicht an der
Technischen Universität Graz

Betreuer:

Priv.-Doz. Dipl.-Chem.Univ. Dr.rer.nat. Frank Wiesbrock
Univ.-Prof. Dipl.-Ing. Dr.techn. Franz Stelzer
Institut für Chemische Technologie von Materialien (ICTM)

May 2012

Deutsche Fassung:

Beschluss der Curricula-Kommission für Bachelor-, Master- und Diplomstudien vom 10.11.2008

Genehmigung des Senates am 1.12.2008

EIDESSTATTLICHE ERKLÄRUNG

Ich erkläre an Eides statt, dass ich die vorliegende Arbeit selbstständig verfasst, andere als die angegebenen Quellen/Hilfsmittel nicht benutzt, und die den benutzten Quellen wörtlich und inhaltlich entnommene Stellen als solche kenntlich gemacht habe.

Graz, am …… ……..

(Unterschrift)

Englische Fassung:

STATUTORY DECLARATION

I declare that I have authored this thesis independently, that I have not used other than the declared sources / resources, and that I have explicitly marked all material which has been quoted either literally or by content from the used sources.

…… ……..

date (signature)

Acknowledgments

Above all, I want to thank Priv.-Doz. Dipl.-Chem.Univ. Dr.rer.nat. Frank Wiesbrock and Prof. Dipl.-Ing. Dr.techn. Franz Stelzer for their exceptional commitment for the supervision of the presented work, many helpful suggestions, and numerous professionally qualified and fruitful discussions.

Moreover, I want to thank all former and present colleagues of the working group Thomas Bodner, Verena Schenk, Andrew Kelly, Inge Mühlbacher, Hannes Offenbacher, Verena Kaltenhauser, Stefan Kalin, Lisa Ellmaier, Stephan Nestl, Andreas Oesterreicher, Bianca Wirnsberger, Martin Fimberger, Volkan Kumbaraci, Claudia Loher, Christina Wappl, Christina Weirer, Peter Neugebauer, Martin Strobl, and Katrin Niegelhell for the excellent working atmosphere which is characterized by respect and cooperativeness. My special thanks go to Barbara Rupp, Elisabeth Rossegger, László Ólah, and Alexandra Schartner for the exceptional collaboration and their valuable contributions to the presented work.

Furthermore, I owe thanks to all my colleagues at the Institute for Chemistry and Technology of Materials for the good working climate. I also thank Renate Trebizan and Liane Hochgatterer for their help with organizational concerns. For his help with all technical challenges, I thank Johann Schlegl and for the GPC measurements and NMR-spectroscopy, I want to thank Josefine Hobisch and Petra Kaschnitz.

Additionally, I thank Johannes Rattenberger from the Austrian Center for Electron Microscopy and Nanoanalysis (FELMI) at the Graz University of Technology for carrying out the focus variation microscopy measurements and Martin Koller of the Institute of Biotechnology and Biochemical Engineering at the Graz University of Technology for the collaboration and the provision of PHB and PHB-HV.

I also want to say thanks to all partners in the BRIC project, the Medical University of Graz, the TU Vienna, the BOKU Vienna, the AT&S Austria Technologie & Systemtechnik AG, and Heraeus Medical for the interesting cooperation and my special thanks go to the consortium leader Priv.-Doz.^{in} Dr.^{in} Annelie-Martina Weinberg.

My greatest gratitude goes to my parents, my daughter Katharina, my brother and his wife and, to the highest possible extent, to Steffi, for her love, kindness, tolerance, and, above all, for keeping me sane during the most challenging time of my life. Thanks honey, you rock!

To my family.

1 Introduction

Since the advent of plastics in every-day life applications in the early 20th century, the interest and the research activities concerning this class of organic macromolecules have been vast. Despite the ever-increasing global production and use of polymer-based materials in all types of applications, concerns regarding disposal, recycling, non-degradability, and raw materials required for the production of synthetic polymers have risen as far back as in the early 1970s.[1;2] Since then, the search for substitutes for oil-based plastic consumables has only partially been successful for alternative bioplastics cannot always fulfill the practical requirements for many applications. Although poly(lactic acid) PLA-based materials have already made their way to commodity applications like disposable coffee mugs or cutlery (Figure 1-1), the generally higher price of bioplastics compared to their oil-based congeners limits their wide-spread application in this field.

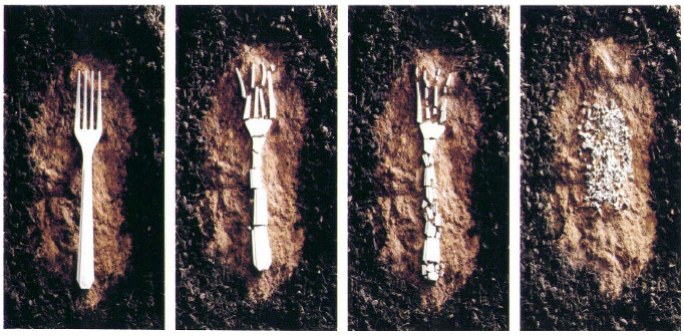

Figure 1-1: PLA-based fork in native and advanced degradation state.[3]

Nevertheless, some synthetically or biologically produced polymers have great potential for higher-priced products (e.g. medical applications), profiting from their non-toxicity, biodegradability, and potential resorbability in physiological systems. With its invention and application in bioresorbable surgical sutures in the late 1960s and 1970s, poly(glycolic acid) (PGA) has paved the way for biopolyesters as medical sewing materials.[4]

Today, PGA and copolymers with PLA and poly(ε-caprolactone) (PCL) are still amongst the most abundantly used polyesters in medicine. Besides the mostly synthetically produced biopolyesters PLA, PGA, and PCL, microbe-derived polyesters

have drawn the attention of polymer chemists, material scientists, and surgeons over the past decades. Bacterial polyesters consisting of hydroxy acid monomers were detected for the first time in 1926 by Lemoigne, but it was not until the 1960s that the scientific community discovered the potential arising from this production pathway.[5-7] The biotechnological production route for these poly(hydroxyalkanoate)s (PHAs) has been exploited for over 40 years now, and since the 1970s, more than 150 different hydroxy acids in the corresponding polymers have been reported.[8]

Starting at the end of the 20th century, possibilities for broader use of bioresorbable materials in modern medicine have been discussed, aiming at the development of new materials for regenerative medicine that can mimic soft or hard tissue, help the human body with the healing process and make multiple operations for implant removal obsolete. Besides polymer-based materials, inorganic materials like hydroxyapatite and other calcium-based compounds[9;10] for bone regeneration or metal-based implants for fracture fixation devices have been proposed. In the area of metal-based materials, magnesium and magnesium alloys have gained considerable attention, driven by their high mechanical stability and high degradation rate.[11;12] Already introduced for the first time in the 1930s, the major drawbacks of these metal alloys still are the severe hydrogen gas evolution upon degradation, sometimes even too fast degradation rates, and potential toxicity of implants containing rare earth elements.[13-15]

Despite the early introduction of polymers in the field of bioresorbable medical materials, wide-spread use of polyesters has been limited because of too low degradation rates, poor mechanical strength and, to some extent, too low biocompatibility. Over the past years, considerable attention has been paid to the increase of the biocompatibility of aliphatic polyesters, mostly aiming at increased hydrophilicity of these generally hydrophobic polymers. Additionally, strategies like crosslinking, blending, and copolymerizing have been brought forward to increase the mechanical stability and to manipulate the degradation characteristics.[15-17] In these developments, material scientists and chemists have been greatly supported by modern medicine and the advances of in-vivo modeling and diagnostics (Figure 1-2).

Figure 1-2: In-vivo diagnostics: Conventional radiograph (left) and 3D CT-reconstruction (right) of a bioresorbable implant in a small animal model.[18]

Inspired by the recent advances in the development of polymer-based biocompatible and bioresorbable materials, current research does not only focus on the synthesis and production of highly sophisticated bulk materials, but almost equally concentrates on the surface design of the targeted product. While the main goal is still the increase of the wettability of hydrophobic surfaces, other parameters such as surface roughness, incorporation of growth factors and antibiotics are considered important with respect to minimized inflammatory reactions and faster tissue regeneration.[19-21]

In summary, the combination of elaborate organic and inorganic materials equipped with smart functional surfaces seems to be the key to perfectly adapted medical materials that can help modern medicine face the challenges of modern life society.

2 Scope and Motivation

The present work has been carried out within the framework of the "BRIC-Laura Bassi Centre of Expertise", which is funded by the Austrian Research Promotion Agency (FFG). The acronym "BRIC" is derived from **B**io**R**esorbable **I**mplants for **C**hildren, and the top-priority of this multi-disciplinary project is the development of bioresorbable implant materials for applications as bone fracture fixation materials in orthopedic infant surgery. With one research focus set on the development of new polymer-based materials, the assignment of the Institute for Chemistry and Technology of Materials within the "BRIC"-project is the modification and processing of polymer-based materials, providing an interface between the biopolymer production/acquisition and the physical and medical evaluation of the developed materials. As basic materials, the biopolyesters poly(3-hydroxybutyrate) (PHB), the statistical copolymer poly(3-hydroxybutyrate-*co*-3-hydroxyvalerate) (PHB-HV), and poly(lactic acid) in both, its L-form and as mixture of L- and D-enantiomers, are considered.

When aliphatic polyesters bearing monomer units with short side-chains (3-5 carbon atoms) are used, one has to face challenges originating from the relatively low stiffness, partially high brittleness, and low hydrophilicity of these compounds. In order to overcome these bottlenecks, different strategies concerning the modification and optimization of the bulk material as well as the resulting surfaces have to be developed. These strategies involve methods for chemical and physical alteration of the basic materials aiming at the production of implants that can meet the high standards of modern medicine.

The term physical modification summarizes all modifications of a certain basic material by processes in which no chemical reactions take place. This involves thermal processing of polymers, control over their crystallinity, blending with other polymers and mixing with organic or inorganic fillers; additionally, physical post-processing of readily prepared polymer molds or coating of polymer and/or metal-based implants are taken into account, like eg. crosslinking.

Chemical modification, on the other hand, allows changes of a given material on a molecular level: These chemical reactions of macromolecular compounds, so-called polymeranalogous reactions, comprise methods for crosslinking a polymer with a

specific crosslinking agent, and chemical surface treatment using wet chemical or chemically active plasma techniques.

From the abovementioned chemical and physical manipulation methods, several strategies are selected and experimentally characterized for their potential within the scope of the present work. The first method selected is the production of organic-inorganic composite materials based on PHB and different inorganic fillers and their characterization in terms of mechanical stability. Also derived from physical processes, the application of polymer-based coatings on metal surfaces will be evaluated. These composites obtained by mixing PHB and inorganic materials or by coating metal surfaces with polymers (PHB, PHB-HV, and PDLLA) will be characterized by means of tensile testing, differential scanning calorimetry (DSC), and microscopic methods.

Another approach about to be tested is the chemical modification of bulk material and surface by crosslinking using highly reactive bifunctional compounds. The aim of this strategy is to pre-compensate for the loss in molecular weight of PHB, PHB-HV, and PLLA occurring during thermal processing in order to provide higher strength and flexibility of the resulting polymer networks. Additionally, the chemical and the physico-chemical characteristics can be tuned by the choice of crosslinking agent and the extent and site of crosslinking (bulk or surface). In terms of post-processing of PHB surfaces, wet chemical and oxygen-plasma techniques will be considered. The characteristics of the resulting compounds and surfaces will be thoroughly evaluated by tensile testing, ^{1}H-NMR- and FT-IR-spectroscopy, sol-gel analyses, swelling experiments, contact angle measurements, microscopic methods, and gel permeation chromatography.

Overall, the abovementioned manipulation strategies and the dedicated methods of analysis are supposed to explore the influences of physical and chemical methods on the characteristics of both, bulk material and surfaces of biopolyester-based materials. Ideally, the outcome of this work should provide materials with increased biocompatibility, mechanical strength and flexibility, and surfaces with increased hydrophilicity and surface roughness in a range that can positively affect bone ingrowth, fracture healing and cell adhesion.

3 Current State of Knowledge

3.1 Biopolymers

The term biopolymer is a general classification for compounds that are, in contrast to synthetic polymers, produced by living organisms. In fact, macromolecular structures are present everywhere in nature and living matter is able to produce a plethora of different polymers. With respect to their chemical structure defined by the repeating units, a classification can be made according to 8 different basic structures:[22]

I. Nucleic acids (e.g. ribonucleic acids, deoxyribonucleic acids)
II. Polyamides [e.g. proteins, poly(amino)acids]
III. Polysaccharides (e.g. cellulose, starch, xanthan)
IV. Organic oxoesters [e.g. poly(hydroxyalkanoic acid)s, poly(malic acid), cutin]
V. Polythioesters
VI. Inorganic polyesters (polyphosphate as only representative)
VII. Polyisoprenoids (e.g. natural rubber or Gutta Percha)
VIII. Polyphenols (e.g. lignin, humic acids)

Due to the abundance and striking variety in structures and essential functions that can be provided by biopolymers, organisms use them for manifold purposes like energy, nutrient, and carbon storage, gene-expression and conservation of genetic information, as catalytically active compounds, and as structural elements.
Originating from the diversity in the structures and functions to be fulfilled, biopolymers must interact very specifically with many different substances. Therefore they need a very high affinity to a variety of molecules. Additionally, many biopolymers, especially natural fibers like silk or other protein-based fibers, exhibit very high strengths, a characteristic which is of considerable interest for many applications. Owing to their biological nature, all biopolymers are not only synthesized, but also degradable under biological conditions. The combination of high strength and biodegradability in organic oxoesters and polysaccharides renders these compounds the most interesting among biopolymers for applications like packaging materials, construction materials, and medical applications.

3.2 Biopolyesters

With the first detection of polyesters in bacterial cells by Lemoigne in 1926 and the deeper understanding of this polymer class originating from extensive research activities since the 1970s, a huge variety of materials with equally diverse properties has been biotechnologically synthesized and characterized up to the present day.[5;22]

3.2.1 Poly(hydroxyalkanoate)s (PHAs)

Since most biopolyesters apart from poly(maleic acid) consist of hydroxy acid building blocks, this kind of polymers is frequently referred to as poly(hydroxyalkanoate)s (PHAs) (Scheme 3-1).

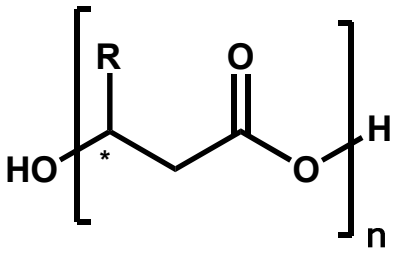

Scheme 3-1: General formula of PHAs.

Owing to their versatile nature and possible production from renewable resources, PHAs have been discussed as substitutes for conventional oil-based plastics, as well as bioresorbable materials for medical purposes.

As depicted in Scheme 3-1, all PHAs have a chiral center in the C-3 or β-position and, hence, are optically active compounds. Due to their natural origin only the R(L-)-configuration of the hydroxy acid monomers is present in the polymers.

A general classification of PHAs can be made by the number of carbon atoms in the respective monomer units: PHAs with monomer units consisting of 3-5 carbon atoms are referred to as short-chain-length PHAs (scl-PHAs), while medium-chain-length PHAs (mcl-PHAs) bear monomer units with 6 to 16 carbon atoms.[23;24] The group of scl-PHAs consists of poly(lactic acid) (PLA), poly(3-hydroxybutyrate) (PHB), poly(3-hydroxyvalerate) (PHV), and the copolymer poly(3-hydroxbutyrate-*co*-3-hydroxyvalerate) (PHB-HV) with PHB being the most abundant PHA produced by

microorganisms. Common mcl-PHAs are poly(3-hydroxyhexanoate) (PHHx), poly(3-hydroxyheptanoate) (PHH), poly(3-hydroxyoctanoate) (PHO), and poly(3-hydroxynonanoate) (PHN), while PHAs with saturated or unsaturated monomers of up to 16 carbon atoms have been reported as well.[25;26]

At this point it is worth mentioning that PLA is frequently not included in the group of PHAs, even though lactic acid is a 3-hydroxy acid and PLA can be synthesized biotechnologically. Nevertheless, PLA is mostly produced by synthetic means, but with respect to its biodegradability is often referred to as biopolyester. Due to the isotactic nature of PHAs they tend to crystallize up to high extents. Especially scl-PHAs reveal high crystallinities of more than 50%, which also has a significant influence on the mechanical properties: Scl-PHAs are hard and brittle materials comparable to polypropylene, while mcl-PHAs are soft and tenacious elastomers that show much lower extents of crystal fractions. PLA bearing the smallest of all PHA-monomer units also has the highest mechanical strength and the lowest flexibility of all PHAs.[27;28]

With respect to possible applications of PHAs in the packaging industry and resorbable medical devices, scl-PHAs have a higher potential than mcl-PHAs for both, commodity bioplastics and implant materials for medical purposes. Additionally, the bacteria that produce these non-functionalized scl-PHAs do not need any specific requirements with respect to the carbon source needed for PHA synthesis. This is, together with the circumstance that PHB and PHB-HV (Scheme 3-2) are the most commonly produced PHAs, the reason why these compounds are the only PHAs that are commercially available in larger quantities.[29-31] Furthermore, PHA-related research has focused on PHB and PHB-HV since the early 1970s and rendered these polymers the best understood materials among all PHAs.

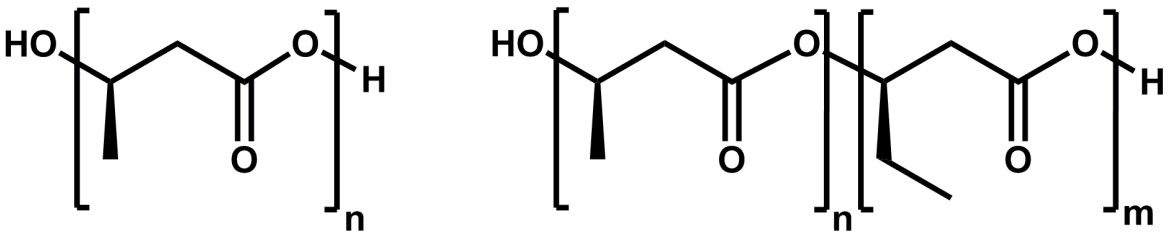

Scheme 3-2: Chemical structures of PHB (left) and PHB-HV (right).

As mentioned before, PHB is a thermoplastic semi-crystalline polymer and reveals crystallinities of over 50%, frequently between 60 and 70%. PHB crystallizes in a right-

handed helical conformation; this PHB-helix has a second rotation axis and a fiber repeat of 5.96 angström.[32;33] These helical units are stabilized by carbonyl-methyl interactions and not, as in many other cases, by hydrogen bridges. In contrast to PHB, pure PHV crystallizes as 2_1-helix in an orthorhombic cell with the space group P_{212121}.[34;35] At low concentrations of HV in PHB-HV copolymers, the copolyester behaves isodimorphous to PHB, which means that the hydroxvalerate and hydroxybutyrate units tend to co-crystallize and are accommodated simultaneously in the PHB crystal lattice. This phenomenon can analogously be observed in copolymers with high HV and low HB contents. Accordingly, PHB-HV with HV-contents of up to 40% generally reaches high crystallinities comparable to those of neat PHB. Only at HV contents of more than 40%, the copolymer crystallizes in the crystal structure of PHV.[34] This is also the reason why attempts to control the crystallinity of scl-PHAs by the incorporation of HV in PHB and vice versa have failed. This goal has partially been achieved by the incorporation of mcl-PHAs comonomers like hydroxyhexanoate or hydroxyoctanoate.[36] Additionally, the incorporation of 4-hydroxybutyrate units in PHB has been shown to decrease the resulting copolymer's crystallinity significantly.[35;37]

3.2.1.1. Biosynthesis of PHAs

Many microorganisms, gram-positive and gram-negative bacteria, and even some archaea produce PHAs as a consequence of metabolic stress caused by limitation of growth factors like phosphorous, nitrogen, and ammonia while at the same time excess carbon is provided. These water-insoluble discrete storage granules can be accumulated up to very high concentrations, sometimes reaching amounts of over 80% with respect to the dry cell weight (Figure 3-1).[8]

In 1961, Marrick and Doudoroff demonstrated the synthesis of PHB from R-3-hydroxybutyryl-CoA in the microorganisms *Bacillus megaterium* KM and *Rhodospirillum rubrum*.[38;39] While the PHA granules produced by *R. rubrum* were considered self-digesting due to the simultaneous presence of PHB synthase and PHB depolymerase, 70% of the protein mass could be extracted from the PHB granules produced by *B. megaterium* via mild alkaline extraction.[40] The protein part was further divided into two components, namely A-I and A-II. It was assumed that A-I, in combination with PHB granules, acted as depolymerase, while for the PHA-synthase, a two-step mechanism was proposed. Since these first attempts of

understanding the production of intracellular storage polymers, a systematic classification of the different PHA-synthases into three types has been made according to the substrate specificity and the primary structures:[41]

- The PHA-synthase type I (*R. eutropha*) consists of one subunit with a molar weight of 61-67 kDa. With its specificity for CoA thioester derivatives of scl-HAs, it produces scl-PHAs exhibiting molecular weights of 500 000 to several million Da.

- The PHA-synthase type II (*Pseudomonas aeruginosa*) has a molecular weight in the range of 61-67 kDa and, like type I, also has one subunit. The specificity of type II synthases towards HA with a chain length of 6-14 carbon atoms accordingly yields mcl-PHAs with molecular weights ranging from about 50 000 to 500 000 Da.

- PHA synthases type III (*Allochromatium vinosum*) consist of two different types of subunits with molecular weights of 40 kDa, PHaC and PHaE that form a 1:1 complex and convert scl-3HA CoA thioesters. With PHaC being the synthase, type III PHA synthases are able to produce PHAs with molecular weights between those of PHAs produced by type I and type II synthases.[41;42]

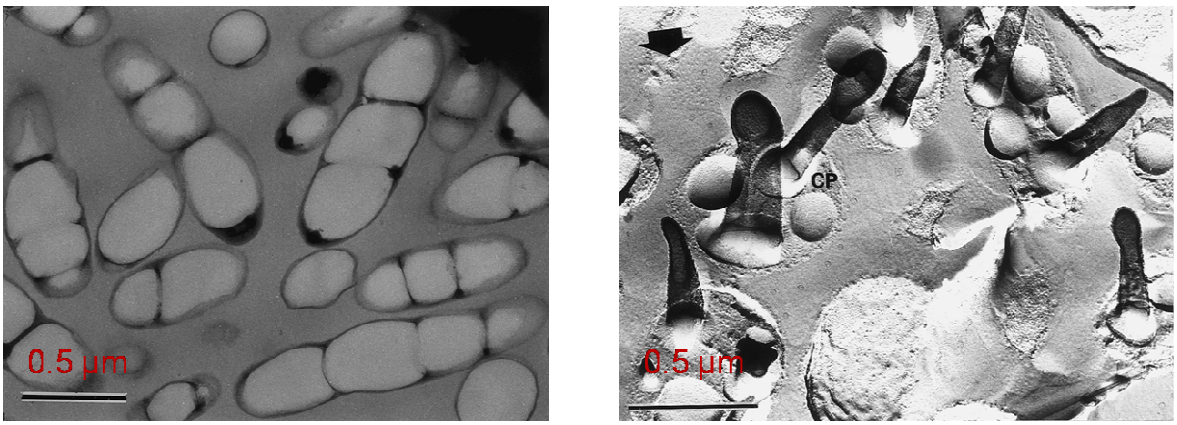

Figure 3-1: Transmission electron microscopic picture of thin sections of *R. eutropha* cells containing 90% PHA (left) and freeze-fracture electron microscopic picture of *R. eutropha* cells containing 50% PHA (right); CP = cytoplasm, arrow indicates the direction of platinum carbon shadowing.[43]

In general, PHAs can be synthesized from different starting materials such as alkanes, fatty acids, and sugars. A systematic overview of the biosynthesis and the catabolism relevant for the microbial PHA synthesis is given in Scheme 3-3.

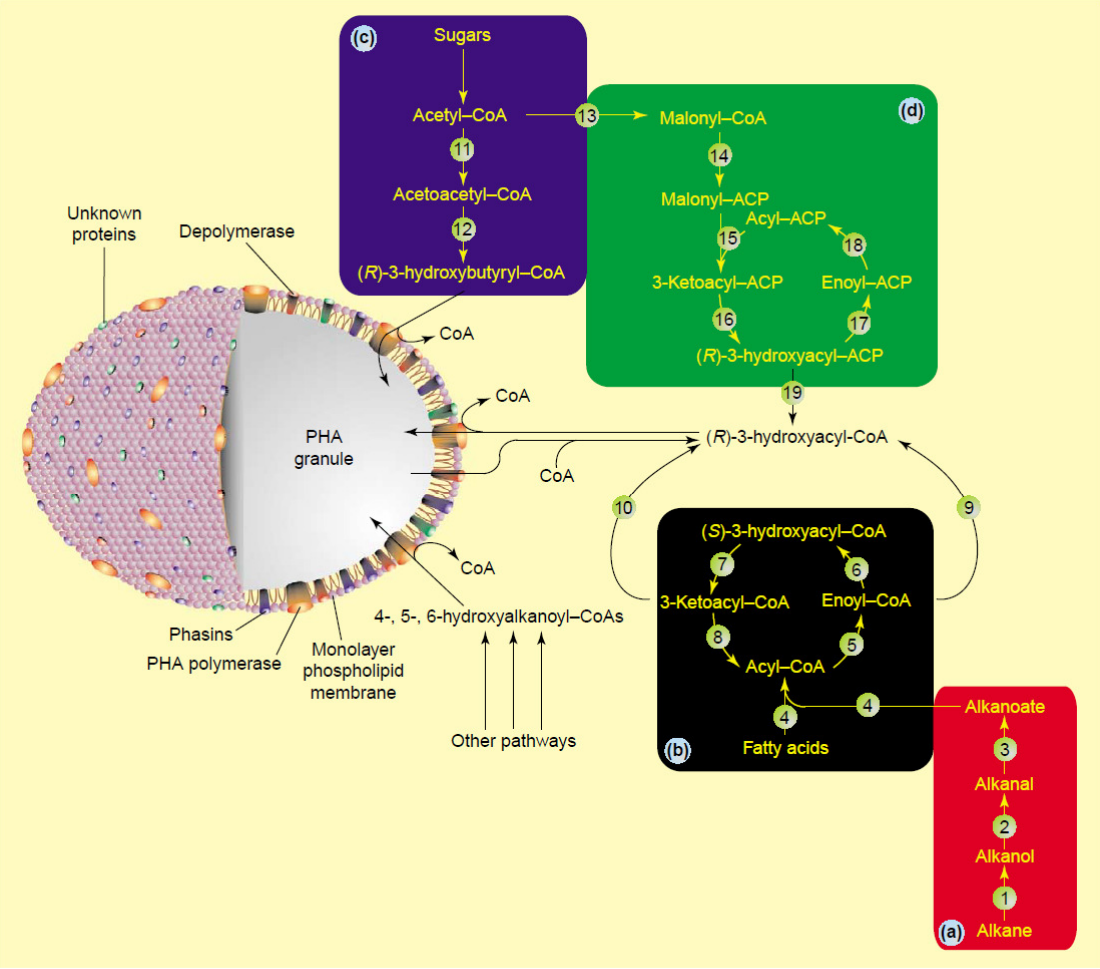

Scheme 3-3: Schematic representation of a PHA granule and the connections between the possible pathways of biosynthesis.[44] **(a)** Alkane oxidation pathway: (1) Alkane 1-monooxygenase, (2) alcohol dehydrogenase, (3) aldehyde dehydrogenase; **(b)** Fatty-acid β-oxidation: (4) Acyl–CoA ligase, (5) acyl–CoA dehydrogenase, (6) enoyl–CoA hydratase, (7) 3-hydroxyacyl–CoA dehydrogenase (8) 3-ketothiolase, (9) (R)-enoyl–CoA hydratase, (10) 3-ketoacyl–CoA reductase **(c)** Biosynthesis from carbohydrates: (11) β-ketothiolase, (12) NADPH-dependent acetoacetyl–CoA reductase. **(d)** De novo fatty acid synthesis: (13) Acetyl–CoA carboxylase, (14) ACP-malonyltransferase, (15) 3-ketoacyl-ACP synthase, (16) 3-ketoacyl-ACP reductase, (17) 3-hydroxyacyl-ACP reductase, (18) enoyl-ACP reductase, (19) 3-hydroxyacyl-ACP–CoA transacylase.[44]

Generally, the activation of the metabolic pathways leading to the formation of PHA-based storage compounds is caused by nutrient limitations.[6] Due to their complexity, the regulation mechanisms are not yet fully understood, but the scientific community has identified the concentration of acetyl-CoA as one of the main factors influencing the PHA synthesis: High levels of acetyl-CoA slow down the PHA synthesis while all processes leading to a decrease in the acetyl-CoA concentration start (or re-start) PHA synthesis.[45]

3.2.1.2. Intracellular Degradation of PHB

First extensive studies concerning the intracellular degradation of PHB have been conducted by Merrick et al. in the 1960s and 70s. Back then, the intracellular breakdown of PHB was studied with PHB granules extracted from *B. megaterium* as substrate for extracts from *R. Rubrum*.[46-48] For depolymerization, a labile factor associated with the granules and three soluble factors are needed, namely a heat-stable activator, a depolymerase, and a dimer hydrolase. With trypsin acting as activator, the attack of the hydrolase yielded 3HB as main product and some dimer and trimer residues. Dimers and trimers, in contrast to PHB are attacked by the hydrolase. The authors suggested a model in which hydrolysis is hindered by an inhibitor associated with the PHB granules and concluded that the inhibitor is destroyed by trypsin or neutralized by another activator.[49] It was also assumed that this behavior was part of the regulatory system for the synthesis and the breakdown of the storage compounds.

3.2.1.3. Extracellular Degradation of PHB

As some bacteria produce PHB in large amounts, it is quite clear that other bacteria and fungi use the released PHB from dead cells as carbon source.[38] The cells living on PHB secrete extracellular depolymerases which, on the other hand, degrade PHB into cleavage products that are used as carbon and energy source. Starting with the breakdown of PHB into oligomers, the oligomers produced are, again, hydrolyzed by oligomer hydrolases to yield HB monomers.

3.2.1.4. Chemical Hydrolysis and Thermal Decomposition of PHAs

Given the fact that all polyesters bear a hydrolytically labile ester-functionality, these compounds are susceptible to mechanical, thermal, irradiation-induced, or chemical decomposition. The decomposition is often based on the cleavage of covalent bonds leading to free-radical formation that subsequently degrades the polymer backbone.
The main reaction mechanism of the hydrolytic polyester cleavage can be referred to as a reversed polycondensation reaction. The degradation rate is mainly influenced by the water diffusion rate and is accordingly strongly dependent on the surface area exposed. The hydrolytic cleavage can be accelerated by the addition of acids, bases, or enzymes as well as by applying elevated temperatures.
The hydrolytic degradation of ester bonds proceeds under formation of small molecules (oligomers) with hydroxy or acid end-groups (Scheme 3-4).[50;51]

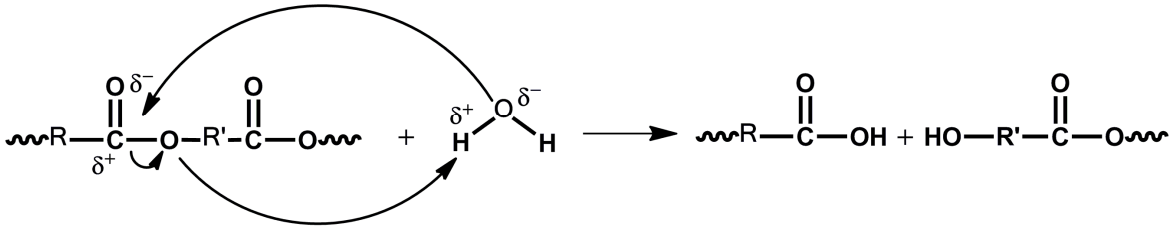

Scheme 3-4: Hydrolytic degradation of polyesters.[52]

Thermal degradation on the other hand, occurs exclusively by non-radical chain scission over a six-membered ring transition state (Scheme 3-5).[53]

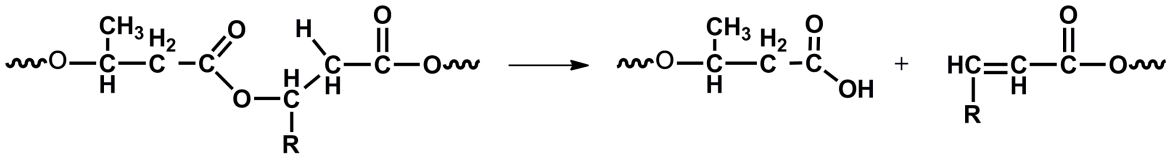

Scheme 3-5: Thermal decomposition of PHB.[53]

Notably, significant thermal decomposition of PHB occurs already at temperatures only slightly higher than the melting point which makes thermal processing without substantial loss of molecular weight impossible.

3.2.1.5. Biotechnological Production of PHAs

The production of PHAs can generally be carried out via fermentative biotechnological processes like batch, semi-batch, or continuous fermentation. The kind of process used and the parameters employed depend on the kind of PHA producing bacteria used.[54;55] Owing to the characteristics in the PHA accumulation, the bacteria can be divided into two groups. The first group begins to accumulate PHAs only after deprivation of essential nutrient factors like N, P, ammonia, or S and under provision of excess carbon, whereas the second group shows growth-related PHA production. Bacteria like *R. eutropha* and methylotrophic bacteria belong to the first group while *Alcaligens latus*, *Azobacter beijerinckii*, and biotechnologically engineered *E. coli* are members of the second group. For nutrient-limited production of PHAs, a two-step culture process has been suggested and widely applied: Cell growth up to a targeted concentration in the first step is followed by nutrient limitation triggering the PHA synthesis.[56;57]

When growth-associated PHA producing bacteria are used, a feeding strategy supporting cell growth as well as PHA accumulation must be employed. Additionally, several nutrient-limiting feeding strategies aiming at the enhancement of PHA accumulation in growth-associated bacteria have been proposed.[58-61]

Despite the various production methodologies proposed concerning the biotechnological synthesis of PHAs, commercial production has only been established for scl-PHAs like PHB, PHV, and the copolymer PHB-HV. PHB-HV, for example has been commercialized by Monsanto under the product name BIOPOL®, but the first consumer product, a biodegradable shampoo bottle launched in 1990 has already been withdrawn from the market due to economic reasons.[24]

Although extensive research on the ecologically and economically sustainable production of PHAs has led to much cheaper and cost-efficient approaches, prices of commercially produced PHB and PHB-HV are still much higher than those of oil-based plastics. Reviewing the literature on PHA-production, Rossel et al. developed an approach for cost efficient and sustainable integration of scl-PHA production in the sugar- and ethanol-based industry.[30] This model is based on sugar, ethanol, and PHB production in an average Brazilian sugar mill with the following assumptions: Crushing an average of 12 000 tons of sugar cane per day in the 180 day-lasting milling-season, the area of land required would be approx. 25 000 hectares. From the

juice obtained, sugar and ethanol are produced and the production of 10 000 tons of PHB per year is planned. Within the plant, thermal, mechanical, and electrical energy from the exploitation of sugar cane and the related by-products such as bagasse are considered. The mass and energy balance of a plant operating at the conditions proposed is depicted in Figure 3-2. From pilot trials carried out by Rossel et al., a production cost of 2.65 US$ per kg not including taxes would be achieved. Notably, Monsanto BIOPOL® products were sold in a price range of 10 000 to 20 000 US$ per kg, depending on the quality.[30]

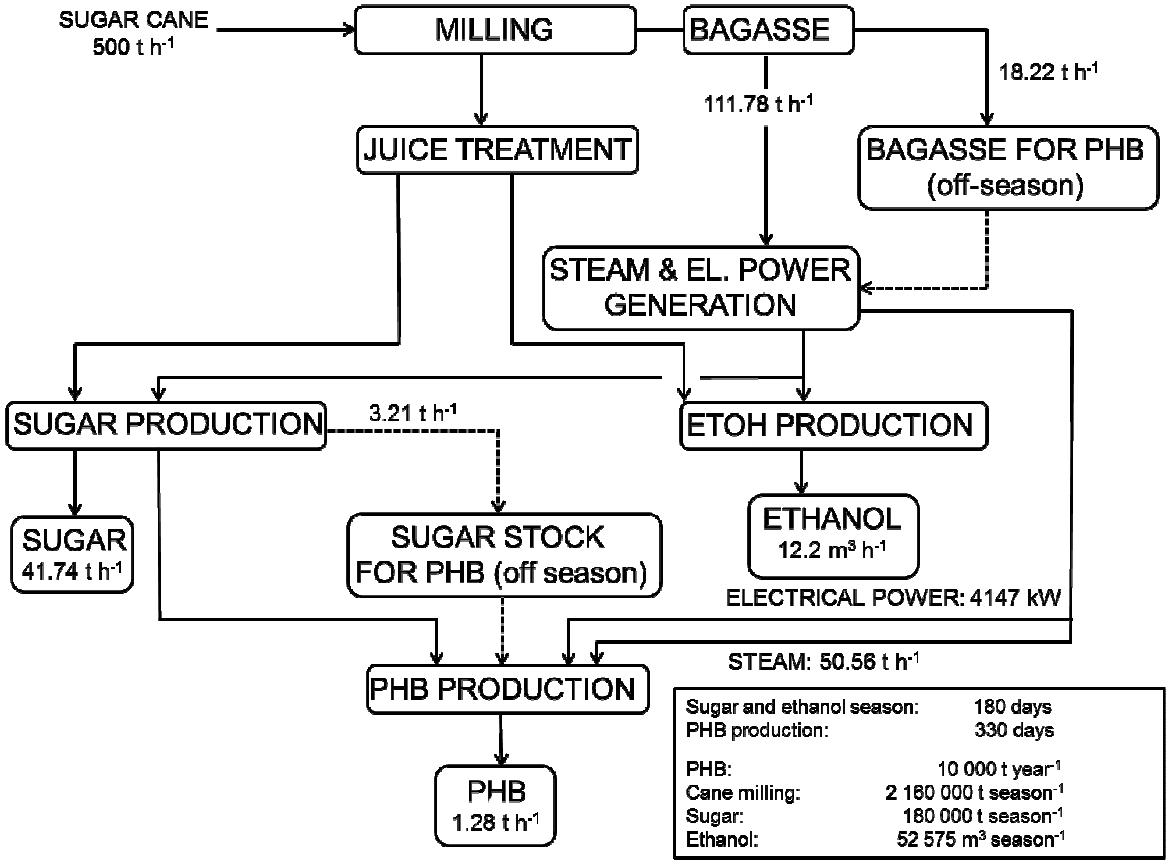

Figure 3-2: Mass and energy balance for PHB production integrated in an average sized Brazilian sugar mill.[30]

3.2.1.6. Material Characteristics of PHAs

As stated before, scl-PHAs reveal mechanical characteristics comparable to those of polypropylene, while their mcl-congeners are rubber-like elastic and tacky compounds.

Given the fact that PHB itself is a highly crystalline and, hence, very brittle material, research in the 1980s focused on the control of the polymer's crystallinity. This has been proven to be feasible by the incorporation of 4-hydroxybutyric acid in PHB rather than by incorporation of HV in PHB (see 3.2.1). Nevertheless, the incorporation of hydroxyvalerate units in the PHB homopolyester has shown potential towards the preparation of more flexible materials from scl-PHAs. PHB and PHB-HV were the first PHAs, the production of which has been commercialized by Monsanto in the 1980s, and which are currently produced and distributed by the German company Biomer.[62] In fact, PHB-HV has significantly increased toughness and lower stiffness compared to the native PHB homopolyester. Depending on the amount of HV present in the copolymer, material characteristics shift from hard and brittle to soft and ductile with increasing HV content.[63] Additionally, the polymer's melting point decreases with increasing HV content.

Another approach for decreasing the brittleness and increasing the toughness of scl-PHAs is the incorporation of 4-hydroxybutyrate units in PHB. Table 3-1 shows the comparison of PHB and different PHB-HV and P3HB-*co*-P4HB copolymers. Notably, the values for PHB-*co*-HV were determined with commercially available Biopol products. As stated before, the addition of HV leads to increased flexibility and decreased melting points and stiffness. Already at low HV concentrations, mechanical characterization reveals significantly decreased values for the tensile strength and the Young's modulus, but 11 mol-% of HV appear to be enough to increase the strain at break by a factor of 3 to 4. These phenomena are even more pronounced with P3HB-*co*-4HB, where 4HB contents of as low as 11 mol-% induce a 100-fold increase in the elongation at break compared to the PHB homopolyester. Additionally, P4HB has significantly superior tensile strength compared to the P3HB homopolyester. According to information retrieved from the Biomer website, the Biomer polymers presented in Table 3-1 are PHB-based, but the tensile characteristics indicate HV contents of more than 10 mol-%. Overall, scl-PHA-based polymers show material characteristics comparable to those of PP, PS, and PET.

Table 3-1: Mechanical characteristics of selected commercial and non-commercial scl-PHA homo- and copolymers as well as three conventional oil-based polymers.[62;64-67]

Polymer	Melting Temp. [°C]	Young's Modulus [GPa]	Tensile Strength [MPa]	Elongation at Break [%]
PHB	179	3.5	40	5
PHB-*co*-HV (7 mol-% HV)	160	1.4	24	2.8
PHB-*co*-HV (11 mol-% HV)	145	1.1	20	17
PHB-*co*-HV (22 mol-% HV)	137	0.62	16	36
P3HB-*co*-4HB (11 mol-% 4HB)	132	-	20.3	698
P3HB-*co*-4HB (22 mol-% 4HB)	128	-	9.9	729
P4HB	60	149	104	1000
Biomer® P209	-	0.84-1.2	15-20	11-18
Biomer® P226	-	1.14-1.9	24-27	6-9
PP	170	1.7	34.5	400
PET	262	2.2	56	7300
PS	110	3.1	50	-

3.2.2 Medical Applications of PHAs

Considering the fact that all PHAs are biodegradable, scl- as well as mcl-PHAs have been proposed for applications in medicine already in the 1970s. PLA has already made its way to medical uses as surgical suture materials and devices for sustained drug delivery applications, often in copolymers containing glycolic acid. Highly pure PLA in its D,L racemic form, as well as D- and L- enantiomerically pure PLA is commercially available for the preparation of medical devices from Evonic under the brand name Resomer®.[68] A main drawback besides the relatively high brittleness and

for some applications even too fast degradation rates is the formation of acidic products upon breakdown of PLA and PGA. This accumulation of strongly acidic compounds at the respective implantation site has been of special concern in the medical community because of the chronic inflammatory reactions caused by this phenomenon.[69] Given the pK_A-value of PLA and PGA of 3.86 and 3.83, respectively, the acidity of 3-hydroxybutyric acid is much lower with a pK_A-value of 4.70.[70] Hence, degradation products of PHB should cause less pronounced chemical irritation. Consequently, PHB and PHB-HV have also been suggested for this field of application. Additionally, softer and less brittle materials derived from mcl-PHAs like poly(3-hydroxyhexanoate) and poly(3-hydroxyoctanoate) have been taken into account for wound dressings, tissue engineering and drug delivery.

3.2.2.1. Medical Applications of PLA, PGA and Copolymers

Approved by the food and drug administration (FDA) for drug delivery applications, PLA-*co*-PGA is among the most common polymer-based materials used for drug delivering microspheres and vaccine development.[71;72] Due to its high degradation rate and sometimes extensive adverse body responses, the PGA homopolymer is frequently used in form of its copolyester with PLA. PLA, on the other hand, is used in both, its homo- and in the copolymer form with PGA, PCL and PEG. Copolymers of PLA and PGA are frequently referred to as poly(lactide glycolide) PLGA. Furthermore, PLA offers the possibility to fine-tune the degradation characteristics and the mechanical properties by covalent incorporation or blending of the two different enantiomers (L and D) of this compound. Stereocomplexation of PLLA and PDLA has been proven to yield materials with significantly higher tensile strength, higher degradation rate and bulk erosion degradation behavior.[73-75] Applications in the area of sustained drug delivery, antigen and DNA delivery have been proposed and tested. Due to their low toxicity apart from acidity-based foreign body reactions and their relatively high degradation rate, PLA-*co*-PGA polymers have been extensively used for drug delivery applications over the past years and as of today, several products are already being marketed or in clinical trials. These products encompass periodontal depots, intratumoral paste, ocular drug delivery devices, drug eluting stents, nanoparticles for inhalation, and parenteral depots (Figure 3-3).

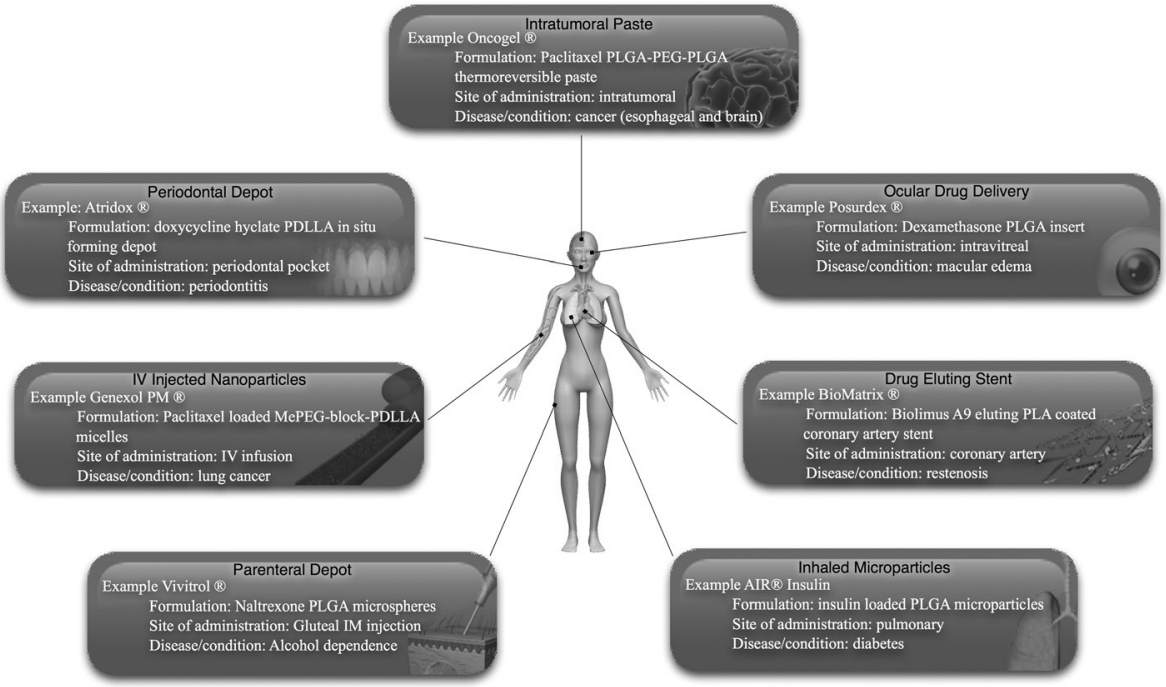

Figure 3-3: PLA and PLGA-based products for drug delivery applications currently being marketed or in clinical trials.[76]

Apart from the considerable use in sustained drug administration, PLA and PLGA have also found to be useful in other applications like arthroscopy, tissue engineering, bone cements and orthopedic implants.[77;78] Biocompatibility and cytotoxicity have been evaluated multiple times and low levels of foreign body responses were found. Notably, basic and application-driven research has focused on drug delivery applications rather than bone implants for fracture fixation or tissue engineering. Nevertheless, intellectual property right (IPR) activities are quite strong for PLA and PLGA in all fields of medical application indicative of growing technical and application-driven interest in addition to the academic research concerning this material class.[79]

3.2.2.2. Medical Application of scl-, mcl-PHAs and their Copolymers

Other than PLA and PGA, aliphatic polyesters like PHB, PHB-HV and mcl-PHAs have not yet been approved for medical use by the FDA. Nevertheless, scl- and mcl-PHAs have been proposed and used for in vivo applications. Especially PHB, which was first

suggested as surgical suture material in 1962 and the copolymer PHB-HV have attracted considerable research interest over the past decades.[80] Owing to the higher versatility of scl- and mcl-PHAs compared to PLA, the potential applications of PHAs cover an even broader range in the field of medicine, but the limited commercial availability of most PHAs has been a major drawback in the evaluation of these materials. Another important issue related to these microbially produced polyesters is the purity. For medical applications, polymer-based materials have to be free from surfactants, residual cell walls, proteins, and, most of all, endotoxins excreted by the PHA-producing bacteria. The FDA has recently set the threshold value for endotoxins in polymers for medical uses to 0.5 $EU \cdot mL^{-1}$.[80]

3.2.2.2.1 Medical Application of PHB and PHB-co-HV

Behrend and co-workers evaluated the use of PHB as soft tissue repair material by implantation of wound patches for gastrointestinal lesions in rats. Preceded by in-vitro testing where moderate adhesion of mouse and rat intestinal cells was observed, the in-vivo experiments revealed better tissue regeneration using a PHB patch than with commercially available Vicryl® (PLGA) patches.[80] The generally good cell adhesion and viability properties were later confirmed for NIH 3T3 and L929 mouse fibroblasts.[81] This effect was found to be significantly enhanced by surface pretreatment with alkaline or lipase solutions.[82]

PHB was first tested for drug release applications as early as in the 1980s. Since then, PHB and PHB-*co*-HV have been used for in-vitro and in-vivo evaluation in sustained drug delivery devices. Depending on the molecular weight, the processing method and the drug used, different observations concerning the release profiles were made. Overall, the devices were tolerated quite well by different host species such as mice, rats, sheep, and cows. Additionally, small human studies and veterinary medical studies have been conducted.[83] Notably, most studies did not profit from the polymer matrix' degradability, either because of high drug loadings and poor mixing or because of the too low degradation rate of PHB and PHB-HV. This is also the reason why the potential of drug delivery based on PHB and PHB-HV is seen in the long-term sustained release of highly potent drugs.[84]

Despite the restricted usability of PHB and PHB-HV in drug delivery, orthopedic applications have shown more promising results. Especially due to the slower degradation rate of PHB and PHB-HV compared to PLA and PLGA, these materials are preferred candidates for such applications.[80]

Doyle et al. observed rapid formation of highly organized bone in in-vivo trials of PHB as bone implant material without chronic inflammatory reactions up to 12 months after implantation.[85]

In combination with hydroxyapatite (HA) [$Ca_5(PO_4)_3OH$], PHB and PHB-HV were found to have a compression strength of 62 MPa, which is within the range of several human bones. Due to the piezoelectric characteristic of PHB, PHB/HA and PHB-HV/HA composites are believed to be beneficial for the bone healing process.[63;86] For in-vitro evaluation of hard tissue applications, PHB/HA composites were placed in simulated body fluid (SBF) at a temperature of 37 °C. Interestingly, the formation of a bone-like layer around the PHB/HA molds was observed and the authors suggested high bioactivity of this material which could, together with the mechanical strength, be tuned by variation of the HA content.[87] These findings are supported by the experiments conducted by Luklinska and Wang, who used PHB/HA and PHB/tricalcium phosphate (TCP) and found that HA crystallites were formed at the interface between implant and bone tissue.[88;89]

Besides PHA/HA composites, porous scaffolds prepared from PHB and coral powder have been proven to be an excellent material for bone tissue engineering. It was stated that the PHB/coral powder composites had optimum pore sizes and porosities ranging from 18 to 25 microns and from 40 to 70%, respectively. The authors concluded that the material prepared would greatly support vascular invasion and bone healing.[90] In-vitro cytotoxicity tests of PHB and PHB composites with HA and coral powder were also carried out by the same working group. These tests confirmed non-cytotoxicity of all the materials evaluated in the study.[91]

In terms of bone formation ability, osteoblast proliferation was observed on O_2-plasma treated PHB-HV foams. Additionally, characterization by means of histology, SEM, and confocal laser microscopy revealed that the osteoblasts could also grow inside the matrix and induce mineralization.[92;93] In-vivo assessment of PHB composites was carried out in the femur of Japanese white rabbits. PHB/HA composites generated increased interfacial shear strength (ISS) up to 8 weeks after implantation. After 8 weeks ISS was lowered by the degradation of the material. Another composite,

namely PHB/glass/HA, showed lower shear strength, which was attributed to soft tissue response at the interface caused by ion release from the glass matrix.[94]
In addition to the above described applications of PHB and PHB-HV in the field of drug delivery and orthopedic tissue engineering, research activities are also strong in nerve regeneration and cardiovascular applications like pericardial patches and artery augmentation.[80]

3.2.2.2.2 Medical Applications of mcl-PHAs and Copolymers

Due to their lower stiffness and higher flexibility, mcl-PHAs and copolymers with PHB have been proposed for soft tissue applications rather than hard tissue regenerative medicine. Copolymers of PHB and PHHx were examined for their potential as injectable in-situ forming implants that can prevent post-operative tissue adhesion. For this, solutions of the polymer in organic solvents like *N*-methyl pyrrolidone or 1,4-dioxane were prepared and directly injected in the respective site.[95] Film formation subsequently occurred due to contact of the solution with the aqueous environment leading to controlled precipitation of the dissolved polymer.[96] Injectable bioresorbable formulations based on polymers have been evaluated for both, tissue repair and drug delivery applications.[97]
In drug delivery applications, on the other hand, nanoparticles consisting of PHB-*co*-HHx were evaluated for targeted drug delivery applications with the binding protein PhaP and ligands fused to PhaP. A schematic representation of this principle is depicted in Figure 3-4. These containers were used as drug delivery vectors for mostly hydrophobic drugs and were taken up in-vivo by hepatocellular carcinoma cells and in-vitro by macrophages and hepatocellular carcinoma cells BEL7402.[98] The authors concluded that the system's drug targeting ability was proven by the in-vivo and in-vitro tests.

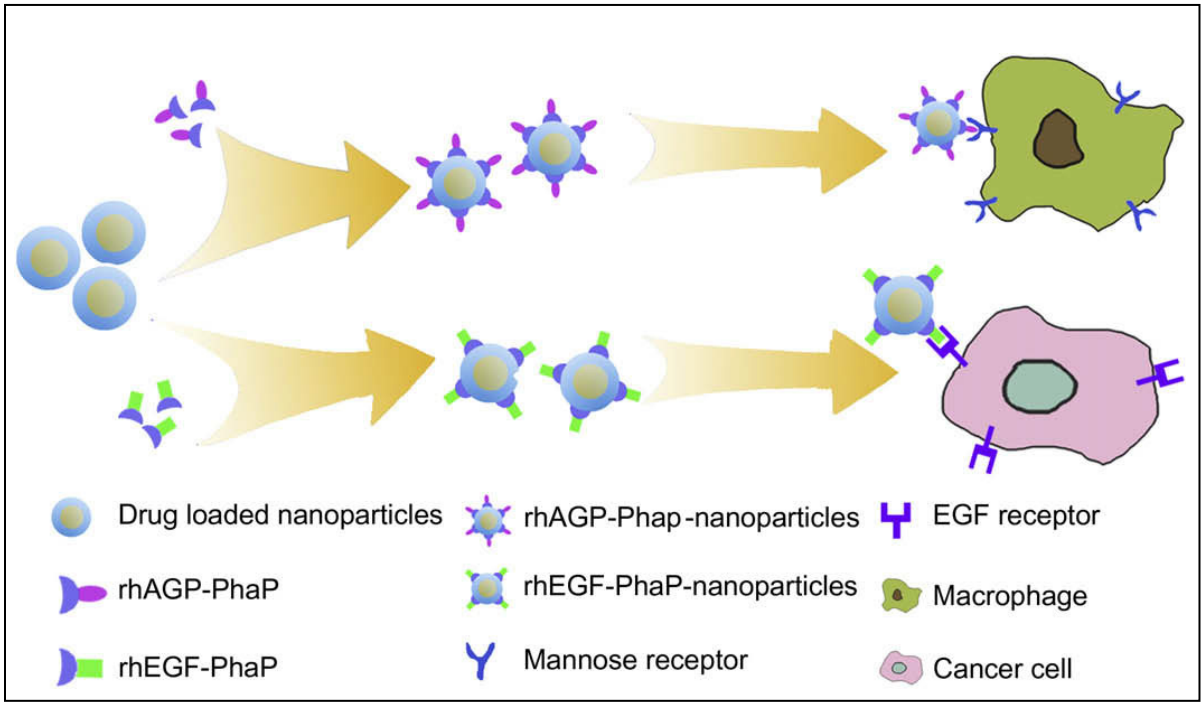

Figure 3-4: Schematic representation of the uptake of drug loaded PHB nanoparticles coated with fusion proteins in order to introduce the recognition sequence. These drug containers were superficially bound on macrophages (up) and cancer cells (bottom).[98]

In addition to soft tissue engineering and drug delivery, porous scaffolds based on PHB-*co*-HHx were tested in other applications like nerve regeneration and cartilage repair. The latter strategy was examined with three-dimensional PHB-*co*-HHx scaffolds in articular cartilage defects in rabbits where repair in the articular cartilage was observed 16 weeks after operation.[99]

The considerably softer mcl-copolymer PHO-*co*-HHx were examined for use as vascular grafts and heart valves but overall, the low degradation rates and the slightly stronger inflammatory reactions compared to other PHA-based materials render these compounds less suitable for this kind of application.[80]

3.3 Modification of Polymer-Based Materials for Medical Applications

As stated in chapter 3.2, the application of biopolyesters for medical purposes in general and the use of PHAs in particular is partially hindered by several challenges arising from the mechanical, chemical, physical, and physico-chemical properties of these materials. The most relevant of these bottlenecks are too fast or too low degradation rates, poor mechanical strength, and low surface hydrophilicity with negative impact on biocompatibility and foreign body response in in-vivo applications. These modifications can be of chemical or physical nature and concern the bulk material as well as the surface state of polymer-based materials for medical applications.

3.3.1 Physical Modification of Polymer-Based Materials

The physical modification of polymer-based materials is mainly based on mixing polymers with other polymers and/or other organic or inorganic fillers in order to yield materials with superior mechanical properties compared to the native polymers. Due to the different characteristics of the components, the resulting polymer/polymer or polymer/filler mixture can benefit from synergistic effects.[100] In addition, nucleating agents can have positive influence on the mechanical properties of semi-crystalline polymers.

3.3.1.1. PHA-Based Composites with Inorganic Fillers

Due to their frequently poor mechanical characteristics and their relatively high price compared to oil-based polymers, PHAs have been mixed with inorganic fillers in order to improve their physical and mechanical characteristics for medical applications, their bioresorbability and biocompatibility. Especially the addition of hydroxyapatite (HA), tricalcium phosphate (TCP), and wollastonite (calcium silicate $CaSiO_3$) for orthopedic devices has been shown to increase mechanical strength, biocompatibility, bone ingrowth, and the resorption behavior (see chapter 3.2.2.2). These so-called

bioceramics can be mixed with PHAs by various methods like injection-molding, compression molding, and salt-leeching.[85;87;94] In fact, composites prepared from PHB or PHB-HV and HA show higher Young's moduli but lower tensile strengths and elongation at break than the native pure polymers. Interestingly, the Young's modulus and the tensile strength of PHB-HV/HA composites decrease with increasing HA content in in-vitro degradation tests carried out in simulated body fluid.[88;89] This finding is attributed to the composites' higher susceptibility to water penetration resulting in higher degradation rates, accompanied with loss of modulus and osteoblast integration in the bone tissue. The reinforcement and bioactive properties of HA and calcium phosphate have been proven to be successful in many studies and is mainly attributed to the fact that HA helps increasing the bonding ability between osteoblast cells and the composite material.[88;94]

TCP, on the other hand, seems to have less a pronounced impact on the mechanical properties of PHB-HV than HA. Accordingly, the mechanical properties of PHB-HV are enhanced with the addition of a certain amount of HA while the addition of TCP has a positive influence on the bioactivity but not on the physical properties of composite materials.[101] Additionally, there is an optimum content of inorganic filler that can fulfill the targeted changes in the material's properties: While HA contents of up to 30% mostly lead to improvements in degradation rate, bioactivity, and stiffness, higher amounts of filler have detrimental effects on the composites' characteristics. This observation can be explained by the formation of filler agglomerates that act as predetermined breaking points in the polymer matrix and render the materials more susceptible to irreversible deformation by external forces.[102;103] In general, the preparation method also has considerable influence on the intensity of the filler effects, and melt-compounding and injection molding have been shown to have more pronounced positive effects than compression molding and solution casting.[94]

Another approach towards the preparation of bioactive reinforced composite materials is the addition of wollastonite and bioactive glasses. Bioactive glasses are a class of silicate or phosphate glass-based materials with broad applications in dentistry and medicine and have potential for preparation of bioactive glass/polymer composites.[104] Commercially available bioactive glass type 45S5 consisting of SiO_2, CaO, Na_2O, and P_2O_5 has been evaluated for the preparation of bioactive composites with PHB. Besides increased stiffness, bioglass PHB composites are found to contribute to the bone healing process by differentiation of human osteoblast cells and it is assumed

that these materials have higher bioactivity than PHB/HA or PHB-HV/HA composites.[105] Besides mixed bioglass/PHA composites, bioactive meshes have been prepared from PHB and bioglass. Bioglass coated PHB meshes were slurry-coated with bioglass and examined by microscopic means and incubation in SBF. The homogeneity as well as the coating thickness can be controlled by variation of the bioglass particle concentrations (Figure 3-5). All coated samples showed formation of HA crystals on the surface, indicative of increased bioactivity. Additionally, minimal polymer degradation 21 days after incubation can be observed and the authors concluded that this time frame was acceptable for bone tissue applications.[106]

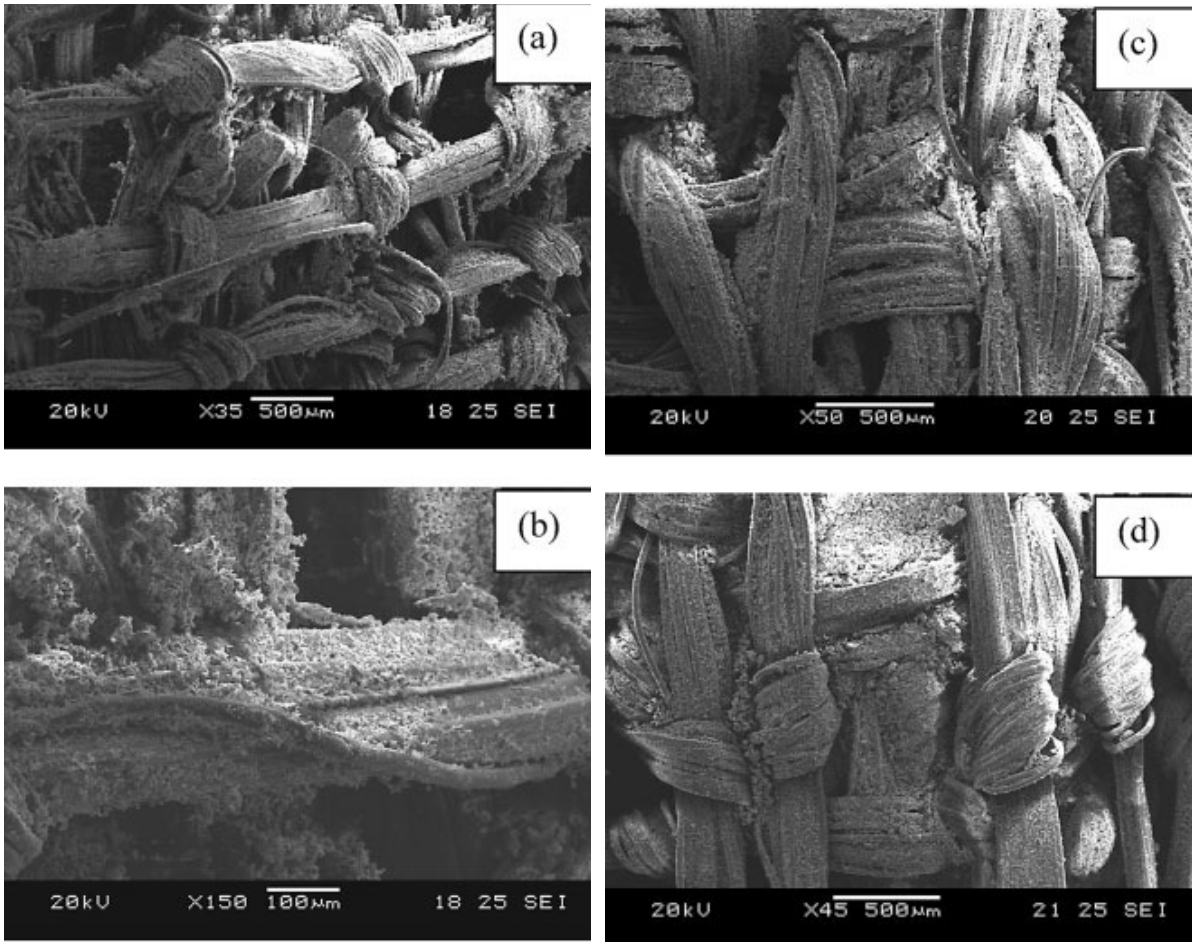

Figure 3-5: SEM micrographs of PHB meshes coated with bioglass from 10% bioglass slurries: (a) Small magnification; (b) large magnification; (c) 5 min dipping time; (d) 10 min dipping time.[106]

Besides polymer matrix/calcium composites, magnesium metal composites offer the possibility for reinforcement of PHAs and, due to magnesium's higher degradation

rate, acceleration of the resorption behavior. Studies concerning the preparation and evaluation of PHA/Mg powder composites are scarce, but significant increases of the composites' stiffness and decreased strain at break can be anticipated by common sense. Additionally, these composites are expected to support the degradation behavior of relatively stable PHA polymers and instable magnesium particles and can lead to synergistic effects between the metal and the polymer part of the resulting material.

Nevertheless, polymer or PHA-based composites have been evaluated as coatings for metal-based implants in orthopedic surgery applications. PHB for example has been used for retardation and fine-tuning of magnesium degradation in Hank's solution for 30 days. The application of PHB coatings on rapidly-eroding magnesium alloys helps to prevent magnesium corrosion and showed uniform degradation of the PHB coating prior to Mg breakdown.[107] This approach has been expanded to a wider range of polymers and biodegradable metal alloys and has also been recognized with a more technical background rather than pure academic interest.[108-112]

Polymer coatings can also be applied on non-degradable materials like titanium. The main goal of this strategy is the increase of the biocompatibility of titanium metal-based implants by adding functional polymer coatings that increase biocompatibility, decrease foreign body reactions and support the healing process compared to the native metal alloy implants. These modifications can be achieved by the incorporation of (bone) growth factors, binding proteins and antibiotics.[113-115]

3.3.1.2. Polymer Blends and Mixing of Polymers

For understanding the basic terms and prerequisites of mixing, some fundamentals concerning the theory of mixing have to be explained at this point.
The term *miscible blend* is applicable for a homogeneous system derived from a mixing process and fulfills the following inequation: [116]

$$\Delta G_M = \Delta H_M - T\Delta S_M < 0 \qquad \textbf{Equation 3-1}$$
$$T,\ p = const.$$

T……. Temperature
p……. Pressure
ΔG_M……..... Change in free energy
ΔH_M……. Change in enthalpy
ΔS_M……. Change in entropy

Since the disorder of the system is increased by mixing, the process is always entropically favored. Although equation 3-1 has to be fulfilled for mixing, it is not sufficient to provide reliable estimation. Notably, a single phase mixture that is thermodynamically stable can only exist when

$$(\partial^2 \Delta G_M / \partial \Phi^2)_{T,p} < 0 \qquad \textbf{Equation 3-2}$$

is fulfilled in the whole range for the mixture (Φ represents the composition). If equation 3-2 is not fulfilled for the whole mixture, the system is referred to as partially miscible, and stable one-phase mixtures can only exist at the ends of the composition range. The factors contributing the most to miscibility are the chemical nature and the molecular weight of the polymers to be mixed. Consequently, a mixture of miscible polymers exhibits characteristics between, or, ideally, even superior to the single components' properties.
In contrast to miscible polymers, compatible polymers are not miscible according to thermodynamical relations. The potential improvement of the properties is based on the interfacial adhesion between the components rather than mixing. From this point

of view, miscible blends have to be separated from compatible blends and composites where one component can be seen as the matrix and the other as the filler or reinforcement. In this case external stress is transferred from the matrix to the reinforcement and the adhesion between matrix and dispersed component is the main contributor to mechanical stability. For the preparation of compatible blends, the compatibility of the components can be improved by the addition of block or graft copolymers, by crosslinking the blend components to yield an interpenetrating network, or by chemical modification of one or both polymer components.[116]

3.3.1.2.1 PHA-Based Blends

PHAs, especially scl-PHAs, have been found to be well miscible with a number of other polymers including biodegradable polymers like poly(ethylene glycol) (PEG), poly(vinyl alcohol) (PVA), PCL, polysaccharides and non-biodegradable polymers like poly(methacrylate) and poly(vinyl acetate).[117]

PHB is miscible with PEG, poly(epichlorhydrin), and poly(vinyl acetate) (PVA), partly miscible with poly(methyl methacrylate) PMMA, and compatible with PCL, ethylene-propylene rubber (EPR) and poly(butylacrylate).

Since research has mainly focused on miscibility, biodegradability and crystallization behavior of PHB-based blends, studies of the mechanical characteristics are scarce. Generally, the addition of other polymers increases the elongation at break of the relatively hard and brittle PHB. This suggestion has been found to be valid for mixtures of PHB with atactic PMMA, EPR, and PVA, where the brittleness of native PHB has been overcome to the disadvantage of stiffness (Young's modulus) and tensile strength.[116]

Also blends within the PHA family have been prepared and characterized. Especially blends prepared from PHB and PHHx have been proven to be much more ductile with significantly increased biocompatibility towards the proliferation of chondrocytes.[118] Additionally, the surface morphology of PHB/PHHx has been determined to be dependent on the degree of crystallinity. Higher contents of PHHx decrease the degree of crystallinity and consequently yield smoother surfaces that allow cell adhesion and growth to a much greater extent than native PHA.[119]

When PHB is mixed with PLLA, the two polymers are found to be miscible with the possibility of co-crystallization and it is concluded that this behavior can strongly

contribute to enhanced mechanical stability.[120] In contrast to that, the miscibility of PHB with PDLLA is found to be dependent on the preparation method: While blends prepared by solvent casting at room temperature are immiscible, samples prepared by melt mixing show greater miscibility. Moreover, the addition of PDLLA yields lower crystallinities for the PHB part and enhances mechanical properties compared to native PHB.[121]

In addition to the abovementioned PHA mixtures, blends of PHAs with chitosan, chitin, cellulose and starch have been prepared mainly in order to prepare cheaper biodegradable materials that can be used for commodity applications.

3.3.2 Chemical Modification of Polymer-Based Materials

In contrast to physical modification, the chemical modification of polymers is based on changes at the bulk polymer or its surface on the molecular level. Polymeranalogous reactions provide a great variety for functionalizing and/or modifying macromolecular compounds without changes in the macromolecular structure. Due to the tremendous diversity of possible reactions and, accordingly, the changes in material characteristics, the field of polymeranalogous reactions has been intensively investigated also in PHA-based polymer chemistry.

These polymeranalogous reactions comprise functionalization by introducing reactive groups like carboxyl-, epoxy-, hydroxy-, amino-, sulfonyl-, and halogen-functionalities and copolymerization as well as grafting of other polymers.[122;123] Furthermore, crosslinking with reactive multifunctional compounds can be carried out in order to prepare polymer networks that exhibit superior properties compared to the native polymers. Besides the overall improvement of material properties, crosslinking reactions are especially targeted towards changes of the degradation characteristics of degradable polymers: While biodegradable polymers tend to undergo random bulk erosion, crosslinking can shift the degradation behavior towards surface erosion and zero-order kinetics.[124] The latter phenomenon is of crucial importance for drug delivery applications where the continuous sustained release of active pharmaceutical ingredients (APIs) can only be obtained by well-defined degradation characteristics.[125]

As low hydrophilicity is one of the main drawbacks of biodegradable aliphatic polyesters in medical applications, extensive research has been conducted in order to improve the wetting characteristics of these polymer-based materials.

3.3.2.1. Graft and Block Copolymers of PHAs

The synthesis of graft and block copolymers is a versatile method for the preparation of new polymers with different characteristics than those of the native basic polymers. Considerable efforts have been made in this field of research in order to incorporate hydrophilic polymers in the generally hydrophobic PHA-backbones and yield amphiphilic materials with tailor-made degradation characteristics and potentially increased biocompatibility.

Poly(ethylene glycol) is one of the most abundantly used polymers for introducing hydrophilic groups into hydrophobic polymers. Profiting from the FDA approval for medicinal applications, PEG is frequently employed as hydrophilic and biocompatible additive for formulations and implants.[126;127]

PHB- and PEG-based triblock copolymers can be synthesized by coupling hydroxy-terminated low molecular weight PHB with methoxy-PEG-monocarboxylic acid using 1,3-*N,N'*-dicyclohexylcarbodiimide as coupling agent. The resulting copolymers exhibit increased crystallinity of the PHB part and decreased crystallinity of the PEG part and were found to form stable micelles in highly diluted aqueous solutions.[128;129]

PHB-PEG diblock copolymers on the other hand can be synthesized analogously to PLLA-PEG copolymers using monomethoxy-PEG and a bis(2-ethylhexanoate) tin catalyst in a melt transesterification. The changes in crystallization and the self-assembling behavior of PHB are attributed to the difference in the hydrophilicity of PHB and PEG and it was concluded that the replacement of PLLA by PHB opened a wider range of morphologies in the resulting block copolymers (Figure 3-6).[130]

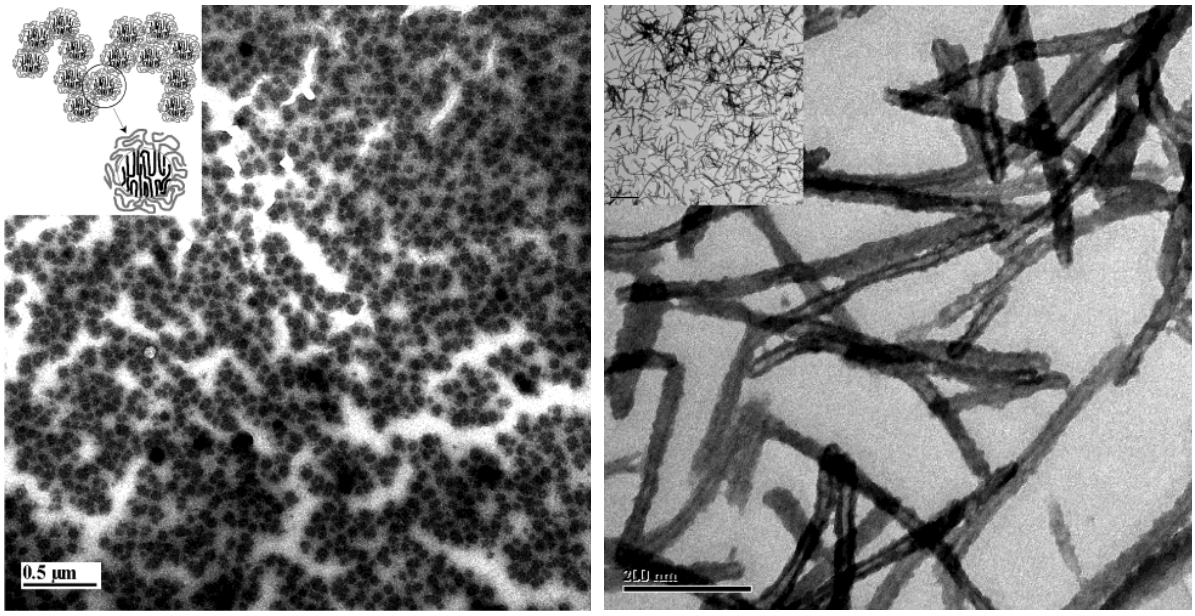

Figure 3-6: TEM micrographs of PHB-PEG diblock copolymers after slow solvent evaporation under stirring (left) and fast solvent evaporation (right) with schematic representation of complete phase separation (upper left) and low magnification inset of random fiber assembly (upper right).[130]

Another approach concerning the synthesis of amphiphilic PHA-based block copolymers with PEG was described by Renard et al. In a first step, length-controlled PHB-HV-, PHB-HHx-, and PHOHHx-oligomers were functionalized with propargylamine and subsequently ligated with azide-terminated PEG in copper(I)-catalyzed cycloadditions. Again, these copolymers formed stable micelles and were suggested for drug delivery applications.[131]

PHB-chitosan can be prepared by reacting carboxy-terminated PHB with chitosan amine functionalities. Despite the fact that both polymers are not soluble in water, the graft copolymers gave stable, viscous aqueous solutions and, after drying, yielded strong elastic films. Similar to PHB, carboxylated PHO can be grafted with chitosan by condensation and in the resulting copolymers, PHO acts as plasticizer for the hard and brittle chitosan.[132]

Chain extension reactions can be employed for the preparation of PHB-PEG block copolyurethanes by reacting PHB-diol and PEG with diisocyantates. PHB-PEG urethanes exhibit a wide range of mechanical properties that can be adjusted by variation of the partner polymers.[133]

Mcl-PHAs can also be used for grafting reactions with monoacrylate-PEG under UV-irradiation with benzoyl peroxide and the copolymers show significantly enhanced

water uptake accompanied with decreased protein absorption with increasing PEG content.[134]

Besides end-group-functionalized saturated PHAs, also unsaturated polyesters can easily be modified with various other polymers like PEG, polystyrene (PS), PMMA, poly(isoprene) (PI) and poly(acryl amide) (PAAm) by either esterification of carboxy groups or free-radical mechanisms.[122;135-138] The resulting graft copolymers have improved film and mechanical properties (PMMA, PS, PI) and give surfaces with increased hydrophilicity (PAAm).

Notably, all above described syntheses are carried out with either functionalized PHAs or with PHAs bearing unsaturated side-chains. Consequently, saturated PHAs have to be functionalized prior to further polymer modification.

3.3.2.2. Functionalization of PHAs

Reactive PHA-derivatives can be obtained by epoxidation, carboxylation, chlorination, and attachment of unsaturated groups. Thermal degradation of PHB for example produces PHB oligomers (approx. 2000 Da) with terminal unsaturated crotonate groups. Esterification of PHB oligomers with hydroxy methacrylate yields functionalized macromonomers.[139] Another method for the preparation of PHB macromers is the maleation of PHB-diol that can be obtained by alcoholysis of PHB with 1,6-hexanediol and subsequent selective reaction with maleic anhydride. This way, PHB macromers with two different functionalities, namely hydroxy double-bond end-groups can be synthesized and subsequently (re-)polymerized with other monomers.[140]

As described in the previous chapter, mcl-PHAs with unsaturated side-chains are more susceptible to modifications than saturated polyesters and, hence, enable for facilitated functionalization. Numerous modifications of unsaturated PHAs have been studied including the introduction of hydrophilic groups and the attachment of reactive sites.

By addition of chlorine to the double-bonds of unsaturated PHAs, chlorinated polymers are formed under partial hydrolysis. The resulting chlorinated polymers have higher glass transition and melting temperatures and can subsequently be converted

to the corresponding sodium sulfate and tertiary ammonium salts as well as phenyl derivatives.[141]

The epoxidation of PHA double-bonds has been studied by several groups and been found to be readily accessible by reaction of PHAs with *m*-chloroperbenzoic acid.[142] This way, the double-bonds are converted into epoxy groups that can be used for crosslinking reactions with succinic acid anhydride in the presence of basic catalysts like 2-methyl-4-methylimidazole.[143]

For converting the double-bonds of poly(hydroxyoctanoate-*co*-hydroxyundecenoate) (PHOU) into hydroxy functionalities, $KMnO_4$ in alkaline solution at room temperature has been reported to be a valid strategy without significant loss of molecular weight. Additionally, extents of 40 to 60% hydroxylation are found to render the polymer soluble in polar solvents like acetone/water, methanol, and DMSO.[144] Complete hydroxylation of poly(hydroxy-undecenoate) homopolyesters can be carried out with 9-borobicyclononane by hydroxylation-oxidation methods.[122]

Besides hydroxylation of double-bonds, $KMnO_4$ in the presence of $NaHCO_3$ or crown ether can also be used for further oxidization to yield carboxy functionalities.[145] Using osmium tetroxide and oxone (a mixture of $KHSO_5$, K_2SO_4, and $KHSO_4$), the double-bonds of PHOU can be converted completely with little influence on the polymer backbone.[146]

3.3.2.3. Crosslinking of PHAs

As stated in chapter 3.3.2, crosslinking is a key strategy for improving a polymer's mechanical, physical, and chemical properties. Given the versatile nature of polymer crosslinking and the possibility of creating new materials with superior properties compared to the native polymer, it is not surprising that extensive research has been conducted in this specific field of macromolecular chemistry.[147]

The idea of crosslinking is the formation of linkages between polymer chains generating a polymer network. Based on the kind of reaction taking place and the resulting interaction between the polymer chains, crosslinking can be divided into three different types:[147]

- Covalent crosslinking where the polymer chains are covalently bound to the crosslinker and/or each other. Covalent crosslinks are believed to be the most stable ones.
- Ionic bonds between the polymer chains.
- Physical crosslinking based on physical interactions between the polymer chains such as Van der Waals-, hydrogen bond-, or ionic interactions.

Covalent crosslinking can be achieved by various methods, either by addition of multifunctional crosslinking agents or by reacting pendant groups present in the polymer chains. Additionally, the introduction of negative charges or macroradical functionalities in the polymer matrix can lead to polymer network formation.[148;149]
Crosslinking of unsaturated mcl-PHAs like PHOU can be carried out by the reaction of double-bonds either by means of ionizing irradiation or chemically with peroxides and multifunctional crosslinking agents.[150] PHOU can also be crosslinked with sulfur-based vulcanization methods.[151] PHA films containing unsaturated side-coppolchains have also been found to be thermally crosslinkable or by UV-irradiation in the presence of benzophenone, peroxides, and/or ethylene glycol dimethacrylate.[122] Using electron-beam crosslinking, Koning et al. prepared a biodegradable rubber from unsaturated mcl-PHAs.[152]
Radiation crosslinking using UV-, electron-, or gamma-irradiation offers an efficient and easily accessible method for crosslinking polymers with unsaturated groups without potential contamination by side-products of chemical crosslinking agents.[153] When using high energy radiation, one has to keep in mind that besides crosslinking reactions, polymer degradation can occur at the same time. The ratio between polymer degradation and crosslinking is dependent on the chemical composition and the radiation dose applied.
Bergmann et al. investigated the effects of electron beam treatment of molten PHB. It was found that the molecular weights and melting temperatures decreased with an increasing radiation dose, indicative of predominant chain scission reactions taking

place. A significant influence of different crystallization stages of PHB on the behavior was observed and the authors concluded that amorphous regions were more susceptible to crosslinking while the crystalline regions were mainly degraded by irradiation. Consequently, electron-beam treatment of molten amorphous PHB can offer significant improvement of the material's properties by the introduction of crosslinks and retardation of crystallization.[154]

Despite the numerous above described crosslinking reactions of unsaturated mcl-PHAs, literature reports on crosslinking non-functionalized saturated scl-PHAs are scarce. The reason for this fact is the chemical inertness of these compounds as well as their high crystallinities which render them susceptible to degradation (thermal or radiation-induced) rather than crosslinking.

For crosslinking chemically inert compounds, highly reactive compounds have to be used. The application of azides has been shown to be quite effective in the course of polymer crosslinking.[155] Besides crosslinking, azides are widely used for click reactions, offering the possibility of reacting small molecules selectively and in high yields.[156]

The crosslinking ability of bisazides is based on the fact that the azide group is labile and can release nitrogen under thermal stress leading to the formation of very reactive nitrenes that can subsequently react with saturated and unsaturated polymer backbones. Nitrenes are electron-deficient compounds containing a nitrogen atom with six valence electrons, which can be seen as nitrogen analogues of carbenes.

Given at least two functionalities, bisazides have the ability to provide crosslinking according to two different mechanisms that have been proposed in literature. As example, a fully conjugated bisazide, namely 2,6-bis(4-azidobenzylidene)-4-methylcyclohexanone is considered:

- After decomposition of the azide groups, nitrene-derivatives of 2,6-bis(4-azidobenzylidene)-4-methylcyclohexanone abstract protons from the polymer backbone yielding 2,6-bis(4-aminobenzylidene)-4-methylcyclohexanone and negatively charged carbon atoms in the polymer chains. Crosslinking subsequently occurs by recombination of the polyester chains (Scheme 3-6 and Scheme 3-7).
- 2,6-bis(4-azidobenzylidene)-4-methylcyclohexanone itself can act as crosslinker; consequently, the nitrenes formed by activation via UV-light or

thermal decomposition are inserted in C-H bonds of the polymer matrix and, due to the bifunctionality, crosslink the polymer chains. In this case, the crosslinker would be present in the form of its amino-derivative in the gel fraction only (Scheme 3-8).[157]

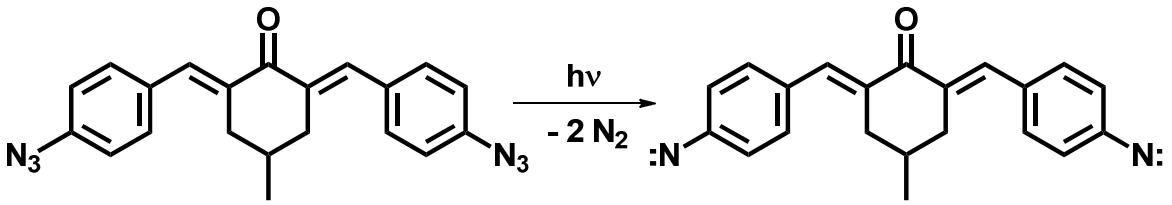

Scheme 3-6: Decomposition of the bisazide 2,6-bis(4-azidobenzylidene)-4-methylcyclohexanone into nitrenes and nitrogen.

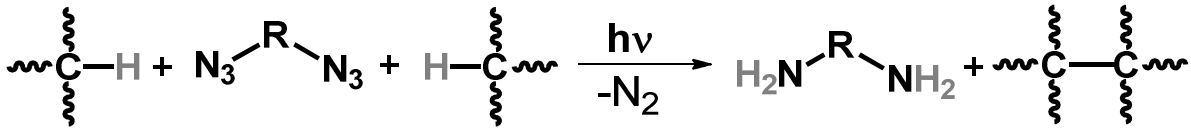

Scheme 3-7: Schematic representation of the proton abstraction and subsequent recombination of the polymer chains for the reaction of bisazides with a polymer matrix.

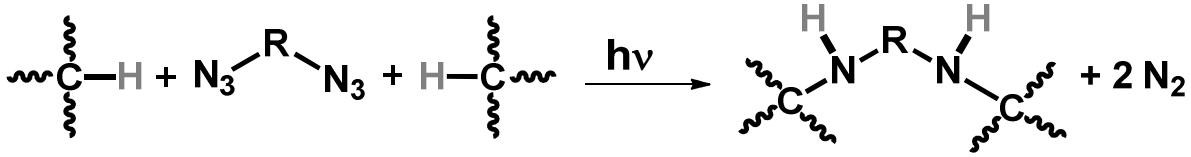

Scheme 3-8: Schematic representation of the insertion of a bisazide into a polymer matrix.

So far, bisazides have not been used for crosslinking reactions involving poly(hydroxyalkanoate)s, but given the high reactivity of these compounds, crosslinking of saturated aliphatic scl-PHAs is very likely to be feasible.

3.3.3 Modification of Polymer Surfaces

When polymer-based materials are used for medical applications, surface manipulation plays an important role for the biocompatibility and the resorption behavior of the resulting materials. Two basic parameters are widely considered as the most influential ones, namely the surface hydrophilicity and the surface roughness. The surface hydrophilicity is believed to be responsible for protein absorption, cell adhesion, and overall biocompatibility while the surface roughness' influence on tissue response appears to be more complex.[158] Nevertheless, the scientific community has agreed on the surface roughness being of significant importance for medical applications, especially for orthopedic surgery, where surface roughness in the range of 1.5 µm are considered to have positive influence on bone integration.[159]

3.3.3.1. Plasma Techniques

Plasma techniques have been widely accepted and applied for surface modifications of metals, semiconductors, and polymers for various purposes. While semiconductors are frequently pre-cleaned by plasma etching, the use of plasma is wide-spread for modification of metal and polymer-based surfaces for potential applications in medicine. The main advantages of plasma techniques are the easy accessibility, short reaction times, and significant changes in the surface characteristics with no or negligible reactions taking place in the bulk material.[160;161]

Generally, two different types of plasma modification are known: Modification by non-reactive gas plasma like nitrogen plasma physically changes the surface in a manner similar to surface blasting methods but does not induce any surface changes in the chemical way while reactive gas plasmas like oxygen- (O_2-) and NH_3-plasmas induce chemical reactions on the treated surface. O_2-plasma introduces mainly hydroxy and carboxylate-functionalities by surface oxidization and NH_3-plasmas yield, among others, amine groups on the surface. Argon-plasmas typically introduce free radicals.[161]

Using N_2- or O_2-plasma, both, the roughness and the surface energy of hydrophobic polymers in general and of polyesters in particular can be increased. When PLLA or

PHB-HV surfaces are treated with oxygen and nitrogen-plasma, significant changes in the surface topology can be observed. O_2-plasma yields more hydrophilic surfaces, indicative of polar groups present on the surface. The increase in the surface energy of nitrogen-plasma treated PHB-HV and PLLA samples is attributed to the changes in the surface topology (Figure 3-7).[162]

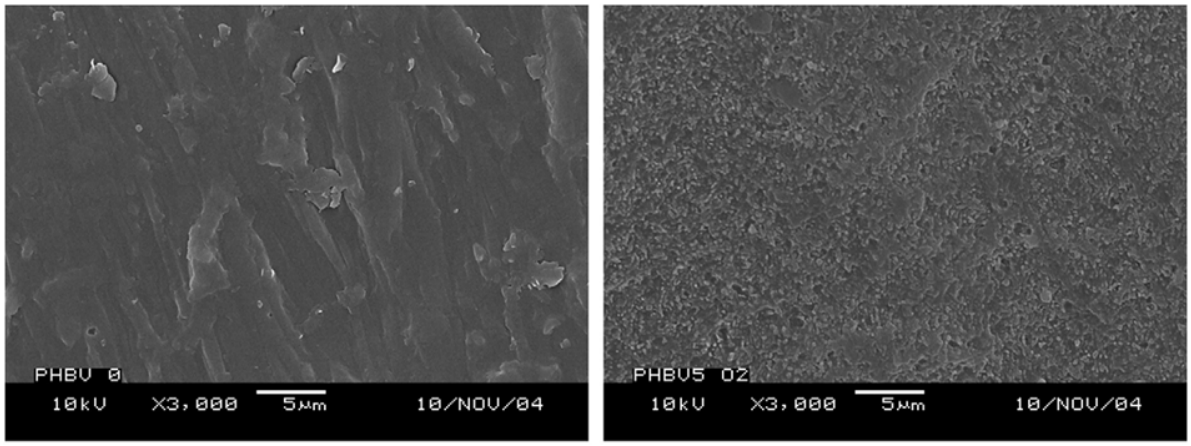

Figure 3-7: Surface topologies of native (left) and O_2-plasma treated PHB-HV samples (right).

3.4 Methods of Analysis

3.4.1 Charlesby-Pinner Analysis

For a deeper understanding of crosslinking reactions in general, one has to be aware of the fact that crosslinking reactions never occur exclusively, but are always accompanied by chain scission reactions challenging the whole crosslinking process. In order to analyze crosslinking processes, Charlesby and Pinner[163] introduced a linearization method for gel curves by assuming that the probability of chain scission and crosslinking are constant for all monomer units and independent of each other and derived the following equation:[164]

$$s + \sqrt{s} = \frac{p}{q} + \frac{1}{P_n^0 \cdot q} \qquad \textbf{Equation 3-3}$$

where s represents the soluble fraction of a polymer left in the polymer network (assumed to be the non-crosslinked part of the polymer), q is the crosslinking density (the relative number of crosslinked monomer units in relation to all monomer units), p is the chain scission density (analogous to the crosslinking density), and P_n^0 is the average polymerization degree.
When both, the rate of chain scission and the rate of crosslinking are constant, for example $q = v_q \cdot t$ and $p = v_p \cdot t$, equation 3-3 can be transformed to:

$$s + \sqrt{s} = \frac{v_p}{v_q} + \frac{1}{v_q \cdot P_n^0} \cdot \frac{1}{t} \qquad \textbf{Equation 3-4}$$

For the range in which this assumption is valid (generally the range before the maximum crosslinking degree is reached), the term $s + \sqrt{s}$ plotted against the reciprocal irradiation time should give linear correlation, the so-called Charlesby-Pinner plot. From the Charlesby-Pinner plot, the ratio between the rate of crosslinking and the range of chain scission can be determined from the y-axis intercept while v_q itself can be derived from the slope.

3.4.2 Surface Characterization of Polymer Surfaces

For applications of polymers in medicine the surface topology and state is of crucial importance for the biocompatibility as well as the degradation characteristics. The methods described in this chapter are useful for the determination of surface roughness parameters and surface energy of polymers.

3.4.2.1. Surface Metrology-Focus Variation Microscopy

Driven by tremendously increased computational power in the past years, 3D measurements and reconstruction of measured 3D surfaces have gained considerable importance. Facilitated by the newest trends in surface characterization where a strong shift from tactile profilometry towards destruction-free measurements

of areas rather than profiles has taken place, this new characterization method has been established in a wide range of technical and research-related applications.[165;166] The main advantages of non-contact methods over tactile methods are the non-destructivity and the possibility of measuring areas instead of profiles. Additionally, 3-dimensional surfaces (round molds, screws) can be characterized and flattened by computational means and provide much more accurate and faster determination of the surface topology.

The principle of focus variation microscopy is based on a conventional light microscope equipped with a precision optical system comprising various lens systems. Light emerging from the in-built light source is inserted in the system's optical path and concentrated on the specimen surface. Light reaching the surface is scattered in all directions in dependence of the surface topology. Light rays scattered from the surface are subsequently bundled by the optical system and collected by a light sensitive sensor. Because of the small field depth only surface areas of the same height are displayed sharply. In order to acquire picture information of the entire sample, the optical system is vertically moved, while simultaneously the optical data are collected. Using the measurement system depicted in Figure 3-8, vertical resolutions of as low as 10 nm can be obtained while the vertical scan range depends on the objective used and varies from 3.2 to 22 mm.

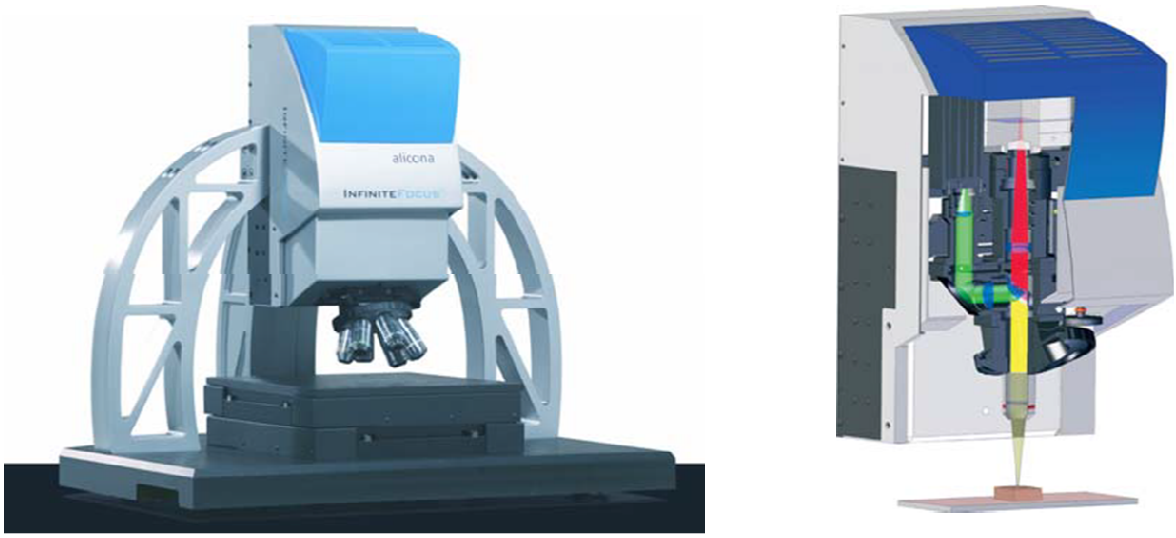

Figure 3-8: Alicona Infinite Focus measurement system IFM G4 (left) and schematic representation of the working principle of focus variation measurement (right).[165]

3.4.2.2. Contact Angles and Surface Energy

As stated before, the wetting characteristics and the surface energy derived thereof are of crucial importance for many applications including medical applications of polymer-based materials. The physical phenomenon of wetting is based on the interaction between a liquid and the surface of a solid phase on the molecular level. The contact angle is formed at the triple point solid/liquid/vapor offering experimental determination of the wetting characteristics of a certain liquid on the solid phase surface. The formation of a certain contact angle is dependent on the interfacial tensions σ_{sv} (solid-vapor), σ_{sl} (solid-liquid), and σ_{lv} (liquid-vapor). The mathematical correlation between the contact angle and the interfacial tensions can be described using the Young's relation for ideal, smooth, inert, homogeneous, and non-deformable surfaces:[167]

$$\sigma_{sv} = \sigma_{sl} + \sigma_{lv} \cdot \cos\Theta_Y \qquad \textbf{Equation 3-5}$$

With Θ being the contact angle, this correlation is schematically represented in Figure 3-9.

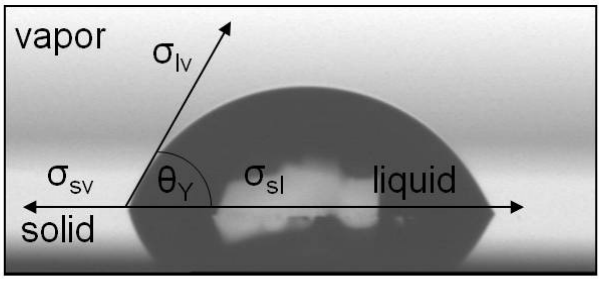

Figure 3-9: Schematic representation of the Young's relation.[168]

Due to the shortcomings in contact angle determination arising from the use of the Young's relation, Wenzel,[169] Cassie and Baxter[170;171] modified this fundamental equation in order to be able to consider surface roughness and inhomogeneities. Given the inaccessibility of the surface tension, a new parameter called wetting tension σ^b is defined by the following relation:

$$\sigma^b = \sigma_{sv} - \sigma_{sl} = \sigma_{lv} \cdot \cos\Theta \qquad \textbf{Equation 3-6}$$

The introduction of the wetting tension allows for the quantitative determination of the difference in the surface tension by contact angle measurements.

Based on equation 3-6, the wetting tension can be numerically positive or negative and the wetting of a solid state is defined by:

- Complete wetting: $\Theta = 0$;
- Wetting: $\Theta < 90°$; the value for the wetting tension is positive, the surface is wetted by the liquid;
- Partial wetting: $\Theta > 90°$; the value for the wetting tension is negative; the surface is not or only partially wetted by the liquid;
- Zero wetting: $\Theta = 180°$;

From the contact angles, the surface energy can be calculated according to the following methods:

- The method according to Owens, Wendt, Rabel and Kaelble enables for the determination of the disperse and the polar part of the surface energy in one single step and can be used for surfaces with a surface energy of up to 35 $mN \cdot m^{-1}$.[172-175]
- The model according to Fowkes can be used for sequential determination of the disperse and the polar part of the surface energy in apolar systems.
- The model following Wu is useful for the determination of the disperse and the polar part of the surface energy of low-energy surfaces (<35 $mN \cdot m^{-1}$).[175;176]
- Employing the method according to Schultz, the surface energy of high energy surfaces can be determined.[177;178]
- The model according to van Oss allows differentiation between Lifschitz-van-der-Waals and acid-base-interactions.[175;179]

Using the method according to Owens, Wendt, Rabel and Kaelble, the surface energy can be split into two parts based on the molecular interactions. Consequently, the surface energy consists additively of a polar part σ^{polar} and a disperse part σ^{disp} corresponding to:

$$\sigma = \sigma^{disp} + \sigma^{pol} \qquad \textbf{Equation 3-7}$$

While the polar part is used for subsuming contributions of polar interactions like dipol-dipol-interactions and hydrogen bridge bonds, the disperse interaction is determined by London forces (induced dipol interactions).

By determination of the geometric mean value, the interfacial tension σ_{sl} can be calculated from the contribution of the solid and the liquid phase according to:

$$\sigma_{sl} = \sigma_s + \sigma_l - 2 \cdot \sqrt{\sigma_s^{disp} \cdot \sigma_l^{disp}} - \sqrt{\sigma_s^{pol} \cdot \sigma_l^{pol}} \qquad \textbf{Equation 3-8}$$

By transformation of equation 3-5 and combination with equation 3-8, the following relation is formed:

$$\underbrace{\frac{(1+\cos\Theta)\cdot\sigma_l}{2\cdot\sqrt{\sigma_l^{disp}}}}_{y} = \underbrace{\sqrt{\sigma_s^{pol}}}_{m} \cdot \underbrace{\sqrt{\frac{\sigma_l^{pol}}{\sigma_l^{disp}}}}_{x} + \underbrace{\sqrt{\sigma_s^{disp}}}_{b} \qquad \textbf{Equation 3-9}$$

Equation 3-9 can be plotted linearly by contact angle measurements of liquids with known polar and disperse part and the polar and disperse surface energy part of the surface can consequently be determined from the slope m and the y-axis intercept b.

3.4.3 Mechanical Polymer Characterization

Tensile testing is considered as a quasi-static testing method in which breakage of a testing specimen or a defined stress capacity (stress or strain) are reached within a defined time range. The application of tensile stress must be carried out slowly and shock-free and the increase in load has to be continuous until specimen breakage.

The resulting elongation $\Delta L = L\text{-}L_0$ of the test specimen is correlated with the base length L_0 and is referred to as strain ε in %:[180]

$$\varepsilon[\%] = \frac{\Delta L}{L_0} \cdot 100 \qquad \textbf{Equation 3-10}$$

According to the DIN EN ISO 527 standard, the following material characteristics can be derived from tensile testing:[202;203]

- The tensile strength σ_M can be determined from the cross sectional area related to the maximum force F_{max} that can be carried by the testing specimen:

$$\sigma_M = \frac{F_{\max}}{A_0} \qquad \textbf{Equation 3-11}$$

- The tensile strain ε_M is based on the elongation of the testing specimen at the tensile strength σ_M:

$$\varepsilon_M[\%] = \frac{\Delta L_{0M}}{L_0} \cdot 100 \qquad \textbf{Equation 3-12}$$

- The strain at break ε_B is the elongation of the testing specimen at the breaking point:

$$\varepsilon_B[\%] = \frac{\Delta L_{0B}}{L_0} \cdot 100 \qquad \textbf{Equation 3-13}$$

The elongation at break and the tensile strength are reciprocally related to each other. Consequently, test specimens with high tensile strength show low elongation at break.[181]

- The Young's modulus (elastic modulus) of plastics at uniaxial load is equal to the proportionality constant in the Hook's law by which the relation between stress σ and strain ε is described as:

$$\sigma = E \cdot \varepsilon$$ **Equation 3-14**

- The Young's modulus is determined in the elastic and linear-viscoelastic deformation range from 0.05 to 0.25% of the stress-strain plot:

$$E = \frac{\sigma_2 - \sigma_1}{\varepsilon_2 - \varepsilon_1}$$ **Equation 3-15**

When computational-assisted evaluation is used, the Young's modulus can also be determined by evaluation of the slope in the stress-strain diagram in the linear range of plastic deformation.

4 Results and Discussion

4.1 PHB Composite Materials

Depending on the targeted properties, polymers can not only be processed and used in their native, pure form, but can also be mixed with other polymers, nucleating agents, plasticizers, and other additives. In this part of the presented work, two main approaches were followed with respect to the aim of producing materials with higher strength on the one hand, and potentially increased degradation rate and biocompatibility on the other hand:

- Mixing of PHB with the bone substitution material Herafill and zirconium oxide (ZrO_2) in order to increase the biocompatibility, resorption rate, and X-ray visibility.
- Mixing of PHB with magnesium powder in order to yield a material with higher stiffness and strength compared to the native polymer.

In order to provide optimum mixing and perfectly shaped shoulder test bars, all polymer composites were produced by mixing the components in a twin screw compounder and subsequent injection molding. For every mixture, the parameters for compounding and injection molding were optimized prior to the production of shoulder test bars.

4.1.1 PHB/Herafill/ZrO_2 Composites

For the production of PHB/Herafill/ZrO_2 composites, the three components were mixed in the compounder and injection molded into a shoulder test bar mold. Three different contents of ZrO_2 and Herafill were tested, namely 3 wt.-% ZrO_2, 3 wt.-% ZrO_2 with 10 wt.-% Herafill, and 3 wt.-% ZrO_2 with 30 wt.-% Herafill (composites I-III). As reference, native commercial grade PHB samples were used.
The resulting test bars were characterized by tensile testing. Indicated by optical inspection and the results obtained by tensile testing, the miscibility of the components was sufficient for the preparation of homogeneous composites. Figure 4-1 shows the

composites' Young's moduli and tensile strength in comparison to the native PHB reference. As it can be seen in the changes in the moduli, the addition of ZrO_2 has a negative influence on the mechanical strength of PHB, whereas the addition of Herafill yields composites with slightly higher resistance towards plastic deformation. This observation is also supported by the tensile strength measurements, which show a significant drop in the mechanical stability for all composites and reach a plateau with approx. 30% loss in tensile strength.

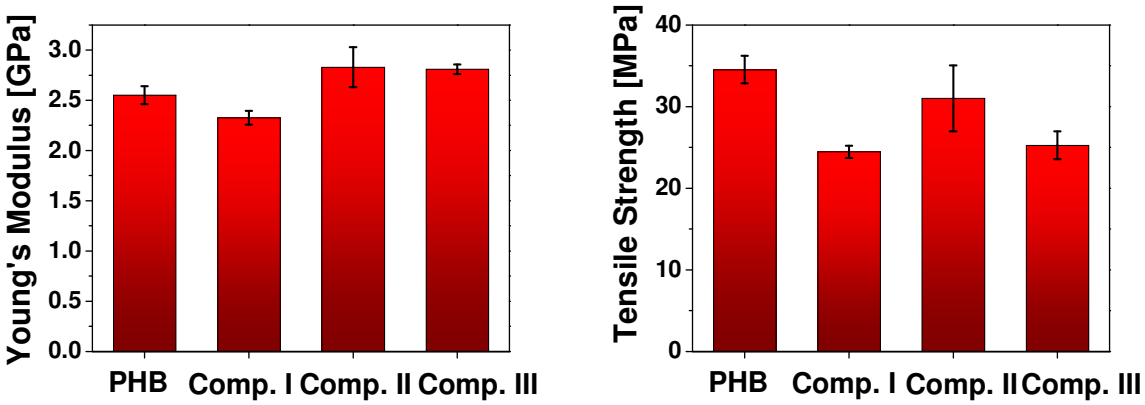

Figure 4-1: Young's modulus (left) and tensile strength (right) for PHB and composites of PHB with ZrO_2 and Herafill.

Additionally, the strain at break of all composites (Table 4-1) is reduced by a factor of 6 compared to the ductile native PHB reference resulting in materials that show brittle fracture behavior rather than plastic deformation. Supported by the fact that polymeric materials with higher crystallinity show higher stiffness and lower elongation at break than less crystalline materials, composite III reveals slightly higher values for the modulus and the tensile strength.[182;183] Moreover, it can be stated that Herafill, used in an amount of 10 wt.-%, can act as a nucleating agent for PHB. The nucleation ability of Herafill is based on calcium carbonate being the main ingredient of the bone substitution material and, besides talcum, is frequently used as nucleating agent for semi-crystalline polymers like linear polyethylene and polypropylene.[184;185]

Table 4-1: Elongation at break and crystallinity of native PHB and composites with ZrO_2 and Herafill.

Composite	Material	Elongation at break [%]	Crystallinity of PHB [%]
	PHB native	19.5 ± 3.3	52.1
I	PHB + 3% ZrO_2	2.8 ± 0.2	43.3
II	PHB + 3% ZrO_2 + 10% Herafill	2.9 ± 0.2	68.0
III	PHB + 3% ZrO_2 + 30% Herafill	2.4 ± 0.1	47.5

Overall, the results of the composites' mechanical testing show no significant improvement in terms of mechanical stability, although the addition of Herafill without ZrO_2 can bring some improvement for the Young's modulus.

4.1.2 PHB/Magnesium Powder Composites

Following the same routine as before, composites of PHB and magnesium powder (44 µm particle size) were prepared by melt-compounding and injection molding. Different amounts of Mg powder ranging from 10 to 50 wt.-% with respect to the polymer mass were used and all resulting shoulder test bars were subjected to mechanical characterization by means of tensile testing. During processing, the magnesium powder was added stepwise in order to prevent clogging of the compounder. For keeping the incorporation of air-bubbles in the molten mixture at minimum, the mixing time was reduced from two to one minute for 30-50 wt.-% Mg; higher amounts of magnesium could not be properly processed. The composites' Young's moduli and values for the tensile strength are summarized in Figure 4-2 which shows the correlation between the changes in the mechanical properties and the amount of Mg powder added to the polymer. According to the correlation chart, the addition of magnesium has a positive impact on the elastic modulus of the resulting composite materials. Starting at around 3 GPa for the PHB reference, the Young's modulus slightly increases continuously with increasing Mg content and reaches a maximum of over 4 GPa with 50 wt.-% Mg. In contrast to these findings, the tensile strength is not positively affected by magnesium. While the mean values of the tensile

strength only slightly decrease with increasing Mg content, the higher error bars indicate lower strength and significantly decreased reproducibility.

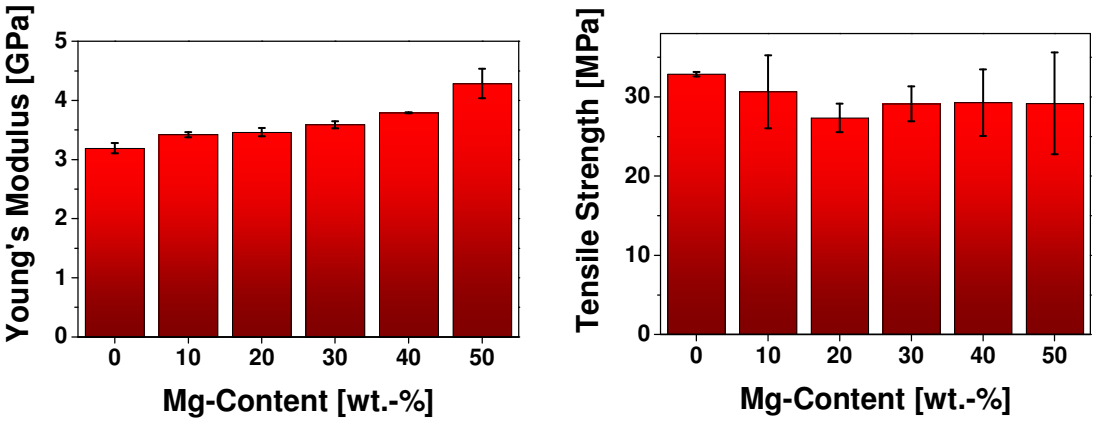

Figure 4-2: Young's Modulus (left) and tensile strength (right) of PHB/Mg powder composites.

Another issue related to the production of PHB/metal powder composites is the change from ductile to semi-brittle fracture behavior. The representative stress-strain curves and the summarized averaged values for the elongation at break to support this claim are shown in Figure 4-3. While the native PHB reference breaks at almost 3% strain, the elongation decreases continuously with increasing Mg content and reaches the lowest values of less than 1% with 50 wt.-% Mg. This fracture behavior can be attributed to the fact that the interaction between the polymer and the metal reinforcement can be described as dispersed metal particles in a polymer matrix.

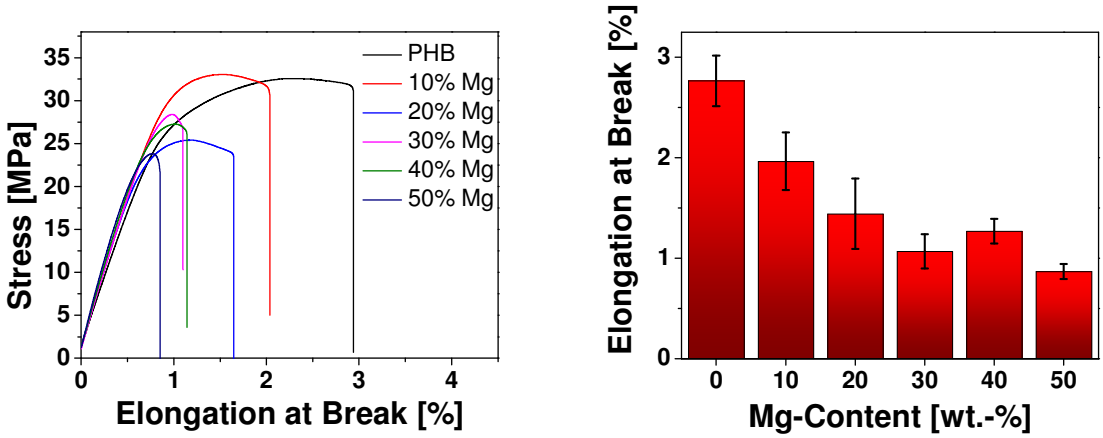

Figure 4-3: Representative stress-strain curves (left) and averaged elongation at break values vs. Mg content (right) for PHB and PHB/Mg composite materials.

The impact of this effect on the macroscopic observations can be explained by the micro-mechanistic model proposed by Gaymans et al. (Scheme 4-1).[184;186]

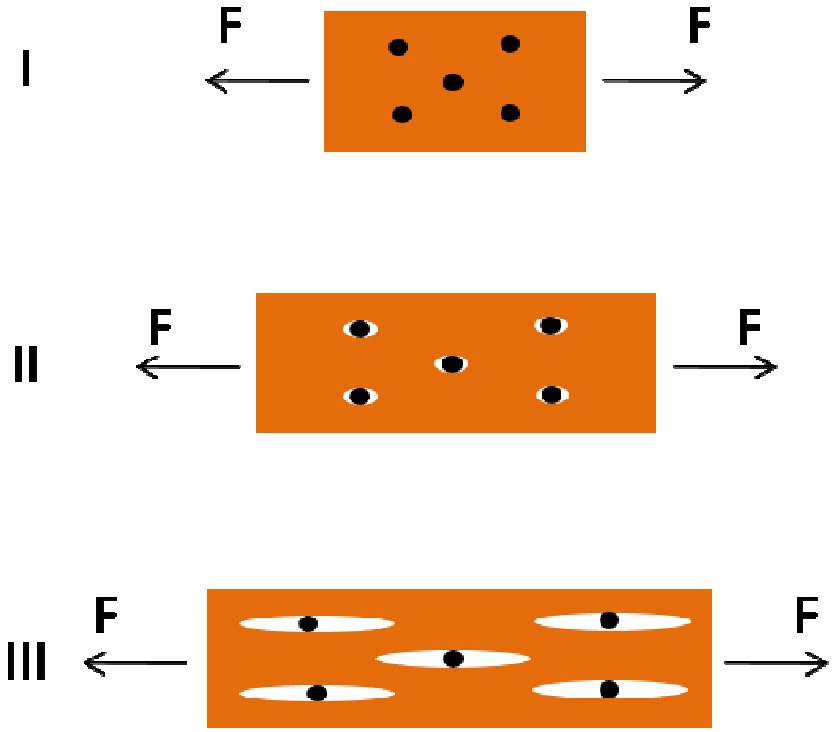

Scheme 4-1: Micro-mechanistic model for the fracture behavior of polymers reinforced with rigid filler particles.[184]

The mechanism depicted in Scheme 4-1 consists of three stages:[184]

I. Stress concentration: Because of their different elastic properties, the rigid filler particles can act as stress concentrators.
II. Debonding: Followed by stress concentration, triaxial stress is built up around the filler particles leading to debonding at the polymer-filler interface.
III. Shear yielding: The stress state in the polymer matrix is altered by the cavities produced by debonding, reducing the sensitivity towards crazing by release of volume strain. After shear yielding takes effect, the material can absorb high amounts of energy upon fracture.

Although hard and brittle metal particles can help to increase the elastic modulus and the tensile strength of a polymer, the shape of the particles plays a tremendously important role for the mechanical characteristics and the fracture behavior: The

magnesium particles used in this study were of a ball-like shape, providing little surface area for interaction between the metal and the polymer matrix. For optimum interaction, and, accompanied with that, more pronounced improvement of the composites' mechanical stability, the metal particles should be span- or rod-like, have a size of under 5 µm, and should be used in such amounts that particle agglomeration can be excluded. Potential agglomeration, non-optimum particle size and shape are the main contributors to the drop in tensile strength and the loss in reproducibility, especially with higher magnesium content.

Putting these findings together, the potential of metal reinforcement of PHB with magnesium powder has been shown, but optimization of particle size and shape is necessary in order to reveal the full potential of this strategy.

4.2 Polymer-Based Coatings on Metal Surfaces

Besides polymeric materials, metal-based devices have gained considerable attention in the field of bioresorbable materials in orthopedic surgery. Magnesium alloys are amongst the most promising candidates of degradable metals. A major drawback of these alloys is the severe hydrogen gas release upon degradation and the rapid degradation rate that eventually leaves the respective site of implantation unsupported.[13-15] Therefore, polymer-based coatings of magnesium implants have been proposed in order to improve biocompatibility and controllability of the resorption rate. In the present work, polymer coatings based on PHB, PHB/TBA, and PDLLA were applied on magnesium-based implants. Prior to the coating of implants, scratch resistance tests were carried out in order to characterize the adhesion of polymer coatings on metal surfaces. The coating procedure of magnesium alloy pins was done by dipping the pins in a solution of the dedicated polymer in DCM and subsequent drying. The amount of coating deposited on the metallic implant was measured gravimetrically. Polymer coatings on the flat copper coated FR4 substrates were prepared by spin coating solutions of the respective polymer on the FR4 plates.

4.2.1 Scratch Resistance Tests of PHB, PHB/TBA, PHB-HV, and PHB-HV/TBA coatings

In order to get an idea about the adhesion between the polymer coating and the metal surface, coatings of PHB, PHB thermally crosslinked with 10 wt.-% tri(ethylene glycol) bis(azidoformate) (TBA), PHB-HV, and PHB-HV crosslinked with 10 wt.-% TBA were applied on copper-coated FR4 polymer-resin plates. The scratch resistance tests were carried out using a CETR UMT2 Microtribometer equipped with a diamond stylus with a tip radius of 5 µm applying a maximum normal force of 3 N; for evaluation, the ASTM G 171-3 standard for scratch hardness was considered. The scratch width and the coefficient of friction were correlated with the normal force applied on the coating (Figure 4-4).

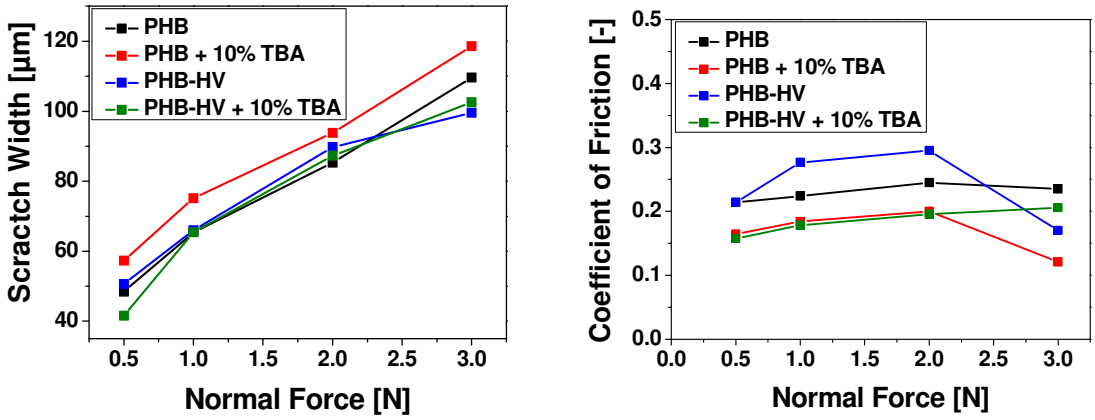

Figure 4-4: Scratch width (left) and coefficient of friction (right) for polymer coatings on metal substrates.

As expected, the scratch width for all polymer coatings increased with higher normal forces, representing deeper penetration of the diamond stylus into the polymer surface. Shown by the coefficient of friction, it becomes clear that not all coatings can withstand the maximum normal force of 3 N. Indicated by a further increase in the coefficient of friction at forces higher than 2 N, coatings consisting of native PHB and PHB-HV crosslinked with 10 wt.-% TBA stay adhered on the copper surface. The drop in the coefficient of friction for crosslinked PHB and native PHB-HV strongly suggests adhesion failures upon forces higher than 2 N. Interestingly, crosslinking of PHB with TBA decreases the maximum force before breakage compared to the native polymer

coating whereas crosslinking of PHB-HV yields coatings with a higher scratch resistance than native PHB-HV. For a deeper understanding of this observation, two facts have to be considered: Firstly, an amount of 10 wt.-% of TBA only yields very low gel fractions of less than 5% with PHB, while PHB-HV with 10 wt.-% of TBA reveals an extent of crosslinking of 20% (see chapter 4.4). Hence, in the case of PHB, the insufficient amount of TBA yielded coatings with lower scratch resistance than the native polymer, most likely due to chain scission occurring as a side reaction of crosslinking polymers with bisazides (see chapter 4.3.2). Secondly, the scratch resistance is not only dependent on the kind of the polymer used as a coating, for the adhesion is majorly influenced by the interaction between the coating and the substrate. This is why adhesive failures occur due to poor interaction between the coating and the substrate, rather than to the mechanical characteristics of the coating itself.

4.2.2 Coating of Mg-Based Fracture Fixation Implants with PHB, PHB/TBA, and PDLLA

Preceded by the preliminary studies concerning the adhesion between polymer coating and metal surface, Mg-LV1-pins were coated by dipping in solutions of PHB, PHB/TBA, and PDLLA in chloroform. In order to provide improved interaction between polymer and metal, the surface of the Mg-pins was roughened prior to coating by immersion in an aqueous HCl solution at pH = 2 for 2 h. From in-vitro degradation tests of PHB performed by Martin Koller at the Institute of Biotechnology and Biochemical Engineering at the Graz University of Technology, a coating mass of approx. 0.4 mg polymer was estimated to be sufficient to retard in-vivo Mg degradation for two months. Consequently, the dip-coating process was repeated until the targeted mass of 0.4 mg per pin was reached. After coating, the coatings' surface roughness was determined by focus variation microscopy (VFM). The microscopic pictures and the surface profiles derived thereof are shown in Figure 4-5. Compared to the pretreated Mg pin (a) and the other polymers (c, d), the visual appearance of polymer coatings prepared from PHB (b) is different. The PHB surface shows fine bubbles dispersed in the polymer coating. This can be attributed to the higher viscosity of the PHB solution compared to PDLLA and PHB/TBA solutions, which

leaves less mobility for bubbles of the evaporating solvent diffusing from the polymer layer. The polymers PLDLA and PHB/TBA yielded clear and translucent coatings. The profiles, on the other hand, show different distributions around the mean value of the surface. Generally, the roughness of the coated samples appears to be higher.

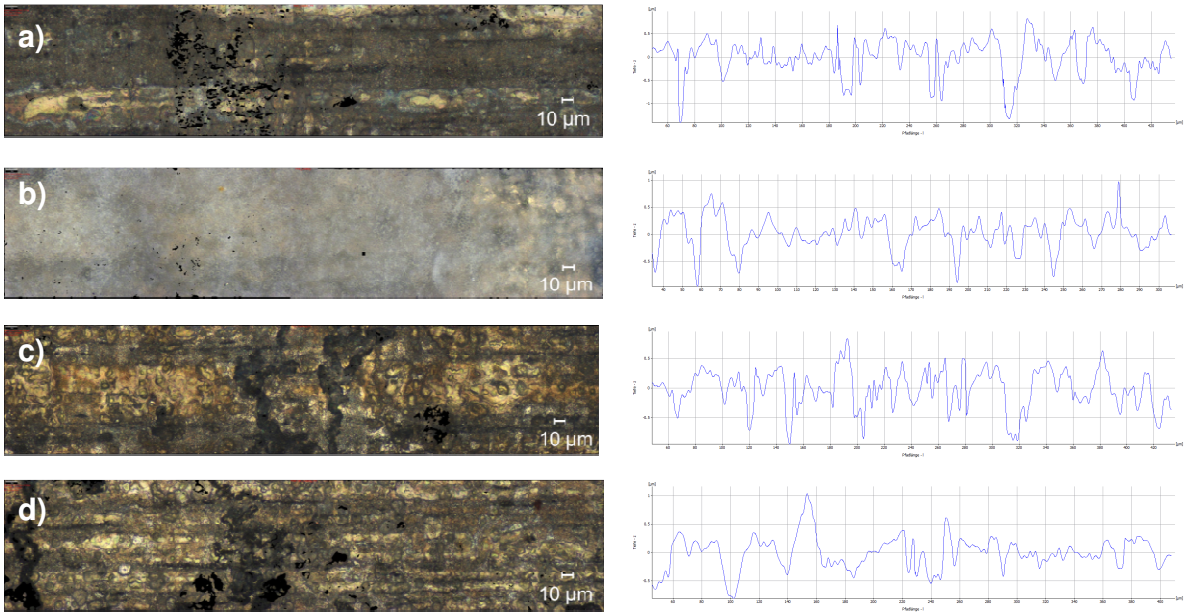

Figure 4-5: FVM pictures (left) and surface profiles (right) of native Mg (a), Mg coated with native PHB (b), Mg coated with PLDLA (c), and Mg coated with PHB/TBA (d).

This assumption was validated by the calculation of the surface roughness parameters R_q, which are shown in Figure 4-6 for comparison of the untreated Mg pin surface with the polymer coated surfaces.

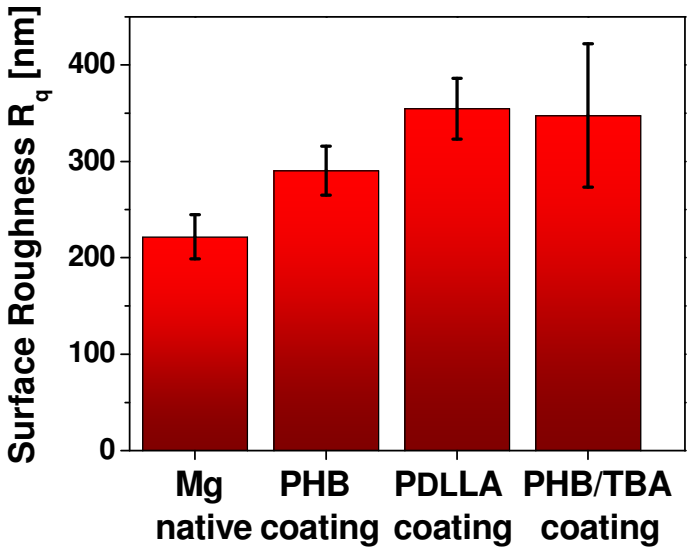

Figure 4-6: Comparison of the surface roughness R_q for native Mg and polymer coated Mg surfaces.

Starting at R_q-values of approx. 200 nm, the mean values for R_q of the native magnesium surface and the polymer coatings increase in the order: Mg native < native PHB coating < PDLLA coating ≈ PHB/TBA coating and reach maximum values of around 350 nm. Notably, the standard deviation of PHB/TBA coatings is significantly higher, indicative of a less ordered surface structure yielded by the crosslinking and/or the heating process. The coating masses reached were in good correlation with the targeted amount of coating per pin and are summarized in Table 4-2.

Table 4-2: Masses of polymer coatings applied on Mg pins.

Coating	Average Mass [mg]	STD [mg]
PHB	0.363	0.033
PDLLA	0.379	0.055
PHB/TBA	0.370	0.033

Supported by the results of the scratch resistance tests, the surface roughness measurements, and the achieved weight distributions of the coating masses, this coating procedure can be used for the production of polymer coated metal surfaces with satisfactory stability and uniformity.

4.3 UV-induced Crosslinking of PHB-HV and PHB

As described in chapter 3.3.2.3, UV-crosslinking of polymers is a versatile and easily accessible method for the fine-tuning of a polymer's mechanical, physical, and chemical characteristics. Due to the known low reactivity of saturated polyesters, a fully conjugated bisazide, namely 2,6-bis(4-azidobenzylidene)-4-methylcyclohexanone (BA) was chosen as a model compound for bisazide-based crosslinking of PHB-HV.[187] Using bisazides as crosslinking agents, the reactive species can be formed in-situ by UV-irradiation or thermal decomposition. The reactive species, so-called nitrenes, can insert into C-H-bonds of the polymer matrix and, due to the bifunctionality of the starting compound, can yield crosslinked polymer networks. In this part of the present work, the crosslinking ability of BA was evaluated by sol-gel-analyses and the mechanism as well as the reproducibility were studied by means of ^{1}H-NMR-, gel permeation chromatography (GPC), and Charlesby-Pinner analyses. Additionally, the proposed insertion-mechanism was verified and the potential application of the PHB-HV/BA system as biodegradable photoresist in a photolithographic process was evaluated. Finally, the proof of concept for crosslinking PHB with BA employing the same process was brought forward.

4.3.1 Sol-gel Analysis

The sol-gel analysis is a well-known and accepted method to quantify network formation between a polymer matrix and a crosslinking agent. In the present work, the crosslinking procedure was done by mixing PHB-HV solutions in chloroform with BA in different amounts ranging from 1 to 5 wt.-% of BA with respect to polymer mass. The resulting solutions were spin-coated on CaF_2-plates to yield thin films with a few µm in height. These films were individually irradiated with UV-light under nitrogen for different time intervals ranging from 0 to 180 s. In order to dissolve the soluble, non-crosslinked part of the polymer, the irradiated samples were developed by immersion in DCM. Via FT-IR spectroscopy, the decomposition of the bisazide-crosslinker could be monitored by the disappearance of the peak at 2115 cm^{-1}, representing the N=N=N-stretching vibration (Figure 4-7).

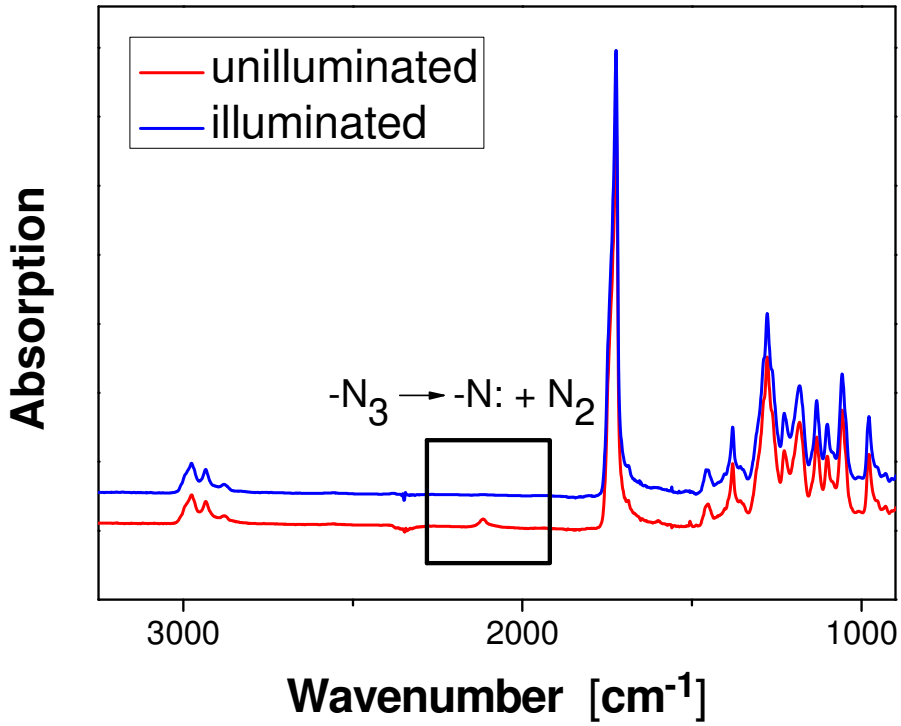

Figure 4-7: FT-IR spectra of PHB-HV/BA-samples before (red) and after (blue) UV-irradiation.

In addition to monitoring the crosslinker decomposition, FT-IR analysis could be used to determine the amount of the insoluble polymer in the samples. The ratio between the height of the polymer's strong ester band at 1724 cm^{-1} before and after development allows for quantification of the residual polymer on the CaF_2 plates and the percentile gel fraction can be calculated according to

$$gel\ fraction\ [\%] = \frac{pht_1}{pht_0} \cdot 100 \qquad \textbf{Equation 4-1}$$

where pht_0 is the ester peak height after illumination and pht_1 is the ester peak height after development, respectively. Being a very fast reaction, the photolysis of BA and the subsequent crosslinking reaction yields maximum gel fractions for all PHB-HV/BA ratios within one minute. The maxima reached for the gel fraction increase according to increasing BA contents from 70% with 1 wt.-% BA to 80% (2 wt.-% of BA) and 90% (3, 4, and 5 wt.-% of BA) (Figure 4-8).

Interestingly, all gel curves reach a plateau after irradiation for at least one minute and even show a slight decrease with prolonged irradiation times of 180 s, indicative of side reactions that partially break the network. Additionally, the time required to reach the maximum gel fraction varies with the amount of crosslinking agent used: An increase of the BA content from 1 to 3 wt.-% not only yields higher gel fractions but also reduces the time needed to reach the maximum gel fraction from 60 to 20 s; a further increase of the crosslinker content yields higher gel fractions but prolonged irradiation times of 30 s are needed for obtaining highest extents of crosslinking. This circumstance suggests that BA-contents higher than 3 wt.-% support chain scission reactions due to a higher concentration of radicals present in the polymer chain. For a comprehensive understanding of the reactions involved in the process, further analyses of the gel curves and the sol- and gel fractions are needed.

In addition, control experiments in which the gel fraction was measured gravimetrically were performed in order to validate the FT-IR-measurements. The results were in good agreement with results of the FT-IR-method: 43% gel fraction after 3 s, 95% after 60 s of UV-irradiation using 3 wt.-% of BA.

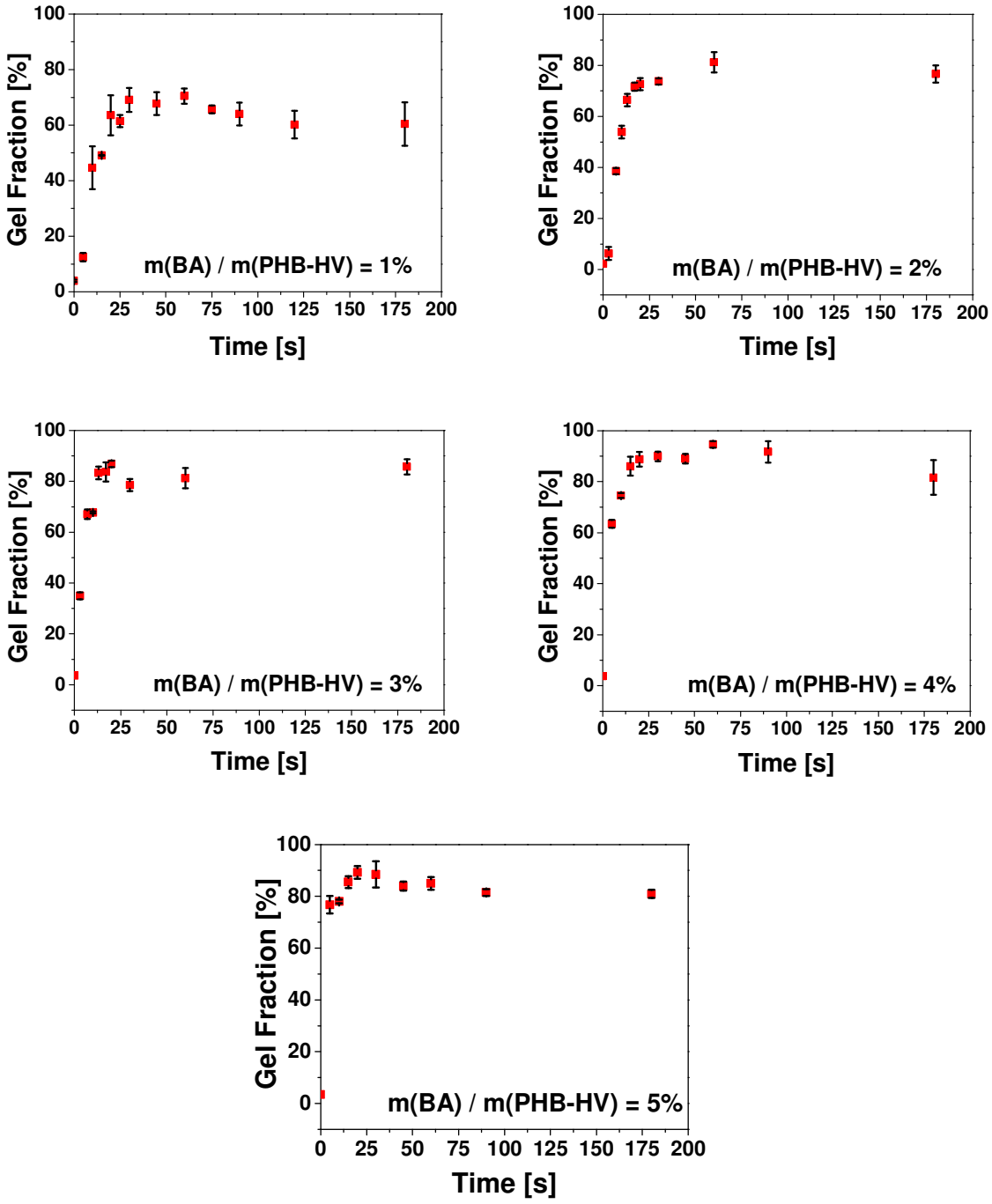

Figure 4-8: Correlation of the gel fractions with irradiation intervals for PHB-HV with 1, 2, 3, 4, and 5 wt.-% BA.

4.3.2 Charlesby-Pinner Analysis

For a deeper insight into the rates of the concurring reactions of crosslinking and chain scission, Charlesby and Pinner proposed a linearization model for the gel curves observed in all crosslinking processes (see chapter 3.4.1). Assuming that the rates for crosslinking and chain scission are constant, the following expression can be used to determine the rates of chain scission and crosslinking from the gel curves:

$$s + \sqrt{s} = \frac{v_p}{v_q} + \frac{1}{v_q \cdot P_n^0} \cdot \frac{1}{t} \qquad \textbf{Equation 4-2}$$

s ..... soluble fraction of the polymer

v_q ..... crosslinking rate

v_p ..... chain scission rate

P_n^0 ..... average polymerization degree (1200, determined by GPC-analysis)

t ..... time

According to equation 4-2, the plot of s + $\sqrt{s}$ against $\frac{1}{t}$ should give a linear correlation for irradiation times shorter than those needed to reach the maximum gel fraction, represented by a linear increase of the gel fraction percentile with time in the gel curves. This assumption could be verified for the present process and the so-called Charlesby-Pinner plots for BA contents of 1, 2, 3, 4, and 5 wt.-% are summarized in Figure 4-9. The plots show good agreement with linearity and from the linear regression, the ratios of $\frac{v_p}{v_q}$, representing the rates of chain scission and crosslinking, can be determined.

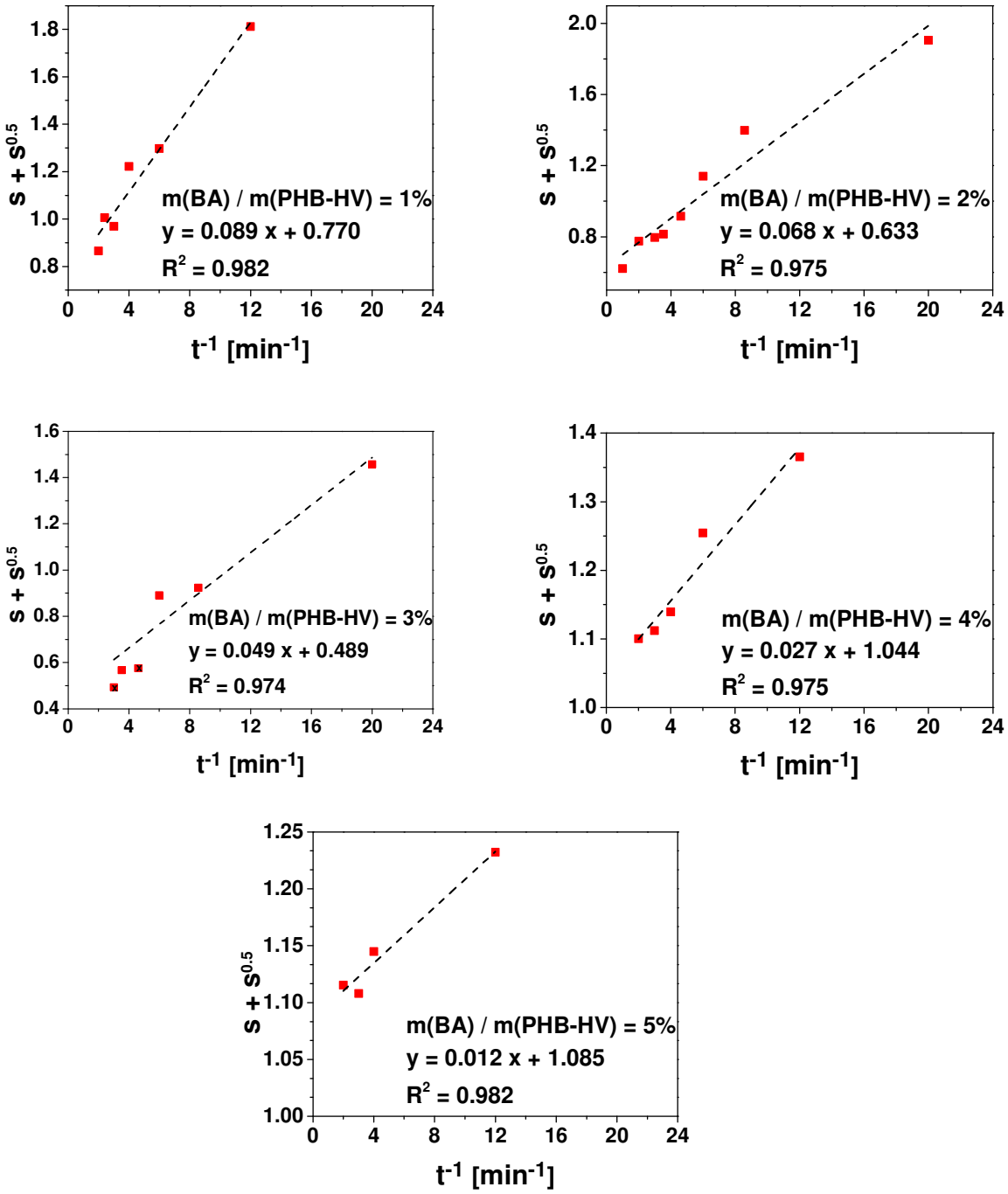

Figure 4-9: Charlesby-Pinner plots derived from the crosslinking of PHB-HV with 1, 2, 3, 4, and 5 wt.-% BA.

Table 4-3: Chain scission v_p, crosslinking rate v_p, and the ratio v_q / v_p for mixtures of PHB-HV with 1, 2, 3, 4, and 5 wt.-% of BA.

m(BA) / m(PHB-HV) [wt.-%]	$10^3 \cdot v_q$ [min^{-1}]	$10^3 \cdot v_p$ [min^{-1}]	v_q / v_p
1	9.32	7.05	1.32
2	12.3	7.79	1.58
3	16.9	8.27	2.04
4	29.9	31.3	0.96
5	68.1	73.9	0.92

For more clarity, the values summarized in Table 4-3 were plotted against the amount of crosslinker and are shown in Figure 4-10. The ratios of chain scission and crosslinking rate exhibit a pronounced maximum at a crosslinker content of 3 wt.-%. A high ratio between v_p and v_q is directly proportional to a high crosslinking rate and a comparably low chain scission rate.

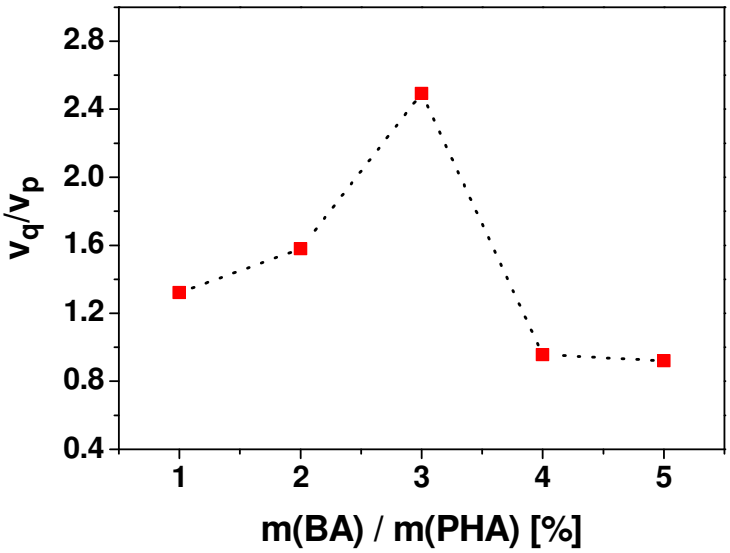

Figure 4-10: Ratio between v_q and v_p plotted against the amount of crosslinker used.

For low BA contents ranging from 1 to 3 wt.-%, the crosslinking rate is higher than the chain scission rate and shows the biggest increase between 2 and 3 wt.-% BA, where v_q increases from $12.3 \cdot 10^{-3}$ min^{-1} to $16.9 \cdot 10^{-3}$ min^{-1}, while at the same time, v_p only increases slightly from $7.79 \cdot 10^{-3}$ min^{-1} to $8.27 \cdot 10^{-3}$ min^{-1}. When more than 3 wt.-% of

BA are used, chain scission and crosslinking rates increase significantly and the ratio drops below 1. This signifies that higher amounts of BA favor the chain scission rate over the crosslinking rate. These findings explain the phenomena pointed out in the discussion of the gel curves in chapter 4.3.1.

4.3.3 GPC-Analysis

The evaluation of the crosslinking process described in the present work was done under the assumption that the non-crosslinked part of the polymer remained soluble while the gel part, representing the polymer/crosslinker network, became insoluble. This presumption is also supported by GPC analyses of the soluble fraction that show a significant decrease in the average molecular weight with progressing irradiation times, accompanied by a broadening of the average molecular weight distribution, represented by the polydispersity index (PDI). In fact, the values for M_n and the PDI change from 191 to 83 kDa and from 2.4 to 3.8, respectively (Figure 4-11). The increasing PDI values indicate that the decrease in the average molecular weight can be traced back to chain scission reactions (see also 4.3.2).

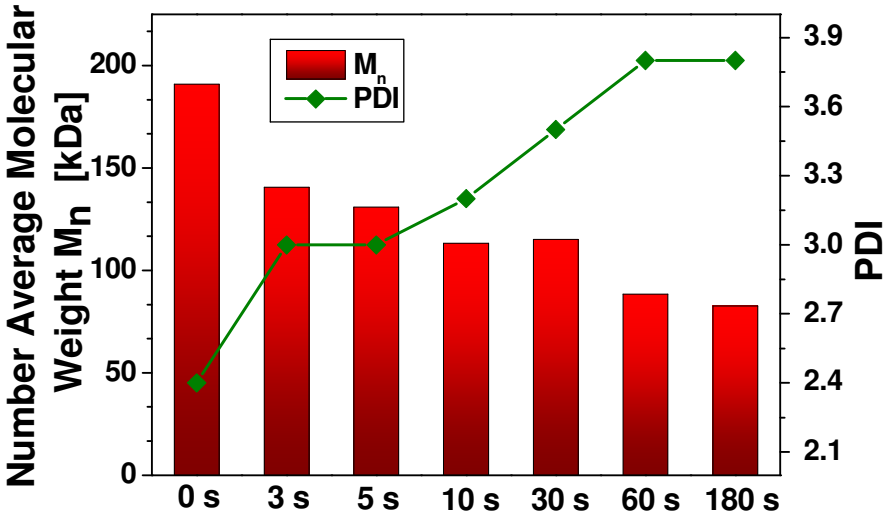

Figure 4-11: Number average molecular weight and corresponding PDI values from the soluble fractions of PHB-HV samples irradiated for different times with 3 wt.-% of BA.

In the GPC curves of the sol fractions shown in Figure 4-12, the broadening effect of chain scission reactions on the molecular weight distribution is also visible and, taking an even closer look at the plot, another phenomenon can be observed: Indicated by the GPC curve's slight tailing effect, the photoreaction increases the average molecular weight of the soluble fraction within the first few seconds (blue curve). This effect is caused by addition of crosslinker molecules to the polymer backbone, combining two or more chains without effectively crosslinking them. Consequently, polymer chains with increased molecular weight persist to be soluble and cause the tailing of the GPC curve. After the first few seconds, this effect is overlapped by the partially linked polymer chains becoming crosslinked, insoluble, and not traceable by GPC analysis.

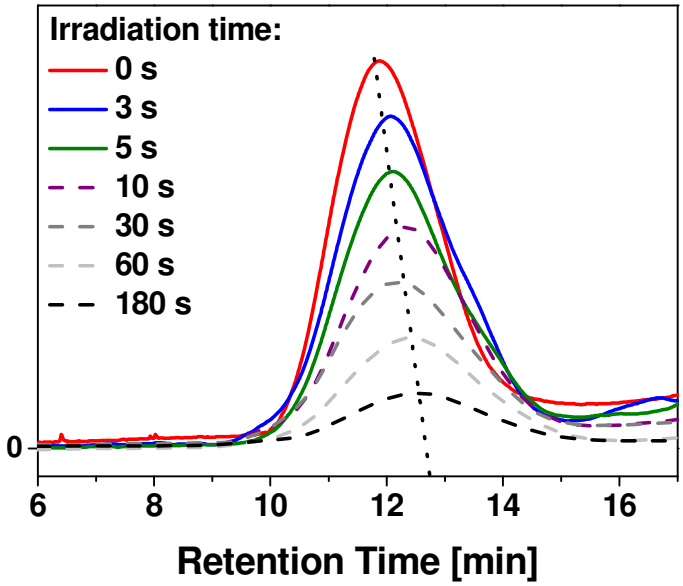

Figure 4-12: GPC curves of the sol fractions of PHB-HV samples irradiated for different times using 3 wt.-% of BA.

4.3.4 ^{1}H-NMR Analysis

Preceded by the GPC analyses of the soluble fractions, further investigations were carried out by means of ^{1}H-NMR spectroscopy. In order to verify the valerate content of the PHB-HV copolyester, the untreated polymer was dissolved in $CDCl_3$ and subjected to ^{1}H-NMR measurements. Figure 4-13 shows the ^{1}H-NMR-spectrum of

PHB-HV in which the two different monomer units hydroxybutyrate and –valerate are visible (Scheme 4-2); from the integral ratio between the doublet at 1.26 (H4') and the triplet at 0.88 ppm (H5) the ratio can be determined to a valerate-content of approx. 20 mol-% in reasonable accordance with the supplier's specification of 18.25 mol-%.

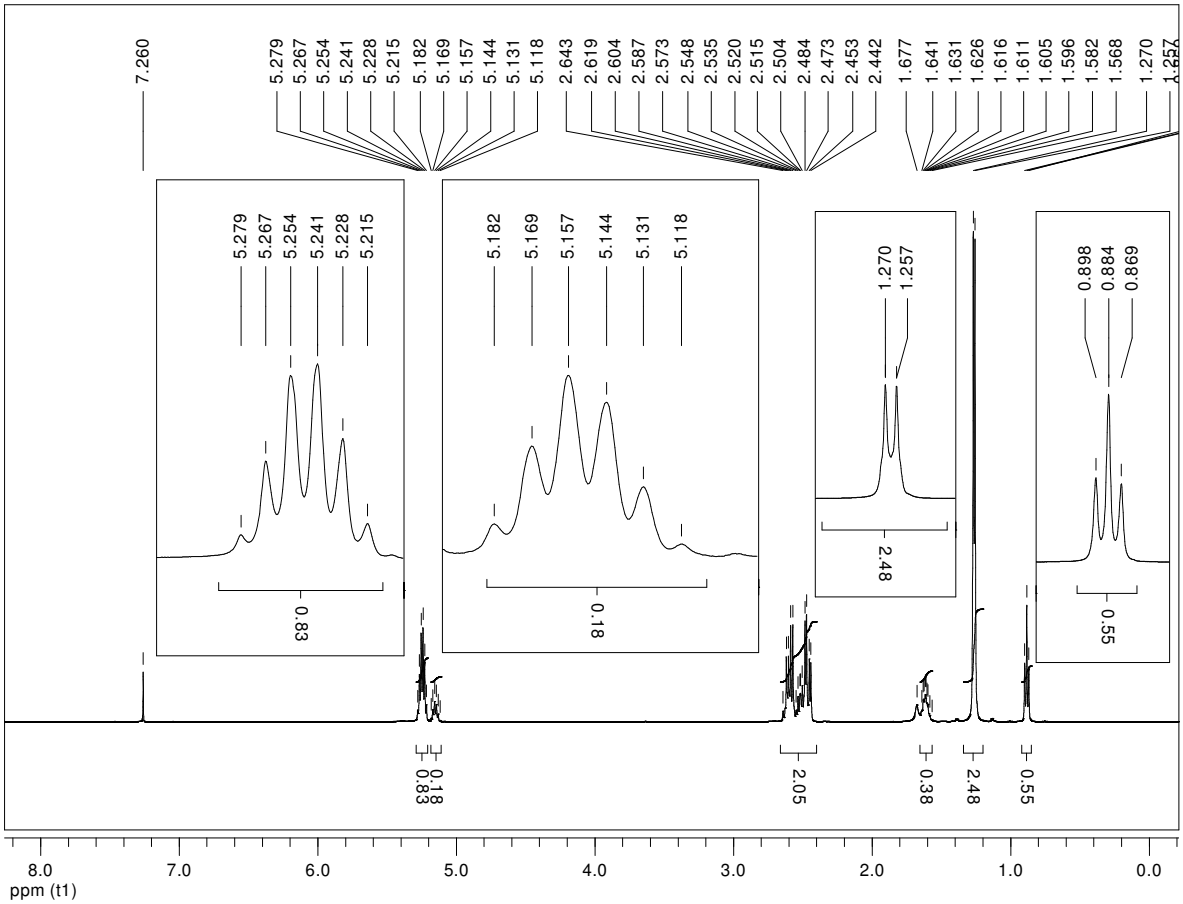

Figure 4-13: ^{1}H-NMR spectrum of PHB-HV in $CDCl_3$.

NMR data: δ (ppm) = 0.88 (0.55; t, 3·0.18 H = 0.54 H, $^{3}J_{H,H}$ = 6.9 Hz, **H5**), 1.26 (2.48; d, 3·0.82 H = 2.46 H, $^{3}J_{H,H}$ = 6.5 Hz, **H4'**), 1.57-1.64 (0.38; m, 2·0.18 H = 0.36 H, **H4**), 2.44-2.64 (2.05; m, 2·0.82 H + 2·0.18 H = 0.36 H, **H2** and **H2'**), 5.12-5.18 (0.18; m (dd), 0.18 H, **H3**), 5.22-5.28 (0.83; m (dd), 0.82 H, **H3'**).

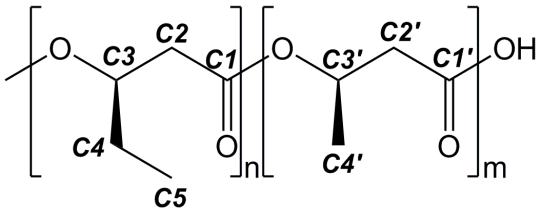

Scheme 4-2: Structure formula of PHB-*co*-HV.

Additionally, ^{1}H-NMR spectroscopy can be used to gather information about the mechanism according to which the crosslinking reaction of bisazides with PHAs takes place. The two alternate mechanisms described in chapter 3.3.2.3 yield differently composed gel and soluble fractions: If the crosslinking mechanism is based on proton abstraction, the crosslinker will be present in the soluble fraction in form of its amino-derivative. If crosslinking occurs due to insertion of the crosslinker in the polymer chains, no traces of the crosslinker will be found in the soluble fraction. In order to validate these mechanisms, ^{1}H-NMR spectra were recorded from the soluble fractions of PHB-HV crosslinked with 3 wt.-% BA after 0, 3, and 20 s irradiation time (Figure 4-14 to Figure 4-16). The spectrum collected from the soluble fractions of non-irradiated samples of PHB-HV and BA shows residues belonging to the aromatic ring-system of the crosslinker (doublets at 7.09 and 7.49, singlet at 7.75 ppm). In contrast to that, the spectra of soluble fractions obtained from UV-irradiated samples reveal no traces of crosslinker at all. In fact, 3 s appear to be enough time for the crosslinker to initiate and incorporate in high yields into the polymer matrix leaving no evidence of 2,6-bis(4-azidobenzylidene)-4-methylcyclohexanone or its 4-amino-derivative in the soluble fraction according to ^{1}H-NMR spectroscopy.

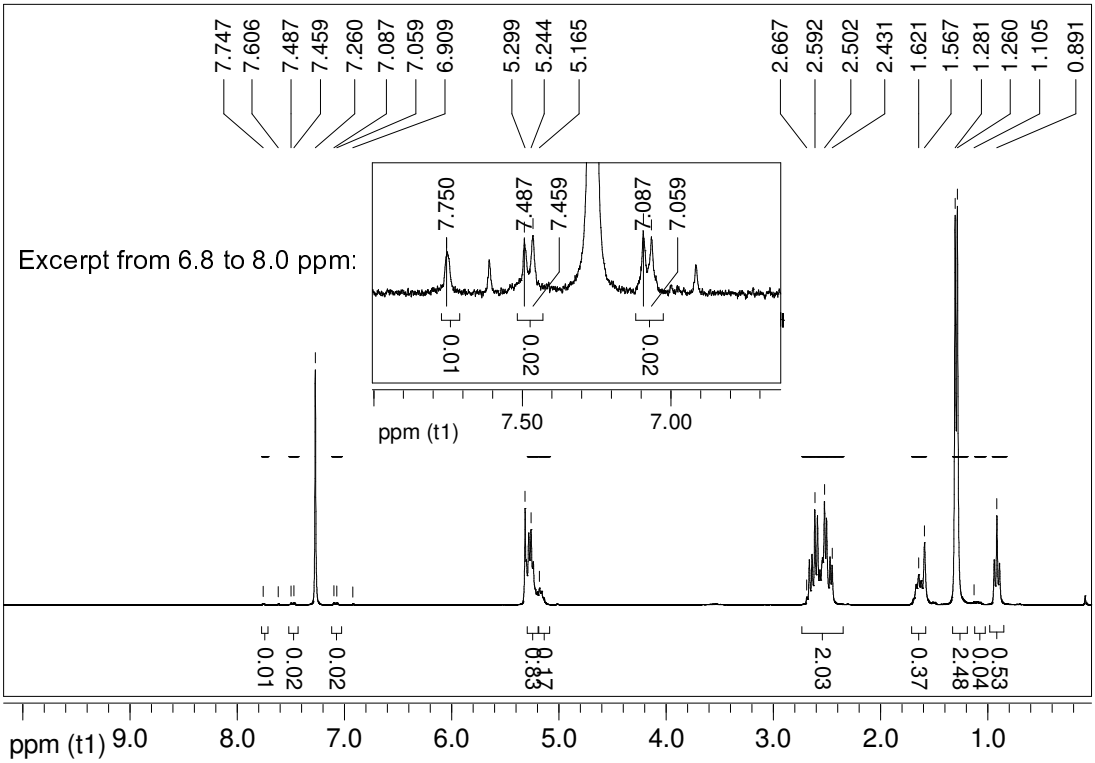

Figure 4-14: ^{1}H-NMR spectrum of PHB-HV samples with 3 wt.-% of BA without UV-irradiation in $CDCl_3$.

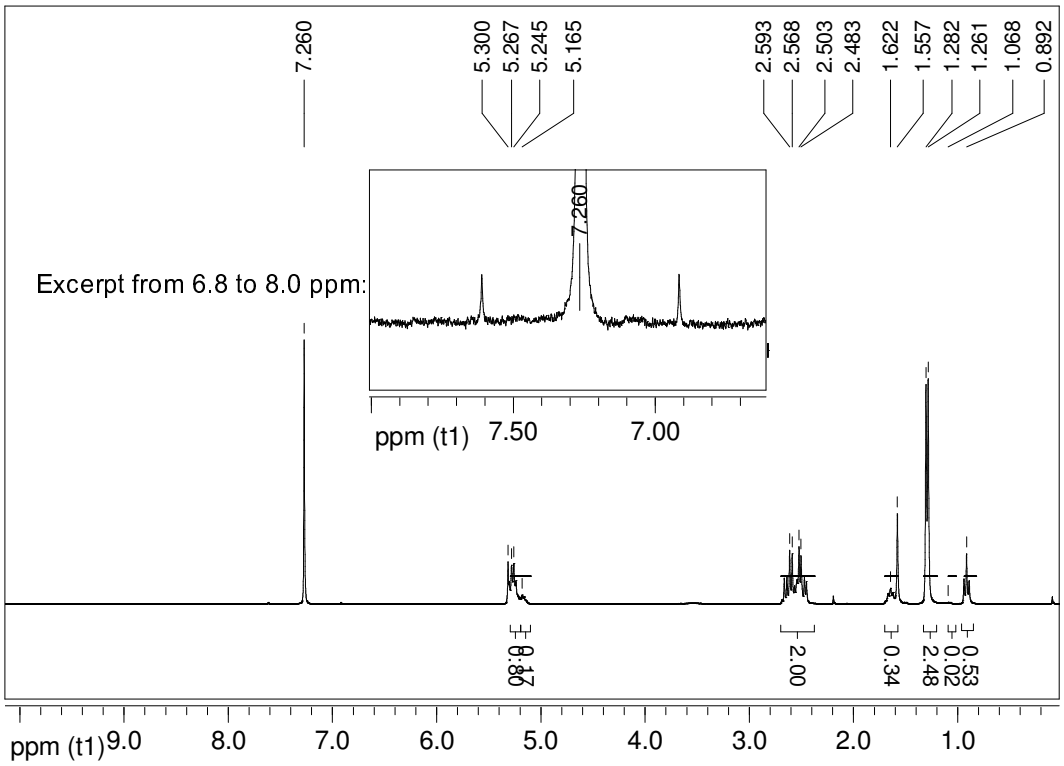

Figure 4-15: ^{1}H-NMR spectrum of PHB-HV samples with 3 wt.-% of BA after 3 s of UV-irradiation in $CDCl_3$.

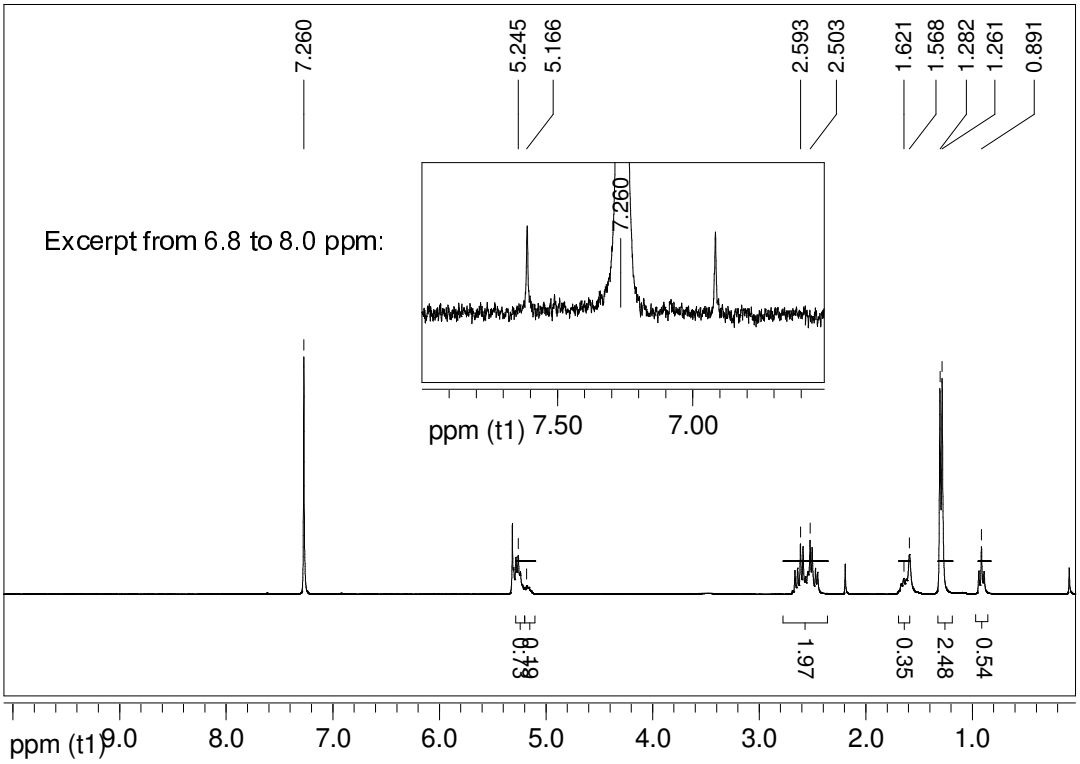

Figure 4-16: ^{1}H-NMR spectrum of PHB-HV samples with 3 wt.-% of BA after 20 s of UV-irradiation in $CDCl_3$.

The results obtained from the ^{1}H-NMR analysis strongly suggest the validity of the insertion mechanism of BA, as no crosslinker or derivative thereof is present in the soluble fraction of UV-irradiated samples. The results also prove the fast initiation of the bisazide and instant reaction with the polymer chains; this phenomenon is also visible in the FT-IR-spectra where the azide peaks disappear within the first seconds of UV-irradiation (Figure 4-7). Furthermore, attempts to crosslink PHB-HV using benzophenone, which is known to provide crosslinking by proton abstraction only, failed to yield any gel fraction at all and can be seen as final proof of the validity of the insertion mechanism.

4.3.5 Photolithography

The optimized photosensitive polymer/crosslinker system consisting of PHB-HV and 3 wt.-% of BA was used as a negative photoresist in a photolithographic process for reproduction of a pattern preset by a quartz photomask. Both, a one-step process on Si-wafers and a two-step photolithographic process on glass/indium tin oxide (ITO)/chrome substrates were employed for these experiments (Figure 4-17). According to Figure 4-17, the steps in the process involved spin-coating of the polymer/BA resist system on the glass/ITO/chrome substrate, followed by UV-irradiation for 30 s using a photomask. During illumination, the parts of the PHB-HV/BA layer not covered by the mask were crosslinked and became insoluble while the covered parts remained soluble and were washed off using DCM in the development step. In the etching step, the parts of the chrome layer not shielded by the polymer film were etched off using cerium(IV) nitrate and reproduced the pattern preset by the photomask in a reasonable resolution of approx. 50 µm. The usability of PHB-HV and BA as photoresist shows the good adhesion between the polymer and the chrome layer as well as the polymer's stability towards oxidization that leaves the covered part of the chrome layer unaffected by the etching step.

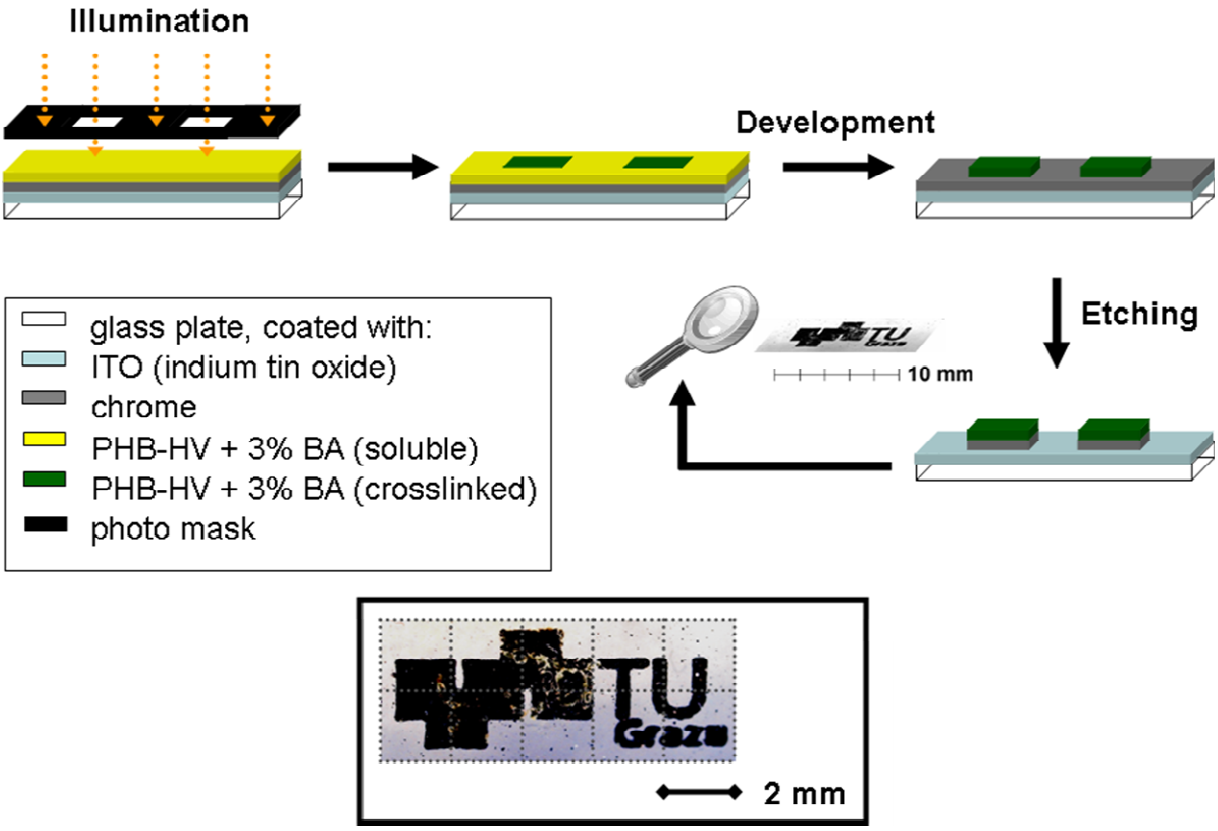

Figure 4-17: Scheme of the two-step photolithographic process on glass/ITO/chrome substrates using PHB-HV with 3 wt.-% BA as negative photoresist.

4.3.6 UV-Induced Crosslinking of PHB

Due to the interesting results obtained by the crosslinking of PHB-HV with BA, the PHB homopolyester was also considered for the same process. Employing the same experimental parameters, a feasibility study was conducted for PHB using an amount of BA of 3 wt.-%. Irradiation times ranged from 0 to 60 s and revealed a very similar behavior of PHB being treated with UV light under the presence of a UV-inducible bisazide (Figure 4-18). The trend revealed by the gel curve of PHB crosslinked with 3 wt.-% of BA is very similar to the trend displayed for PHB-HV with 3 wt.-% BA (Figure 4-8): Maximum gel fractions of over 90% are reached within 20 s rendering the homopolyester PHB and its copolymer with hydroxyvalerate equally suitable for the UV-induced crosslinking process using BA.

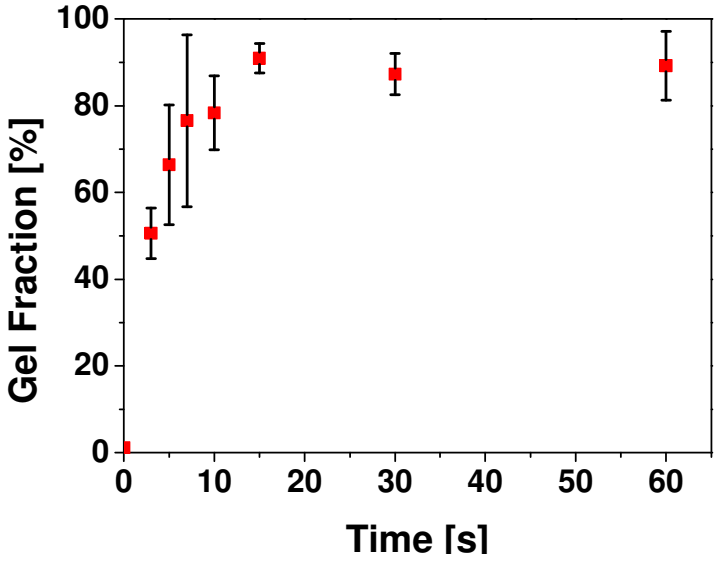

Figure 4-18: Gel fraction vs. time for the UV-induced crosslinking of PHB using 3 wt.-% of BA.

4.4 Temperature-induced Crosslinking of PHB, PHB-HV, and PLLA

Considering the results obtained in the study of the UV-induced crosslinking of PHB-HV and PHB, experiments towards thermal crosslinking of biopolyesters were conducted. UV-induced crosslinking bears one very important disadvantage over thermal crosslinking: The low penetration depth of UV-light makes crosslinking of the bulk material and the production of 3-dimensional crosslinked molds impossible in one-step routines.

4.4.1 Temperature-Induced Crosslinking of PHB Using BA

In principle, the conjugated bisazide used in chapter 4.3 can be initiated not only by UV-irradiation: The energy needed for the decomposition of azides can also be of thermal nature. In fact, all organic azides tend to decompose into nitrenes and nitrogen at elevated temperatures, which makes this substance class very interesting for the crosslinking of non-functionalized polyesters (see chapter 3.3.2.3).[188] For that reason, experiments using the aforementioned bisazide as crosslinker in combination

with melt compounding PHB at elevated temperatures and subsequent injection-molding were conducted. Mixtures of PHB and 3 wt.-% of BA were prepared and filled in the compounder at a temperature of 177 °C. After mixing for 3 min, the melt was transferred to the cylinder (167 °C) and injection molded in a shoulder test bar mold preset to a temperature of 110 °C. This procedure yielded well-shaped shoulder test bars with an intense red-brownish color. These samples were subjected to sol gel analyses and tensile testing and the results of the mechanical characterization are summarized in Table 4-4. While the values for the tensile strength and the elongation at break were not significantly changed by crosslinking, the Young's modulus dropped from almost 3 to 1.8 GPa for the samples containing 3 wt.-% of BA and, hence, did not provide the targeted improvement of the material's properties. The assumption that the bisazide used is too reactive for compounding at elevated temperatures is supported by the fact that the samples failed to form any gel fraction insoluble in DCM. This indicates that chain scission is predominantly active and considerably stronger than the effect of crosslinking. Additionally, the lack of nitrogen-purging in the compounder favors side reactions of the nitrenes with oxygen to form intensely colored nitrous oxides.[189] Overall, these results prove that the system is not applicable for melt compounding due to too high reactivity of BA on the one hand and non-optimum reaction conditions during this kind of processing on the other hand.

At this point it must be emphasized that the considerably lower tensile strength and elongation at break of the reference sample compared to other native PHB samples (see 4.1.1 and 4.1.2) can be traced back to the time of measurement: All samples (reference and PHB/BA) were injection-molded and measured within two days after processing. Semi-crystalline polymers like PHB, poly(trimethylene terephthalate), polyethylene, or polyamide are known to increase in mechanical strength, depending on the conditions and time period of storage. This ageing-induced increase in mechanical stability is ascribed to changes of the extent of crystallinity and orientation processes of the amorphous phase of the semi-crystalline polymers.[190-192] Hence, a minimum time of two weeks should be kept between the processing of PHB and the time of measurement. This way, the permanent mechanical behavior of PHB and similar semi-crystalline polymers can be determined more accurately.

Table 4-4: Summary of the mechanical characteristics of native PHB and PHB compounded with 3 wt.-% of BA.

Sample	Young's modulus [GPa]	Tensile strength [MPa]	Elogation at break [%]
PHB native (reference)	2.94 ± 0.38	13.19 ± 0.01	0.47 ± 0.02
PHB + 3 wt.-% BA	1.82 ± 0.10	12.92 ± 0.02	0.75 ± 0.05

4.4.2 Temperature-Induced Crosslinking of PHB, PHB-HV, and PLLA using Tri(ethylene glycol) bis(azidoformate) (TBA)

Due to the challenges arising from the high reactivity and the processing conditions using BA as thermosensitive crosslinker, another bisazide was chosen for the temperature-induced crosslinking of biopolyesters. Furthermore, 2,6-bis(4-azidobenzylidene)-4-methylcyclohexanone and its amino-derivatives have not yet been fully characterized in terms of toxic effects and, hence, cannot yet be used for medical applications. For the selection of the crosslinker, the reactivity as well as the chemical structure, apart from the azide groups needed for crosslinking, were considered. For that reason, the ethylene glycol-based bisazide tri(ethylene glycol) bis(azidoformate) (TBA) was selected for further crosslinking experiments. This compound is less reactive than BA and contains hydrophilic ethylene glycol groups that can change the crosslinked polymer's hydrophilicity, which is frequently aimed for in medical applications of saturated, hydrophobic polyesters like PHB, PHB-HV, and PLLA (see chapter 3.3.2). Due to the reasons mentioned in the previous chapter, the processing route was changed from melt-compounding and injection-molding to thermoforming in a vacuum platen press. The samples were prepared by mixing the respective polymer with TBA in different amounts in solution and, after drying, the mixtures were ground in order to yield granulate material for processing. The amounts of crosslinker and the number of resulting copolymers are summarized in Table 4-5.

Table 4-5: Summary of amounts of TBA used for crosslinking PHB, PHB-HV, and PLLA, processing temperatures, and the number of resulting polymers.

Biopolyester	TBA-contents [wt.-%]	Processing temperature [°C]	# of polymers
PHB	10, 20, 30, 40, 50	180	5
PHB-HV	10, 20, 30, 40, 50	170	5
PLLA	10, 20, 30, 40, 50	180	5

These 15 polymers were processed in a vacuum platen press at the respective temperatures. In order to prevent side reactions with oxygen and to facilitate the evaporation of the in-situ formed nitrogen, heating was initiated only after complete evacuation of the platen chamber. Once the targeted temperature was reached, the samples were kept under a pressure of 5 bar for 10 min. This way, thin samples of 200 µm height were produced. All 15 polymers were subjected to sol-gel analyses, swelling experiments in DCM and water, and tensile testing.

4.4.2.1. Sol-Gel Analysis

In order to prove network formation, all samples were subjected to sol-gel analyses in DCM at elevated temperatures of 100 °C for 10 min in closed vessels in a microwave reactor. The gel fractions were determined gravimetrically and the percentile gel fractions were calculated according to:

$$gel\ fraction\ [\%] = \frac{m_{gel}}{m_0} \cdot 100 \qquad \textbf{Equation 4-3}$$

where m_0 is the mass of the crosslinked polymer sample and m_{gel} the mass of gel fraction.

While the native reference samples dissolved quantitatively in the course of sol-gel analysis, all samples containing TBA showed increasing gel fractions with increasing TBA content starting at less than 5% and reaching up to 80% gel fraction in the case of PHB-HV (Figure 4-19). The maximum gel fraction for PHB and PLLA was higher than 40%. Interestingly, the threshold of TBA content from which significant gel

fraction is observed, is at 20 wt.-% TBA for PHB (24% gel fraction) and PLLA (23 % gel fraction), but already at 10 wt.-% TBA for PHB-HV (22% gel fraction). Generally, the gel fractions of PHB-HV are considerably higher than those of PHB and PLLA. Overall, the trends for PHB and PLLA are very similar to each other.

Notably, these copolymer networks of polyesters and triethylene glycol can also be prepared using 1-methoxy-2-propanol as a solvent instead of DCM or chloroform if the solutions are prepared at elevated temperatures in closed vessels in a microwave reactor. Additionally, sol-gel experiments using 1-methoxy-2-propanol instead of DCM led to the same amount of gel fractions. This enables for replacing the harmful, toxic halogenated solvents with less harmful compounds in most solvent-based steps in this process.

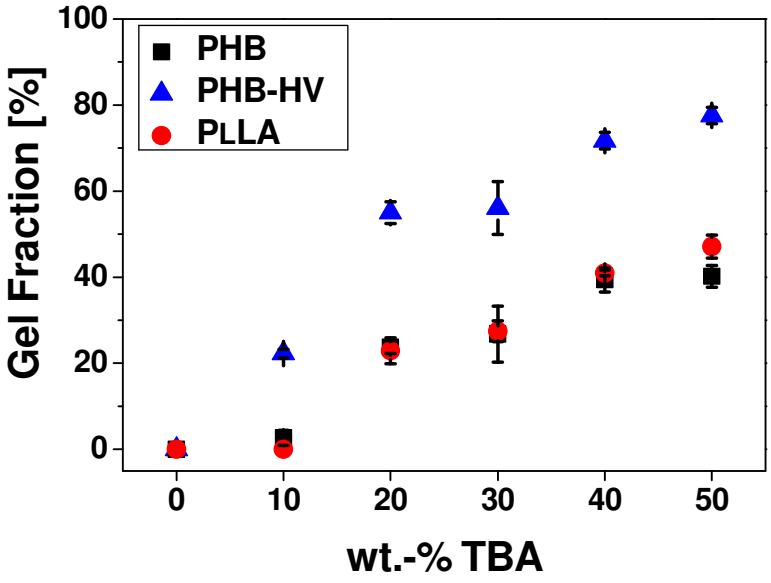

Figure 4-19: Gel fractions for PHB-, PHB-HV-, and PLLA/TBA networks as function of TBA content.

4.4.2.2. Swelling Experiments in H_2O and DCM

In order to determine the physico-chemical behavior of polyester/TBA networks prepared from PHB, PHB-HV, and PLLA with TBA, the films were immersed in DCM and water for at least 3 days until maximum swelling degrees were reached. Notably, only gel fractions were used for swelling experiments. The swelling degrees, representing the ability of a polymer network to take up solvents of particular polarity, were determined by calculating the mass balance between the native dry gels and the swollen samples according to:

$$\text{swelling degree} = \frac{m_{swollen} - m_{gel}}{m_{gel}} \qquad \textbf{Equation 4-4}$$

where $m_{swollen}$ is the mass of swollen gel fraction and m_{gel} the mass of dry gel fraction.

Due to the hydrophobic nature of saturated polyesters, all copolymers showed high swelling degrees in DCM ranging from around 20 to up to 60 (Figure 4-20). Because of too small gel fractions, the swelling degrees of polyesters crosslinked with 10 wt.-% of TBA could not be determined. The highest swelling degrees of 60 were achieved for PLLA crosslinked with 20 wt.-% TBA, followed by PHB-HV (20-30 wt.-% TBA) with 52, and PHB (20 wt.-% TBA) with a maximum swelling degree of 31. Higher TBA contents representing higher crosslinking degrees and more rigid network structures led to lower solvent uptake. Generally, two different phenomena contribute to the extent of solvent uptake of polymer networks: The pore size and the amount of covalent crosslinks constituting the network. Higher amounts of TBA lead to more crosslinking sites that yield networks with smaller pore size and a more rigid structure resulting and decreasing ability of the network to expand upon solvent uptake.
A completely different trend was observed for the water swelling behavior of the prepared polymer networks: Induced by the crosslinker's polar ethylene glycol units, the water swelling degree increased with increasing TBA content (Figure 4-21). Due to the relatively low swelling degrees compared to those in DCM, the effect of higher crosslinking density and lower pore size is not the limiting factor for the extent of water uptake. Additionally, the water molecule is much smaller than the bulkier

dichloromethane molecule and can penetrate the network more easily. Interestingly, the PHB-HV/TBA networks revealed the highest water uptake of 0.2 g per g polymer at a crosslinker content of 50 wt.-%. By comparison of the water swelling and the amount of gel fraction formed (Figure 4-19) using PHB-HV, it becomes clear that the higher concentration of crosslinker left in the samples is responsible for the higher swelling degrees. Notably, the threshold of TBA for overruling the hydrophobic nature of PHB-HV is relatively high; 50 wt.-% of TBA, corresponding to 80% gel fraction are needed for PHB-HV in order to take up more water than the other two polyesters. Water swelling of PLLA and PHB-based networks was less pronounced, but still significantly increased compared to the native polymers. PLLA, being the least hydrophobic polymer of all three, took up almost 3% of water already in its native state and reached the lowest maximum swelling degrees of 0.1. PHB, on the other hand, took up 1% of water in its native state and reached swelling degrees of 0.14 with 50 wt.-% of TBA.

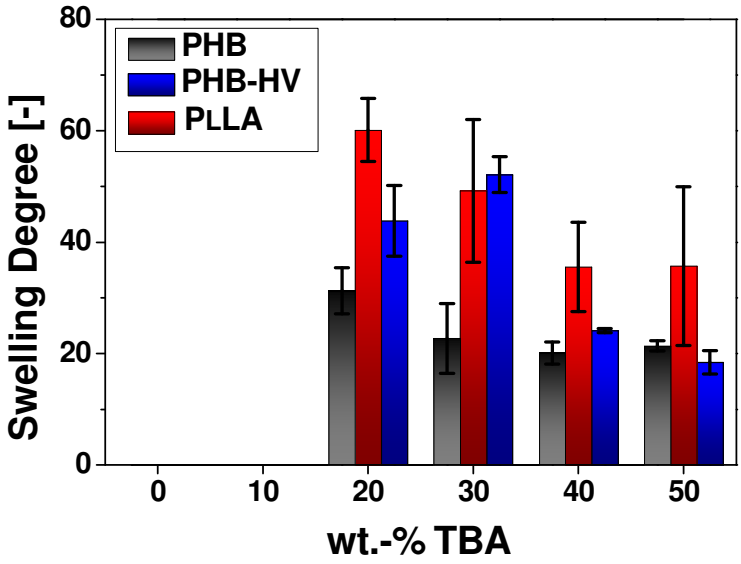

Figure 4-20: Swelling degrees of PHB-, PHB-HV-, and PLLA/TBA networks in DCM.

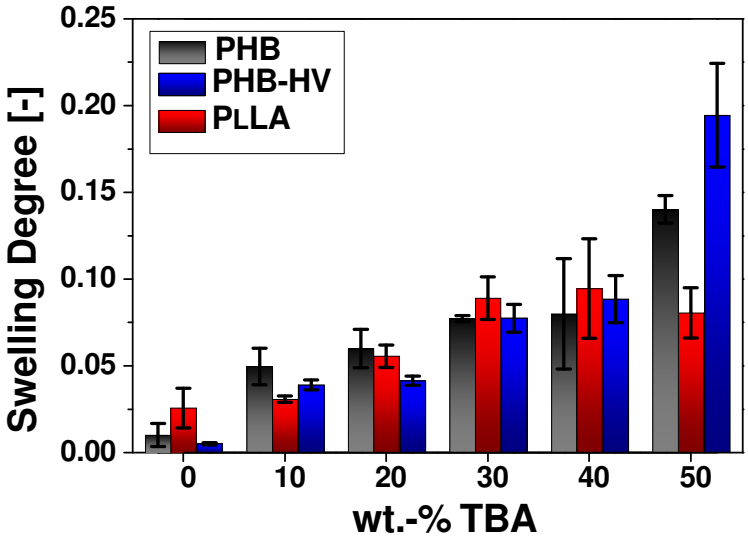

Figure 4-21: Water swelling degrees of PHB-, PHB-HV-, and PLLA/TBA networks.

Overall, the incorporation of TBA in PHB, PHB-HV and PLLA yielded polymer networks that showed significant swelling in DCM and swelling in water, indicative of significantly increased hydrophilicity. The water uptake was increased by factors of 20 and 14 for PHB-HV and PHB while PLLA's maximum hydrophilicity induced by TBA was only three times higher than for native PLLA. As stated in chapter 3.2.2 and 3.3.2, the hydrophilicity of polymer-based materials is of great importance for medical applications. Increased hydrophilicity does not only potentially promote cell adhesion and proliferation in physiological systems, but enables the material to swell. The latter phenomenon can be of special interest for bone surgery applications, as the water uptake also leads to volume expansion and gives rise to adaption of the implant to the environment and promotes the physical interaction between bone tissue and implant material while, at the same time, the implant's surface is increased and can potentially alter the degradation rate.

4.4.2.3. Mechanical Characterization of Polyester/TBA Networks

Crosslinking of polymers is not only aiming for manipulation of the physico-chemical properties but is also used for the production of materials with higher physical strength and elasticity. For the mechanical characterization of PHB-, PHB-HV, and PLLA/TBA networks, samples in the size of 40 x 10 x 0.2 mm were cut from the platen-press processed samples and subjected to tensile testing. Due to the swelling in water and this work's aim of developing materials for medical applications, tensile testing was done with samples in the dry as well as water-swollen state. This way, potential changes in the materials' properties due to water uptake can be estimated for applications in the targeted field. The Young's moduli of dry PHB-HV and PLLA networks show a distinct loss of stiffness with increasing TBA content, while the modulus of PHB is widely unaffected by the incorporation of TBA (Figure 4-22). After swelling in water, all samples revealed decreased resistance towards plastic deformation as the crosslinker content and the water uptake increased (Figure 4-23). In perfect agreement with literature, this observation can be attributed to the water uptake which slightly expands the network inducing stress and rendering it more susceptible to additional external forces.[50;52;193]

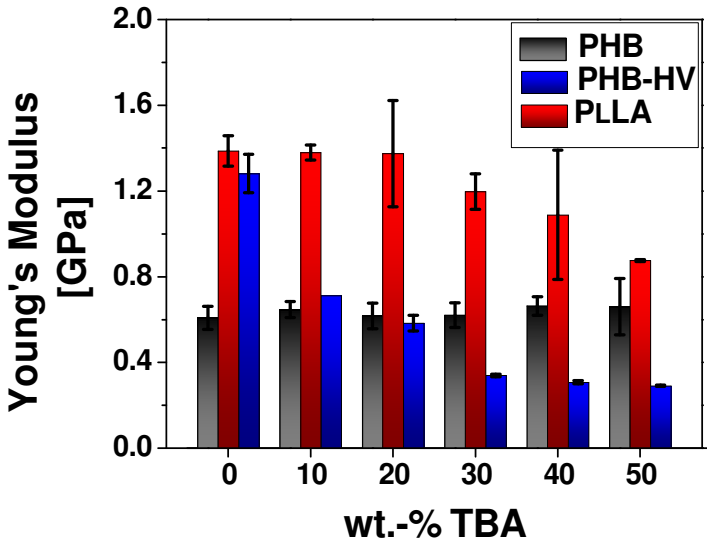

Figure 4-22: Young's modulus of dry samples of PHB-, PHB-HV-, and PLLA/TBA networks.

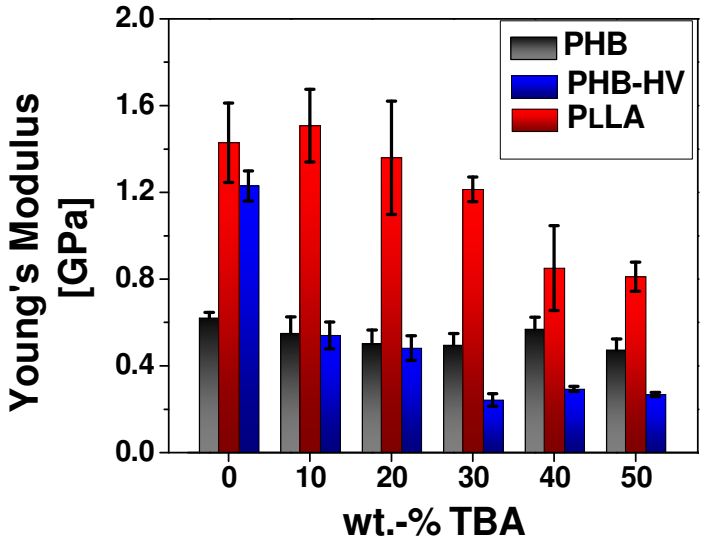

Figure 4-23: Young's modulus of water-swollen samples of PHB-, PHB-HV-, and PLLA/TBA networks.

For the changes in the tensile strength, very similar trends were observed (Figure 4-24). Again, the mechanical strength of PHB-HV and PLLA is negatively affected by the reaction with TBA while the tensile strength of PHB benefits from crosslinking: PLLA and PHB-HV lose about 40 and 30% of tensile strength with 50 wt.-% of TBA, whereas PHB's tensile strength is increased by more than half with 50 wt.-% of TBA. Even in the water-swollen state, crosslinked PHB is able to take up higher tensile forces than native PHB (Figure 4-25). Interestingly, lower concentrations of TBA did not significantly affect the strength of PHB-HV which even showed a slight increase for 10 and 20 wt.-% of TBA (dry and water-swollen), even though the Young's modulus was almost halved (Figure 4-22). The most pronounced negative changes are observed for PLLA, which considerably loses strength in terms of Young's modulus and tensile strength in the dry and in the water-swollen state. This indicates a softening effect of TBA on PLLA as well as PHB-HV.

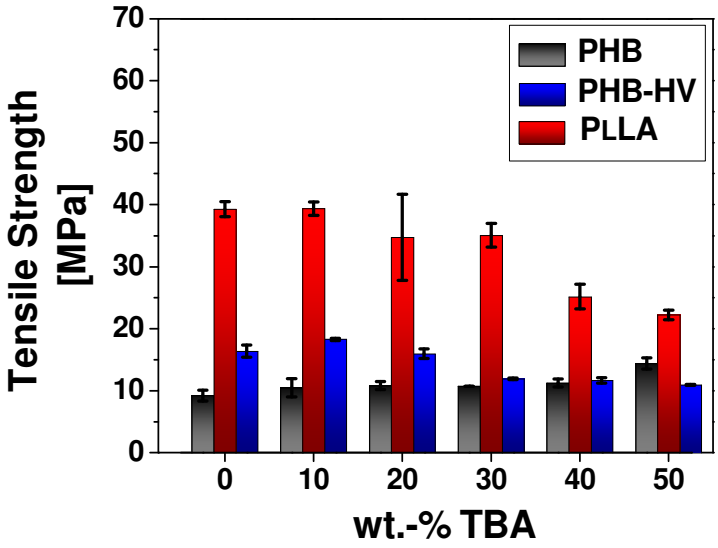

Figure 4-24: Tensile strength of dry samples of PHB-, PHB-HV-, and PLLA/TBA networks.

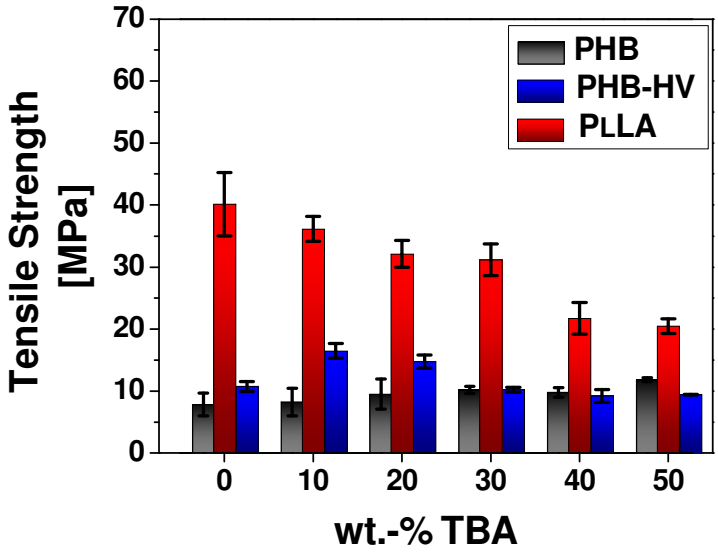

Figure 4-25: Tensile strength of water-swollen samples of PHB-, PHB-HV-, and PLLA/TBA networks.

The assumed plasticizing effect of TBA on PHB-HV and PLLA is further supported by the strain at break, where a tremendous increase in flexibility can be observed for dry PHB-HV and also, but less dramatic, for dry samples of PLLA and PHB: The addition of 50 wt.-% TBA increased the elongation at break of PHB-HV by almost 9000%, followed far behind by PLLA with 530%, and PHB with 240% (Figure 4-26). In the

water-swollen state, PHB-HV loses flexibility with increasing TBA content, but crosslinked PHB-HV still elongates at least 10 times more than the native PHB-HV reference (Figure 4-27). On crosslinked PHB and PLLA samples, water has a plasticizing effect leading to higher strains at break with higher TBA contents. Therefore, the values for the strain at break of swollen PHB- and PLLA-based networks were slightly higher than those of the dry materials.

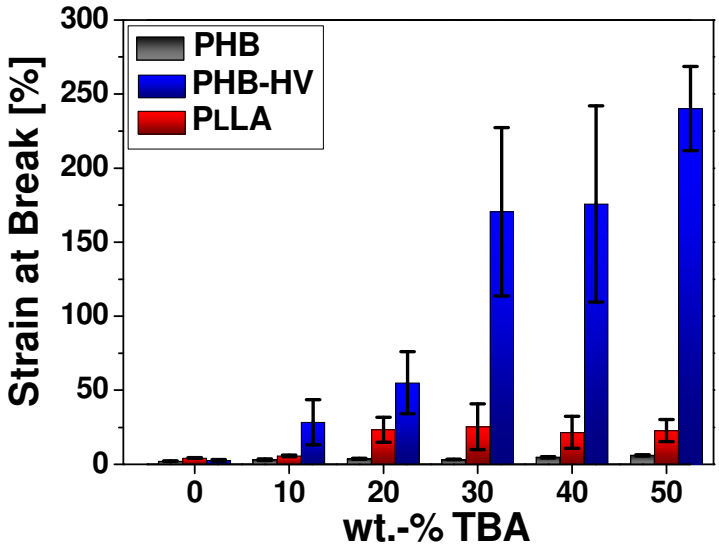

Figure 4-26: Elongation at break of dry samples of PHB-, PHB-HV-, and PLLA/TBA networks.

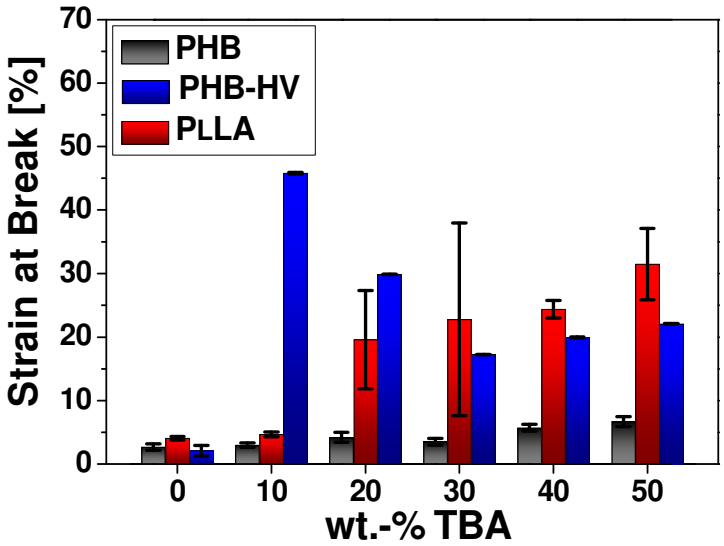

Figure 4-27: Elongation at break of water-swollen samples of PHB-, PHB-HV-, and PLLA/TBA networks.

All in all, crosslinking of the biopolyesters PHB, PHB-HV, and PLLA with TBA novel materials with modified mechanical parameters. The crosslinking routine enables for the manipulation of the swelling behavior in apolar and polar solvents and can yield stronger (PHB) and considerably more flexible materials (PHB-HV, PLLA, and PHB) that have potential for applications in medicine, especially in orthopedics.

4.4.2.4. Hydrolysis of PHB and PHB/TBA Copolymer Networks

Considering the potential application of PHB and PHB/TBA networks in the medical field, hydrolysis experiments were carried out in order to identify potentially harmful degradation products. Additionally, the recovery rate of TBA from the crosslinked samples and the purified gel fractions was determined. For hydrolysis, all samples were treated at a temperature of 160 °C in DCl/D_2O in closed vessels under microwave-assisted heating. After hydrolysis, all samples were completely dissolved. According to Figure 4-28 and in full agreement with literature, PHB is degraded into water-soluble PHB oligomers and crotonic acid (Figure **Fehler! Verweisquelle konnte nicht gefunden werden.**).[194] Due to the fast acid-catalyzed elimination of the hydroxy functionality of 3-hydroxybutyrate, no monomers were found in the hydrolyzed polymer solution.

Scheme 4-3: Structure formulas of PHB (left) and crotonic acid (right).

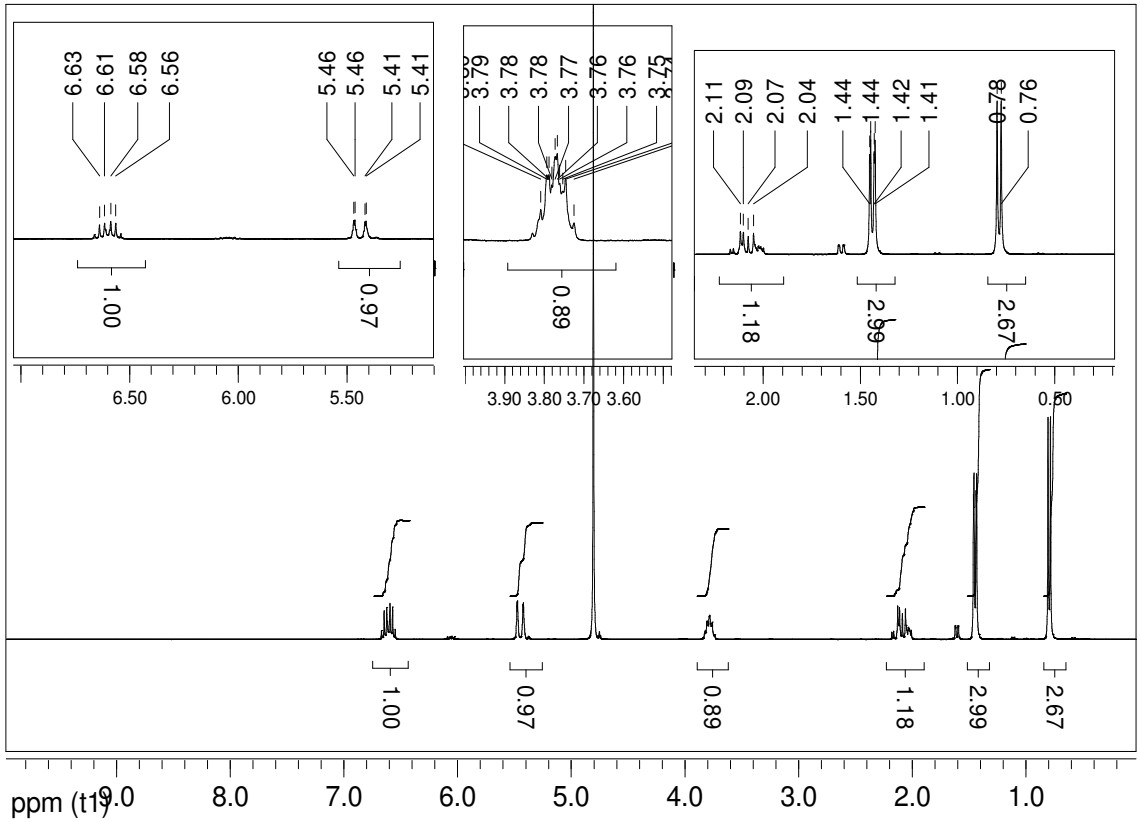

Figure 4-28: ^{1}H-NMR spectrum of PHB hydrolyzed with 1 M DCl/D_2O.

NMR data: δ (ppm) = 0.78 (2.67; t, 3·0.89 = 2.67 H, $^{3}J_{H,H}$ = 6.3 Hz, **H4**), 1.41-1.44 (2.99; m, 3·1 H = 3 H **H4'**), 2.04-2.11 (1.18; m, 2·0.59 H = 1.18 **H2**), 3.74-3.80 (0.89, m, 0.89 H, **H3**), 5.41-5.46 (0.97; m, 0.97 H, **H2'**), 6.54-6.66 (1.00; m, 1 H, **H3'**).

The ^{1}H-NMR spectrum of the purified gel fraction of PHB crosslinked with 50 wt.-% TBA shows the 12 protons from the crosslinker at 3.18-3.41 (Figure 4-29). From the molar ratios between PHB oligomers/crotonic acid and the TBA protons, the recovery rate was calculated for the purified gel fractions as well as the entire crosslinked PHB/TBA samples (Figure 4-30). For the purified gel fraction, good agreement with the theoretical values was achieved, while the recovery rate for TBA and TBA derivatives in the entire samples was low. Considering the increasing difference between theoretical and the experimental ratios with increasing TBA content, it was assumed that the missing amount TBA was lost due to side reactions that mainly form nitrous oxides that are not detectable by ^{1}H-NMR analysis.

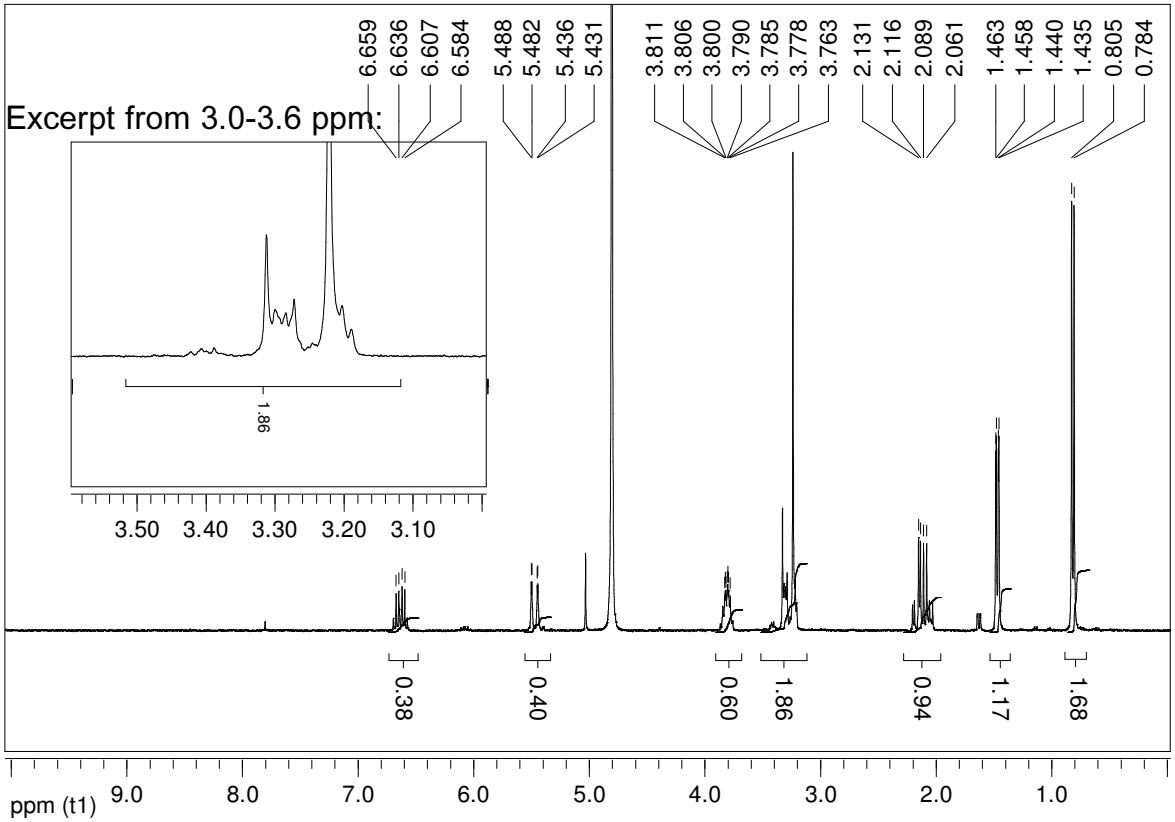

Figure 4-29: Representative ^{1}H-NMR spectrum of the purified gel fraction of PHB crosslinked with TBA (50 wt.-%) hydrolyzed with 1 M DCl/D_2O.

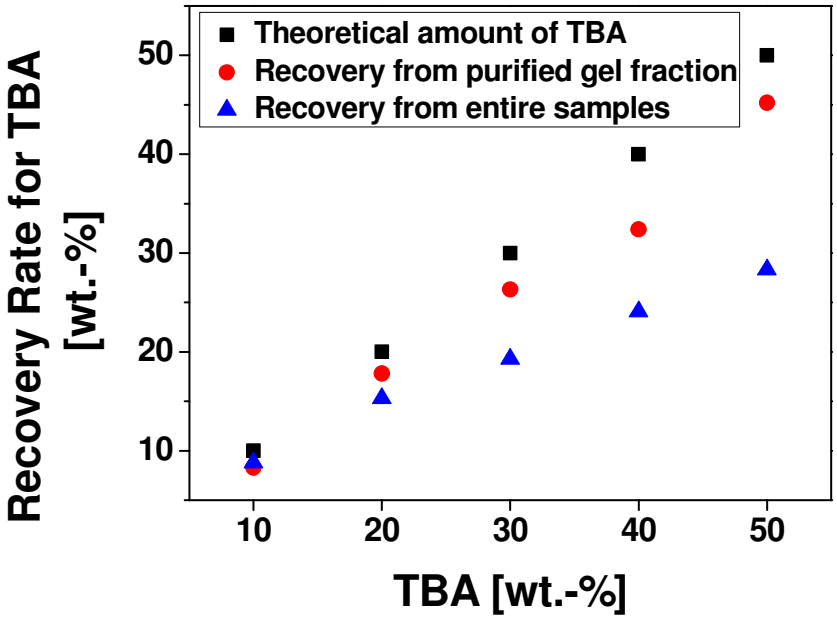

Figure 4-30: Recovery of TBA and TBA derivatives from entire samples, purified gel fractions, and comparison with the theoretical value.

4.5 Surface Modification of Injection-Molded PHB

With the advent of polymeric materials in medical applications, surface modification of polymer-based materials has frequently been discussed as a method for the increase of biocompatibility. Surface modification aiming at the increase of the material's hydrophilicity has been studied by a variety of working groups worldwide, for hydrophilicity is of considerable importance for applications of polymers in physiological environments. Besides surface functionalization and grafting of hydrophilic polymers, plasma techniques are among the most abundant processes used for surface modification of polymer-based materials.

4.5.1 O_2-Plasma Modification of PHB Surfaces

For O_2-plasma plasma modification of injection-molded PHB, flat shoulder test bars were subjected to O_2-plasma treatment and subsequently characterized by means of contact angle measurements with water and diiodomethane from which the surface energy was calculated according to the Owens-Wendt-Rabel-Kaelble method (see chapter 3.4.2.2). Injection-molded samples of PHB were treated in a plasma oven for times ranging from 0 to 8 min and characterization was done by means of contact angle measurements, the results of which are summarized in Figure 4-31. In good agreement with literature reports, the water contact angles decreased significantly from 70 to less than 40° after two min of treatment time; continued treatment of 4-8 min yielded surfaces with water contact angles of as low as 20°, indicative of significantly increased surface hydrophilicity. The contact angles for the apolar solvent diiodomethane, on the other hand, did not change to a significant extent in the course of plasma treatment. This observation can be attributed to the fact that the surface modifications achieved using O_2-plasma are based on surface oxidization reactions yielding polar groups like –COOH, =O, and –OH. These functional groups contribute to changes in the polar part of the surface energy rather than of the dispersive one. The observations and the related explanation are supported by the surface energy displayed in Figure 4-32.

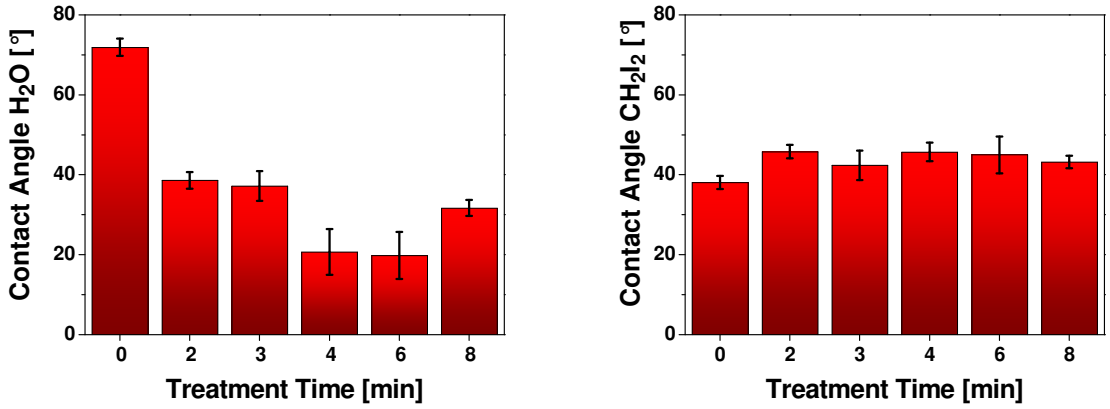

Figure 4-31: Water- (left) and diiodomethane (right) contact angles of O_2-plasma treated PHB samples.

As stated before, the polar part of the surface energy is significantly increased by O_2-plasma treatment resulting in maximum surface energy of up to 70 $mN \cdot m^{-1}$ compared to 43 $mN \cdot m^{-1}$ for the native surface. At the same time, the contribution of the dispersive component remains nearly unchanged by plasma treatment.

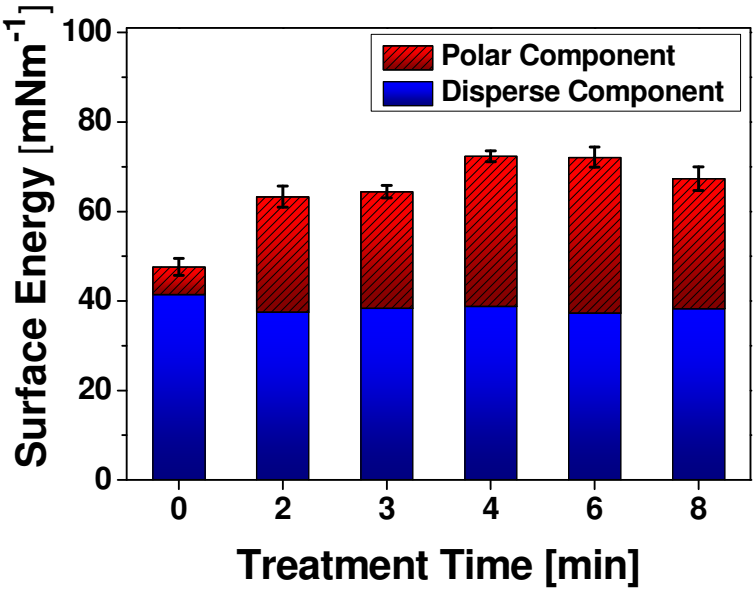

Figure 4-32: Surface energy calculated from the water- and diiodomethane contact angles of O_2-plasma treated PHB samples.

When plasma techniques are used for surface manipulation, surface ageing is considerably important, because surface rearrangement reactions can lead to

complete regression of the contact angles. For that reason, additional samples were prepared according to the same routine and left for ageing under ambient conditions. The influence of time-dependent regression of the surface energy is displayed in Figure 4-33. In agreement with literature, the comparison between the native untreated reference and the aged O_2-plasma treated samples reveals a relatively short-lived character of the oxidization-induced surface changes: While most of the formerly increased surface energy is lost already after 4 days, 12 days appear to be enough for the PHB surface to regain its original surface state in terms of surface energy and wettability.

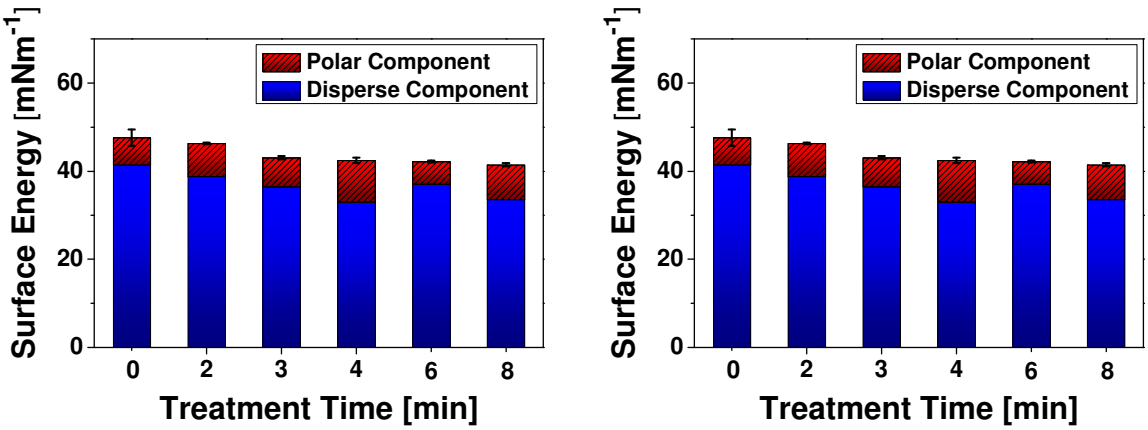

Figure 4-33: Surface energy calculated from the water- and diiodomethane contact angles of O_2-plasma treated PHB samples after ageing for 4 (left) and 12 days (right).

The results from the O_2-plasma treatment of PHB surfaces suggest that enhanced wettability of the naturally hydrophobic polyester can be achieved within 4-6 min in an inexpensive, fast and easily accessible process. Nevertheless, the shelf-life of these modified surfaces is very short, but methods as simple as storage in water, longer treatment times, and thermal ageing have been proposed and proven to partially overcome hydrophobic recovery.[195-197]

4.5.2 Surface Roughness of Injection-Molded PHB Using O_2-plasma, Mechanical, and Chemical Surface Treatment

Another important issue related to surfaces of polymeric materials in medical applications is the surface roughness, which has been shown to have great influence on the biocompatibility, cell adhesion promotion, and osseointegration. Therefore, the influence of different treatment techniques on the surface roughness of injection-molded PHB was characterized by means of focus variation microscopy. Small cylindrical PHB pins with a size of 1.5 x 8 mm were produced by injection-molding and subjected to surface treatment using Mg powder, O_2-plasma, and a combination of acidic surface hydrolysis and Mg powder treatment. Mg powder treatment was done using Mg powder with two different particle sizes, namely 297 µm (Mg I) and 44 µm (Mg II) average particle size. The PHB samples as well as the Mg powder were placed in a glass vial and ultra-sonicated in deionized water for 30 min. Preceded by acid treatment in concentrated HCl in a microwave reactor for 10 min, the same procedure was applied according to the routine described in chapter 4.5.1 on the other group of pins. O_2-plasma treatment was applied for 8 min on the third group of pins. All pins were subjected to focus variation microscopy and the surface roughness parameters R_a and R_q were calculated from the measured surface area with a size of 290 x 220 µm. The representative arbitrarily colored 3D-reconstructed microscopic pictures are summarized in Figure 4-34. According to the 3D-reconstructed surfaces, Mg powder treatment seems to have minimal influence on the surface morphology in comparison to the native untreated surface (Figure 4-34, a, c, and d), whereas the O_2-plasma treated surface shows a slightly different surface state (b). The most pronounced changes in surface morphology were obtained with the combined method of surface hydrolysis and subsequent Mg powder treatment (e, f). For more precise comparison, the calculated values for R_a and R_q of all characterized surfaces are summarized in Figure 4-35. In accordance with the optical appearance of the surfaces, Mg powder treatment resulted only in minor increase of the surface roughness, whereas O_2-plasma treatment yielded approx. 20% increase in R_q. The highest values for R_a and R_q were achieved using surface hydrolysis followed by magnesium powder treatment; maximum R_q in the range of 1.5 µm was realized.

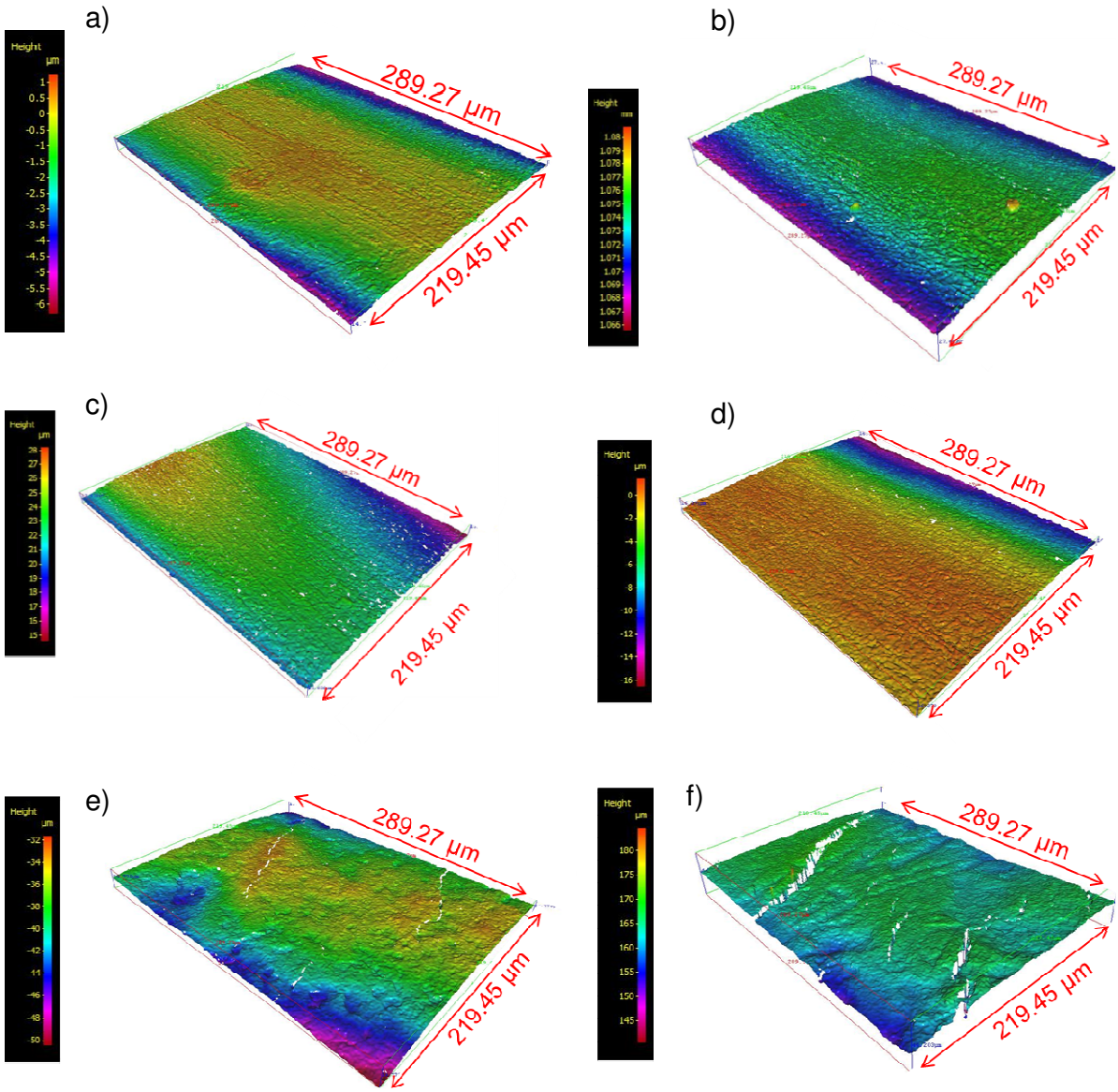

Figure 4-34: Representative 3D-reconstructed surface topologies of native PHB- (a), O_2-plasma treated PHB- (b), 297 µm Mg powder treated PHB- (c) 44 µm Mg powder treated PHB- (d), HCl and 297 µm Mg powder treated PHB- (e), and HCl and 44 µm Mg powder treated PHB-samples (f).

The more pronounced impact of the combined method of surface hydrolysis and Mg powder treatment can be explained by a softening effect of HCl treatment facilitating the attack of the Mg particles.

Higher surface roughness and wettability of polymer and metal-based implant materials are known to have positive influence on cell adhesion, strength and proliferation as well as enhanced osseointegration.[198;199]

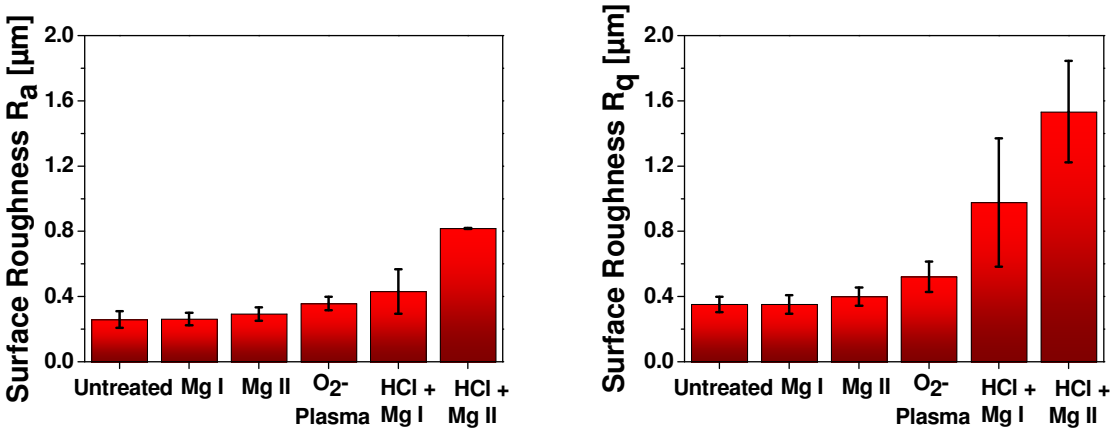

Figure 4-35: Summarized values for R_a (left) and R_q (right) of differently treated PHB surfaces.

Hence, the surface treatment of hydrophobic polymers using surface hydrolysis, Mg particle surface blasting, and O_2-plasma developed in the present work can be described as useful methods for the increase of surface roughness on the one hand, and for increased surface energy and wettability on the other hand.

5 Summary

The aim of the present work was the development of polymer-based materials for medical applications, especially for the field of orthopedic surgery. Due to their biodegradability and biocompatibility, biopolyesters were chosen as substance class for the experiments. As candidates, poly(3-hydroxybutyrate) (PHB), the copolymer poly(3-hydroxybutyrate-*co*-3-hydroxyvalerate) (PHB-HV), and poly(lactic acid) (PLA) were used. When using biopolyesters, challenges arise from their relatively low stiffness, especially in comparison to metal-based materials, their low surface hydrophilicity, and the frequently too low resorption rate in physiological environments. For overcoming these bottlenecks, different approaches to manipulate the mechanical stability, the hydrophilicity, and the surface state of bioresorbable implant materials were followed. The approaches can roughly be divided in two main classes, namely the physical approach based on mixing and physical treatment of implant materials and the chemical approach aiming at the alteration of the polymer-based materials' mechanical, physico-chemical, and chemical characteristics.

Starting with mixing polymeric materials with inorganic fillers in order to improve X-ray visibility, mechanical stability and resorption rate of the resulting materials, composites based on polymers and ZrO_2, the bone substitution material Herafill, and magnesium particles were produced. Additionally, Mg-alloy-based pins and copper-coated substrates were coated with PHB, PHB-HV, PLDLA, and bisazide-crosslinked PHB and PHB-HV.

The addition of Herafill and ZrO_2 to PHB led to increased X-ray visibility and potentially increased biocompatibility, but did not yield materials with higher mechanical strength. In fact, the addition of ZrO_2 to PHB decreased the Young's modulus, the tensile strength, and the elongation at break, while Herafill showed some increase of the Youngs's modulus and the tensile strength, most likely due to the seeding ability of calcium carbonate, the main ingredient of Herafill. The addition of Mg powder to PHB, on the other hand, yielded higher Young's moduli of approx. 4 GPa compared to 3 GPa determined from tensile testing of the native pure PHB

samples. Nevertheless, high amounts of Mg powder did not have any positive influence on the tensile strength and the flexibility of the resulting composite materials.

Polymer coatings applied on metal surfaces showed scratch resistance towards a diamond stylus at forces of up to 2-3 N maximum force before mechanical failure. The coatings based on PHB, PHB-HV, PHB/TBA, and PLDLA, revealed sufficient uniformity and surface roughness that increased in the order Mg native < native PHB coating < PLDLA coating < PHB/TBA coating and reached maximum values of aprox. 350 nm.

The chemical modification of the polyesters described in this work was motivated by the idea that crosslinking can alter the mechanical stability, the chemical behavior, and the physico-chemical characteristics of polymers. Due to the relatively low reactivity of saturated polyesters, 2,6-bis(4-azidobenzylidene)-4-methylcyclohexanone (BA), a UV-inducible, fully conjugated bisazide from which nitrenes as active species can be formed, was investigated as model substance for crosslinking thin films of PHB-HV. The results showed significant extents of crosslinking of over 90% gel fraction at room temperature at irradiation times of less than one minute with low crosslinker contents. As suggested by the Charlesby-Pinner analyses, the process has high reproducibility and a BA content of 3 wt.-% according to the polymer mass was found to yield high rates of crosslinking (v_q) compared to relatively low rates of chain scission (v_p). A further increase of the BA content resulted in significantly increased chain scission to the disadvantage of crosslinking. Additionally, the optimized polymer-crosslinker system could successfully be used as a negative photo-resist in a two-step photolithographic process (Figure 5-1), and the proof of concept for crosslinking biopolyesters with bisazides was transferred for PHB. Proven by ^{1}H-NMR-spectroscopy and reference crosslinking experiments using benzophenone, the crosslinking mechanism of saturated polyesters with bisazides was verified: Bisazides induce network formation with saturated aliphatic polyesters by insertion into the polymer matrix.

Inspired by the UV-induced crosslinking of biopolyesters, the approach was expanded to other bisazides and the temperature-inducible, hydrophilic bisazide tri(ethylene glycol) bis(azidoformate) (TBA) was chosen for further investigations. Using high

amounts of crosslinker of up to 50 wt.-% with respect to polymer mass, PHB, PHB-HV, and PLLA were treated thermally under vacuum. The resulting copolymer networks of polyesters and amine-linked ethylene glycol showed medium to high gel fractions of up to 40 (PHB, PLLA) and 80% (PHB-HV), significant swelling in apolar solvents like DCM and low swelling in polar solvents like water.

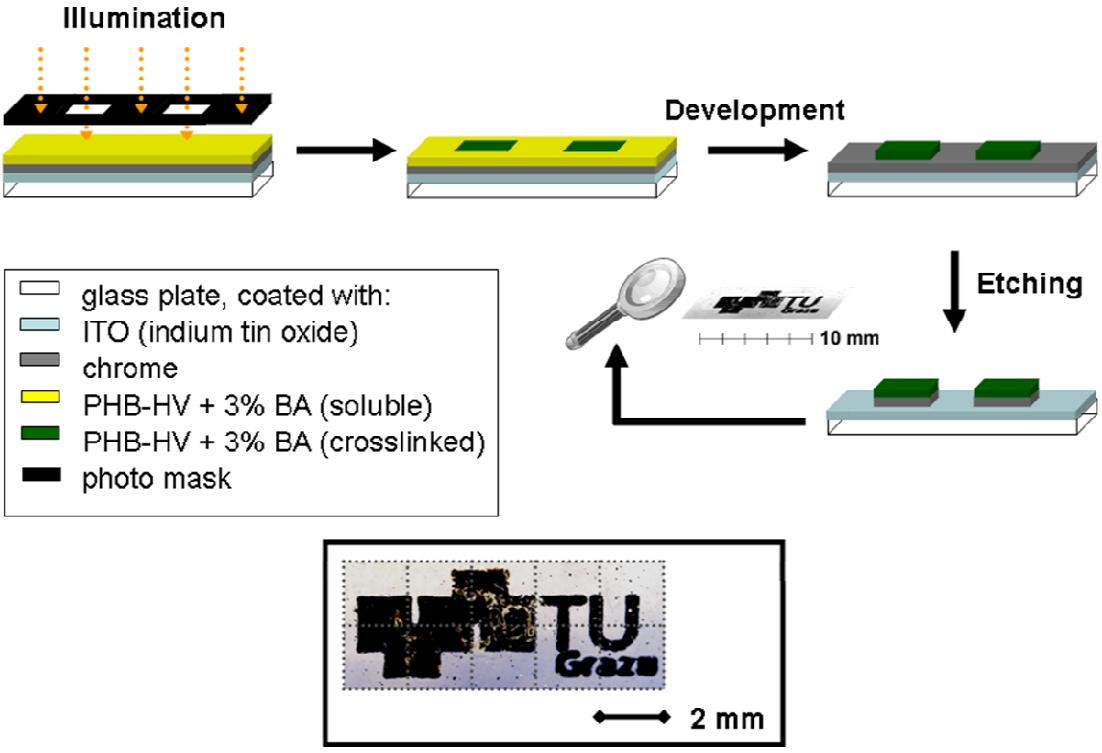

Figure 5-1: Scheme of the two-step photolithographic process on glass/ITO/chrome substrates using PHB-HV with 3 wt.-% BA as negative photoresist.

The ability to swell in water enables a material to expand in a physiological environment and can help to increase the interaction between the implant material and the surrounding tissue, which is of special interest in orthopedics. In terms of mechanical characteristics crosslinking had a negative impact on the Young's modulus of PHB-HV and PLLA, while PHB/TBA networks revealed higher tensile strength upon crosslinking. The most interesting results were obtained for the elongation at break, representing the flexibility of the polymer networks. While the elongation at break showed a 2-5-fold increase for PHB and PLLA, crosslinked PHB-HV elongated up to 90 times more than the native reference. Additionally, hydrolysis experiments of PHB/TBA networks gave good recovery rates for TBA and its derivatives and no toxic hydrolysis products were found.

The last part of the present work was dedicated to the surface modification of injection molded PHB forms. Employing O_2-plasma techniques, the surface energy of PHB, indicating significantly increased surface hydrophilicity, could be raised from less than 50 to over 70 $mN \cdot m^{-1}$ (Figure 5-2), but without further surface treatment or specialized storage conditions this effect was reversible within days. Additionally, O_2-plasma could be proven to slightly increase the surface roughness of injection-molded PHB, while surface-blasting using ultra sonication with water and magnesium particles did not significantly influence the surface roughness.

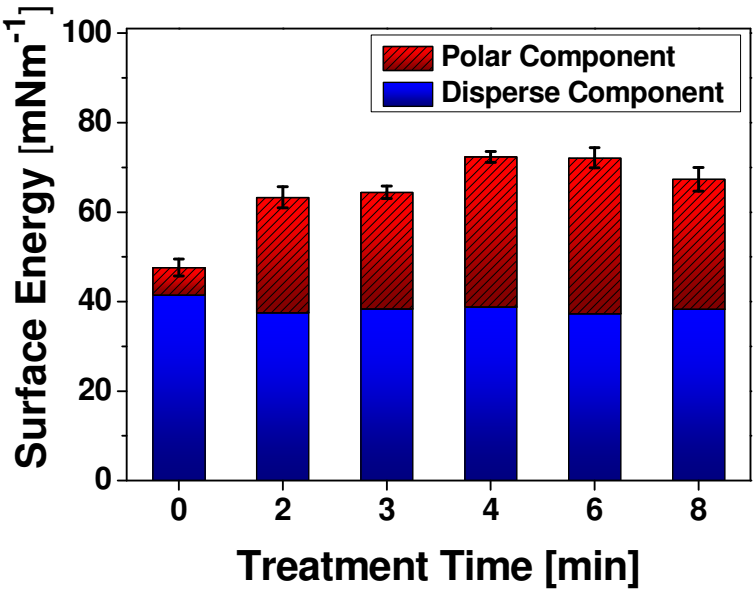

Figure 5-2: Surface energy calculated from the water- and diiodomethane-contact angles of O_2-plasma treated PHB samples.

In terms of enhanced surface roughness, a combined method of acidic surface hydrolysis for softening the top layer of the mold, followed by surface blasting with Mg particles was found to have the greatest influence on the surface topology and up to 1.5 µm surface roughness were achieved. This value is generally accepted to have positive influence on cell adhesion, strength, and viability as well as on the osseointegration of orthopedic implants.

5.1 Abstract

The application of biopolyester-based materials in orthopedic surgery has gained considerable attention over the past decades because of their good biocompatibility, biodegradability, and versatile nature with respect to the different monomer units that can be incorporated in the respective (co-)polymers. Nevertheless, there are still some challenges to be handled, such as too low stiffness and mechanical stability, too low degradation rates and partially limited biocompatibility caused by the hydrophobic nature of these compounds.

The aim of the present work was the development of novel biopolyester-based materials for applications in orthopedic surgery, especially for bone fracture fixation devices. As basic materials, poly(3-hydroxybutyrate) (PHB), poly(3-hydroxybutyrate-*co*-3-hydroxyvalerate) (PHB-HV), and poly(lactic acid) (PLA) were considered. In order to overcome the abovementioned shortcomings, different strategies aiming at the alteration of the bulk material's characteristics and the manipulation of the surface characteristics were followed. Starting with the production of composites from PHB with inorganic fillers, especially magnesium powder, improvements in terms of mechanical strength were achieved. The UV-induced crosslinking of PHB-HV and PHB films with a fully conjugated bisazide BA, on the other hand, revealed high gel fractions within short irradiation times at low to moderate crosslinker contents. Additionally, the insertion mechanism on which the bisazide-induced crosslinking of polyesters is based was verified and the BA-polyester system was used as a negative photoresist in photolithography. Based on the knowledge derived from bisazide-based UV-crosslinking, another temperature-inducible hydrophilic group-bearing crosslinking agent TBA was chosen for the preparation of polymer networks from PHB, PHB-HV, and PLLA. These polymer networks revealed medium to high gel fractions at high crosslinker contents and were proven to be mechanically stronger (PHB) and much more flexible (PHB, PHB-HV, and PLLA). Given the hydrophilic nature of TBA and the hydrophobic behavior of the polyesters used, the resulting crosslinked networks showed significant swelling in dichloromethane and swelling in water, enabling the materials for physical adaption to the respective implantation site (e.g. bone) and potentially increased biocompatibility. Eventually, the treatment of injection-molded PHB with O_2-plasma, Mg particle surface blasting and acidic surface hydrolysis

yielded hydrophilic surfaces with a roughness in a good range for enhanced cell adhesion and osseointegration.

5.2 Kurzfassung

Wegen ihrer guten Biokompatibilität, biologischen Abbaubarkeit und der Vielzahl an Monomeren, aus denen sie aufgebaut werden können, sind Biopolyester-basierte Materialien während der letzten Jahrzehnte in den Fokus der orthopädischen Chirurgie gerückt. Nichtsdestotrotz weisen diese Verbindungen noch Optimierungsbedarf in Bezug auf Festigkeit, Abbaurate und, wegen ihrer hydrophoben Eigenschaften, teilweise zu geringen Biokompatibilität auf.
Das Ziel der vorliegenden Arbeit war die Entwicklung von neuen biopolyesterbasierten Materialien für Anwendungen im orthopädischen Bereich, insbesondere als Materialien zur Schienung und verbesserten Heilung von Knochenbrüchen. Als Grundmaterialien wurden die Polymere Poly(3-hydroxybutyrat) (PHB), das Copolymer Poly(3-hydroxybutyrat-*co*-3-hydroxyvalerat) (PHB-HV) und Poly(Milchsäure) (PLA) verwendet. Hierbei wurden verschiedene Strategien zur Verbesserung der Eigenschaften des Bulkmaterials und der Oberfläche entwickelt. Durch die Herstellung von Kompositmaterialien aus PHB und anorganischen Füllstoffen konnte, vor allem durch die Zugabe von Magnesiumpartikeln, eine Erhöhung der Festigkeit erzielt werden. Die chemische Vernetzung von PHB-HV und PHB mit einem konjugierten Bisazid BA führte wiederum zu hohen Vernetzungsgraden nach kurzen Belichtungszeiten mit niedrigen bis mittleren Vernetzergehalten. Zusätzlich konnten der der bisazidbasierten Vernetzung von Polyestern zugrunde liegende Mechanismus aufgeklärt und das optimierte BA/Polyester System als Photoresist in der Photolithographie eingesetzt werden. Mit den Erkenntnissen aus den UV-Vernetzungsexperimenten wurde ein weiteres, thermisch induzierbares Bisazid TBA mit hydrophilen Funktionalitäten für die Vernetzung von PHB, PHB-HV und PLLA ausgewählt. Die so hergestellten Polymernetzwerke zeigten mittlere bis hohe Vernetzungsgrade bei hohen Vernetzerkonzentrationen, höhere mechanische Stabilität (PHB) und deutlich erhöhte Flexibilität (PHB, PHB-HV und PLLA) verglichen mit den nativen Polyestern. Durch die hydrophoben Eigenschaften der Ausgangspolymere und die hydrophilen Gruppen des Vernetzers zeigten alle

Polyester/TBA Netzwerke starke Quellung in Dichlormethan und leichte Quellung in Wasser. Dementsprechend kann das Material bei Einsatz in physiologischen Umgebungen Wasser aufzunehmen und sich so physikalisch der Umgebung (z.B. dem Knochen) anzupassen. Zusätzlich kann zusammen mit der Hydrophilie auch die Biokompatibilität erhöht werden. Zuletzt konnten mit der Oberflächenbehandlung von spritzgegossenem PHB durch O_2-Plasma, mechanische Behandlung mit Magnesiumpartikeln und saure Oberflächenhydrolyse stark erhöhte Benetzbarkeit (Hydrophilie) und erhöhte Oberflächenrauigkeiten in einem für die Osseointegration förderlichen Bereich erreicht werden.

6 Experimental

6.1 Materials

The following chemicals were bought from or supplied by the indicated sources and used without further purification.

Chemical	Supplier	Purity
Tri(ethylene glycol) bis(chloroformate)	Sigma	97%
Dichloromethane	Sigma	≥99%
Chloroform	Sigma	
Sodium sulfate	Sigma	
Sodium azide	Acros	99%
2,6-bis(4-azidobenzylidene)-4-methylcyclohexanone	Sigma	97%
Hydrochloric acid	Fluka	12 M
Deuterium chloride 1 M in deuterium oxide	ABCR	
Magnesium powder (44 µm particle size)	ABCR	99.8%
Magnesium powder (297 µm particle size)	ABCR	99.8%
Zirconium oxide	Heraeus Medical	
Herafill	Heraeus Medical	
Poly(L-lactide) Resomer 206S	Aldrich	
Poly(D,L-lactide) Resomer 203	Aldrich	

Commercially available poly(3-hydroxybutyrate) homopolyester (Biocycle, Brazil) was provided by Martin Koller of the Institute of Biotechnology and Biochemical Engineering at the Graz University of Technology. Purification was achieved by repeatedly dissolving the polymer in chloroform and subsequent precipitation in ethanol. The PHB homopolyester was delivered in three different batches. Samples of poly(3-hydroxybutyrate)-*co*-(3-hydroxyvalerate) (PHB-HV) with 18.25 mol-% of HV were also provided by Martin Koller and were purified by soxhlet extraction in ethanol

for 24 h, followed by two precipitation cycles, in which the copolymer was dissolved in dichloromethane (within 4–5 days under vigorous stirring), filtered, and reprecipitated in ethanol. The PHB-HV copolyester was purified in two batches. The average molecular weights and the polydispersity indices were determined by GPC measurements and are summarized in Table 6-1; the batches used are indicated in the dedicated subchapters.

Table 6-1: PDI values and number average molecular weights of the different polymer batches used.

Polymer	M_n [kDa]	PDI
PHB commercial grade	107	2.8
PHB batch I	165	2.4
PHB batch II	87	3.1
PHB batch III	128	2.7
PHB-HV batch I	102	2.8
PHB-HV batch II	191	2.4
PHB-HV commercial grade	173	2.4

The bone substitution material Herafill® was provided by Heraeus Medical and used as received. The material is composed of calcium carbonate, calcium sulfate dihydrate, and hydrogenated triglyceride, the proportions of which were not provided by the supplier.

Tri(ethylene glycol) bis(azidoformate) was synthesized from tri(ethylene glycol) bis(chloroformate) using a previously published recipe in 98% yield.[200] The purity was confirmed by ^{1}H-NMR-spectroscopy. **^{1}H-NMR data:** δ (ppm) = 3.64 (s, 4 H); 3.69-3.76 (m, 4 H); 4.31-4.39 (m, 4 H).

6.2 Methods

6.2.1 Melt Compounding and Injection-molding

For the preparation of three-dimensional molds, the dedicated polymers were melt-compounded in a Haake MiniLab Micro-compounder and subsequently injection-molded using a DSM Research 3.5 mL injection-molding machine (Figure 6-1).
For all experiments, the pressure limit was set to 5 bar and two different kinds of molds were used: A shoulder test bar mold type 1BA for mechanical testing according to the ISO-standard 527 and a nail-shaped mold for the production of small, cylindrical pins. The compounder screws were set to counter-rotation at a speed of 100 rpm and the temperatures were adapted individually for each polymer/mixture and are described in the following chapters. For the characterization of the mechanical behavior of PHB and PHB composites, at least three samples of each mixture were prepared for tensile testing according to the ISO standard 527.

6.2.1.1. PHB-Homopolyester

The preparation of injection-molded forms from the PHB homopolyester was done using the parameters summarized in Table 6-2. In order to provide optimum mixing and to keep thermal and shear force-induced degradation of the material at minimum, the mixing time following the filling procedure was set to 2 min.

Table 6-2: Parameters for melt-compounding and injection-molding of PHB homopolyester.

	Mass [g]	Time [s]	Vent-position	Rotation speed [rpm]
Filling I	2.00	30	Bypass	100
Filling II	2.00	30	Bypass	100
Filling III	2.00	30	Bypass	100
Mixing		120	Bypass	100
Cylinder filling		60	Flush	150
Injection-molding		15		
Pressing		10		

PHB from every batch (commercial grade and batch I-III) was used for the determination of PHB's mechanical characteristics as well as for referencing the PHB -based composite materials.

6.2.1.2. PHB and PHB-Based Composite Materials

6.2.1.2.1 PHB/ZrO_2/Herafill Composites

For the preparation of highly filled PHB-based composite materials, the temperatures had to be adjusted in order to provide optimum conditions for mixing and injection-molding (Table 6-3). The parameters for filling and injection-molding were employed according to 6.2.1.1 for the preparation of all PHB/ZrO_2/Herafill composites.

Table 6-3: Temperature parameters used for melt-compounding and injection-molding of PHB composite materials.

Zone	Temperature [°C]
Compounder	177
Cylinder	170
Mold	106

Three specimens each were produced with 3 wt.-% ZrO_2, 3 wt.-% ZrO_2 + 10 wt.-% Herafill, and 3 wt.-% ZrO_2 + 30 wt.-% Herafill, respectively. For the PHB/ZrO_2/Herafill composites, commercial grade PHB was used.

6.2.1.2.2 PHB/Mg Powder Composites

Composite materials based on PHB and magnesium powder with an average particle size of 44 µm were prepared using precleaned PHB from batch II. Employing the same temperatures as in 6.2.1.2.1, the filling procedure and the mixing time had to be adapted in order to prevent clogging of the compounder and inclusion of air bubbles in the resulting shoulder test bars (Table 6-4). Mg contents of up to 50 wt.-% with respect to polymer mass were properly processed, while higher contents of Mg led to compounder clogging and excessive bubble formation. PHB and Mg powder were mixed prior to filling the compounder in three steps.

Table 6-4: Parameters for melt-compounding and injection-molding of PHB/Mg powder composites.

	Mass [g]	Time [s]	Vent-position	Rotation speed [rpm]
Filling I	2.00	30	Bypass	100
Filling II	2.00	30	Bypass	100
Filling III	2.00	30	Bypass	100
Mixing		60	Bypass	100
Cylinder filling		60	Flush	100
Injection-molding		15		
Pressing		10		

6.2.1.2.3 PHB/BA-Photoinitiator Composites

For the preparation of crosslinked PHB samples with the bisazide-photoinitiator BA, the mixing time had to be increased in order to push out the in-situ formed nitrogen gas (Table 6-5). The temperatures were set to the same values as in 6.2.1.2.1.

Table 6-5: Parameters for melt-compounding and injection-molding of PHB/BA-photoinitiator mixtures.

	Mass [g]	Time [s]	Vent-position	Rotation speed [rpm]
Filling I	2.00	30	Bypass	100
Filling II	2.00	30	Bypass	100
Filling III	2.00	30	Bypass	100
Mixing		240	Bypass	100
Cylinder filling		60	Flush	100
Injection-molding		15		
Pressing		10		

6.2.2 Polymer Coatings on Metal Substrates

6.2.2.1. PHB, PHB-HV, PHB/TBA, and PHB-HV/TBA Coatings on Copper Coated Substrates

Coatings of PHB (batch III), PHB with 10 wt.-% TBA, PHB-HV (batch II) and PHB-HV with 10 wt.-% TBA were prepared from spin-coating (20 s, 1000 rpm) solutions of the respective polymers in DCM (20 $mg \cdot mL^{-1}$) onto copper-coated FR4 substrates. In order to induce crosslinking of the polymer/TBA samples, the dried films were subjected to thermal treatment at a temperature of 150 °C under vacuum for 1 h. All samples were characterized by scratch resistance experiments (chapter 6.3.13).

6.2.2.2. Coating of Mg LV1 Pins

Prior to coating, the native Mg pins were roughened by immersion in an aqueous HCl solution at pH = 2. The pretreated Mg pins were coated from solutions of PHB (batch III), PHB/TBA, and PDLLA in chloroform (15 $mg \cdot mL^{-1}$) and subsequently air-dried. The coating procedure was repeated until the targeted coating mass of approx. 0.4 mg per pin was reached. After coating, the PHB/TBA coatings were subjected to thermal

treatment under vacuum at a temperature of 150 °C for 1 h. The coatings were subjected to characterization by means of focus variation microscopy (FVM) in collaboration with the Polymer Competence Center Leoben GmbH using the Alicona Infinite Focus measurement system (chapter 6.3.9).

6.2.3 UV-Induced Crosslinking of PHB-HV and PHB using BA

Thin films with a height of a few µm consisting of PHB-HV (batch I) and the photoinitiator (1, 2, 3, 4, and 5 wt.-% with respect to polymer mass) 2,6-bis(4-azidobenzylidene)-4-methylcyclohexanone (BA) were prepared from spin-coating freshly prepared solutions of 20 $mg \cdot mL^{-1}$ polymer in DCM on CaF_2 plates (20 s, 1000 rpm). After spin-coating, the dry films were characterized by means of FT-IR-spectroscopy and subsequently irradiated individually under nitrogen purge using a mercury lamp set to a power of 3000 $mW \cdot cm^{-2}$. The distance between sample and the UV-lamp's lightguide was adjusted to 7 cm. After UV-irradiation, the samples were developed by immersion in DCM for 20 min and after drying, another set of FT-IR-spectra was recorded. From the difference in the height of the ester band at 1724 cm^{-1} before and after development, the residual amount of polymer film, representing the insoluble polymer/BA gel fraction, was calculated (equation 4-1). The gravimetrical control experiments were carried out by irradiating films of PHB-HV (batch II) and 3 wt.-% of BA with a mass of approx. 80 mg for the targeted times. After development in DCM, the solvent was removed by filtration and the residual mass was determined gravimetrically. All experiments were carried out in triplicate. For the GPC analysis of the soluble fractions, several polymer-coated CaF_2 plates were irradiated for the targeted times and developed in DCM while the soluble fractions were collected. After solvent evaporation, GPC measurements were carried out according to 6.3.3. The proof of concept for crosslinking of PHB homopolyester (batch III) was brought forward according to the same routine with a BA content of 3 wt.-%.

6.2.4 Temperature-Induced Crosslinking of PHB, PHB-HV, and PLLA Using TBA

Due to challenges arising from the melt-compounding and injection-molding of crosslinked polymer samples, the processing route was changed to platen pressing. Solutions of the respective polymer (PHB batch III, PHB-HV batch II, and PLLA) and different amounts of tri(ethylene glycol) bis(azidoformate) TBA (10, 20, 30, 40, and 50 wt.-% with respect to polymer mass) in DCM were prepared. After solvent evaporation, the mixtures were ground and dried again overnight under vacuum. The dry ground mixtures were pressed in a vacuum platen press with a platen pressure of 5 bar (Figure 6-2). Before heating was applied, the platen chamber was evacuated in order to prevent side reactions of TBA with oxygen. All samples, except for PHB-HV (170 °C) were heated to 180 °C and kept at the respective temperature for 10 min. This way, films with a height of approx. 200 µm were produced from which samples for tensile testing (4 x 2 x 0.2 mm), sol-gel experiments, swelling experiments, and hydrolysis were cut.

6.2.4.1. Sol-Gel Analyses, Swelling Experiments, and Tensile Testing

The TBA-crosslinked samples of PHB, PHB-HV, and PLLA were subjected to sol-gel analyses by thermal treatment in DCM at a temperature of 100 °C under microwave-assisted heating in closed vessels. After heating, the gel and the soluble fraction were separated and the mass of the gel fraction formed by crosslinking was determined gravimetrically. For the swelling experiments, purified gel fractions of PHB, PHB-HV, and PLLA crosslinked with TBA were immersed in DCM and water for at least 3 days until the maximum swelling degrees were reached. The amount of solvent taken up by the polymer networks was determined gravimetrically and the swelling degree was calculated according to equation 4-4.

The mechanical characterization of polyester/TBA networks was done with small specimen sizes (40 x 10 x 0.2 mm) in order to keep swelling-induced size changes at minimum and provide optimum comparability between the dry and the water-swollen

samples. Prior to testing the samples were immersed in water for at least 3 days. The principles based on which tensile testing was done and evaluated are described in chapter 6.3.10.

6.2.4.2. Hydrolysis of PHB/TBA Networks

The hydrolysis of PHB/TBA networks was done in 1 M DCl in D_2O at 160 °C in closed vessels under microwave irradiation. The resulting solutions were characterized by ^{1}H-NMR spectroscopy and the relative amounts of TBA as well as the degradation products derived from PHB degradation were determined.

6.2.5 Surface Modification of Injection-Molded PHB

6.2.5.1. O_2-Plasma Treatment

The surface modification of injection-molded PHB was done on flat shoulder test bars for contact angle measurements and on cylindrical PHB pins with a size of 1.5 x 8 mm for the surface roughness manipulation. All surfaces were etched with O_2-plasma in a Diener FEMTO Plasma System at a power of 100 W and a frequency of 40 kHz (Figure 6-3). Treatment times ranged from 1 to 8 minutes and, in order to provide reproducible surface states, both sides of the flat samples were etched individually. Characterization of O_2-plasma etched samples was done by contact angle and focus variation microscopy measurements.

6.2.5.2. Mg-Surface Blasting and Hydrolysis-Facilitated Surface Blasting Using HCl and Mg Particles

For surface manipulation, small cylindrical PHB pins (1.5 x 8 mm) were subjected to Mg particle surface blasting using magnesium powder with two different particle sizes (44 and 297 µm average particle size). Surface blasting was done by ultra sonicating the samples and the Mg particles in deionized H_2O for 1 h. Facilitated surface blasting

was done by pretreatment of the PHB samples in concentrated HCl at a temperature of 100 °C under microwave-assisted heating for 10 min. The surface-hydrolyzed samples were surface blasted in the same manner as the non-hydrolyzed samples. All surface treated as well as the native PHB reference samples were characterized by focus variation microscopy.

6.2.6 Contact Angle Measurements and Surface Energy

The static contact angle was measured under ambient conditions with an automatic goniometer Krüss DSA 100 employing the sessile drop method. For evaluation of the contact angle a drop of the dedicated testing liquid was applied on the surface using a microliter syringe. The analysis of the drop profile was done video-assisted using a CCD camera while the fitting procedure was carried out under software-assistance using the software package *"Drop Shape Analysis"*. Employing the tangent method 2, the function $y = a + b \cdot x + c \cdot x^{0.5} + \frac{d}{\ln x} + \frac{e}{x^2}$ was adjusted to the drop shape near the base line.[201]

The contact angle was determined from the slope in the triple point. As testing liquids deionized water (Milli-Q quality, 18 MΩ·cm) and diiodomethane were employed. For every sample and both testing liquids at least five single drops of 3 µL in volume were evaluated for the contact angles. The surface energy was subsequently calculated according to Owens, Wendt, Rabl and Kaelble using the following equation (see also chapter 3.4.2.2):

$$\underbrace{\frac{(1+\cos\Theta)\cdot\sigma_l}{2\cdot\sqrt{\sigma_l^D}}}_{y} = \underbrace{\sqrt{\sigma_s^P}}_{m}\cdot\underbrace{\sqrt{\frac{\sigma_l^P}{\sigma_l^D}}}_{x} + \underbrace{\sqrt{\sigma_s^D}}_{b} \qquad \textbf{Equation 6-1}$$

Θ represents the contact angle, σ_l^D and σ_l^P are the disperse and the polar component of the testing liquid's surface energy, and σ_s^D and σ_s^P represent the disperse and the polar component of the solid phase's surface energy.

6.3 Equipment

6.3.1 Melt-compounder and Injection-molding Machine

Figure 6-1: Haake MiniLab Micro Compounder (left) and DSM Research Injection Molding Machine (right).

The Haake MiniLab Micro-compounder is specially designed for compounding small amounts of material starting from 5.5 g, can be operated at temperatures of up to 350 °C and pressures of up to 200 bar, and is equipped with two, either co- or counter-rotating screws. During homogenizing, the vent inside the compounder is set to "*bypass*", while for obtaining the homogenized molten material, the vent can be set to "*flush*" and the material is extruded into the cylinder of the injection-molding unit. Using the DSM Research Injection Molding Machine, molten thermoplastic materials can be injection molded with a maximum pressure of 16 bar.

6.3.2 NMR Spectroscopy

All NMR-spectra were recorded on a Bruker Avance III 300 MHz NMR spectrometer. All polymer-spectra were recorded with a minimum delay of 5 s; in general, a

minimum number of 32 scans (^{1}H-NMR) was employed. As solvents, $CDCl_3$, D_2O, and CD_2Cl_2 were used. The following peak shapes are indicated: s (singlet), d (doublet), t (triplet), m (multiplet). For referencing, the residual solvent peaks were used.

6.3.3 GPC Analysis

The average molecular weights as well as the polydispersity indices were determined using gel permeation chromatography GPC. As eluent, a mixture of $CHCl_3$/Et_3N/^{iso}PrOH (94/4/2) was used. The GPC system consisted of a Merck Hitachi L-6000A pump, separation columns from Polymer Standards Service, 8\ 300 mm STV linear XL 5 µm-grade size, and a differential refractometer Waters 410 detector. For calibration, polystyrene standards from Polymer Standard Service were used.

6.3.4 UV-Lamp

For irradiating the thin films consisting of polymer and the photocrosslinker BA, a polychromatic mercury lamp EFOS Novacure from EXFO was used.

6.3.5 Spin-Coater

For the preparation of thin polymer films on CaF_2 platelets and copper coated FR4 substrates, a Karl Suss CT-62 Spin Coater was used at rotation speeds of 1000 rpm and an acceleration rate of 1000 rpm·s^{-1} for 20 s.

6.3.6 Laboratory Platen Press

For processing films of PHB, PHB-HV, PLLA, and polymer films crosslinked with TBA, a Collin P 200 Laboratory Platen Press was used (Figure 6-2). The press can be used at temperatures of up to 180 °C and pressures of up to 250 bar. The press is equipped with a vacuum pump and a water-cooling system.

Figure 6-2: Collin Laboratory Platen Press.

6.3.7 O_2-Plasma System

O_2-plasma treatment was done using a Diener FEMTO Plasma System at a power of 100 W and a frequency of 40 kHz (Figure 6-3). The oxygen gas flow was adjusted to 15 standard cubic centimeters per minute. The injection-molded PHB samples were placed inside the plasma system and treated for the targeted times.

Figure 6-3: Diener FEMTO Plasma System.

6.3.8 Biotage Initiator 8 Microwave Reactor

The Biotage Initiator microwave reactor was used for dissolving the polymers PHB, PHB-HV, and PLLA at elevated temperatures as well as for the sol-gel experiments of TBA-crosslinked polymer networks (Figure 6-4).

Figure 6-4: Initiator 8 microwave reactor from Biotage.

6.3.9 Focus Variation Microscope

For surface roughness measurements, a focus variation microscope type *Alicona Infinite Focus IFM G4* was used. Prior to the measurements, the polymer samples were sputtered with a 10 nm palladium layer to yield optimum contrast. The measurements were carried out with a cutoff wavelength of λ = 80 nm and the surface roughness parameters R_a and R_q of all polymer samples were calculated from the measured area of 290 x 220 µm. The polymer coated magnesium samples were not sputtered and the roughness parameters were calculated from profiles derived from the measured area. All roughness measurements were performed in duplicate. The FVM measurements were carried out in collaboration with the Polymer Competence Center Leoben GmbH and the Austrian Center for Electron Microscopy and Nanoanalysis (FELMI) at the Graz University of Technology.

6.3.10 Shimadzu AGS-X Universal Testing Machine

All tensile tests were performed using a Shimadzu AGS-X universal testing machine (Figure 6-5). The test mode was set to tensile and, depending on the samples, crosshead speeds of 5-10 mm·s^{-1} were used. For tensile testing according to the ISO standard 527, shoulder test bars type 1 BA were tested using a preload of 10 N, 100 mm gage length, and a crosshead speed of 10 mm·min^{-1}.[202;203]

Figure 6-5: Shimadzu AGS-X series Universal Testing Machine.

Tensile testing of the crosslinked polyester/TBA networks was done with small film-like samples with a size of 40 x 10 x 0.2 mm, a preload of 1 N, a gage length of 20 mm, and a crosshead speed of 5 mm·min^{-1}. All tensile tests were carried out in triplicate. For the evaluation of the mechanical characteristics, also the ISO standard 527 was considered.

6.3.11 Differential Scanning Calorimetry

The thermal properties of PHB and PHB composite materials were determined by differential scanning calorimetry (DSC) using a Netzsch DSC 204 calorimeter in a temperature range from -90 to 200 °C and a heating/cooling rate of 10 K·min^{-1} under

inert gas conditions (N_2). The degree of crystallinity of semi-crystalline PHB samples was determined from the first heating run and calculated according to:

$$X_c\ [\%] = \frac{\Delta H_m}{\Delta H_m^\circ} \cdot 100 \qquad \textbf{Equation 6-2}$$

ΔH_m .....Melting enthalpy [J g^{-1}].

ΔH_m° .....Melting enthalpy of 100% crystalline PHB (146 J g^{-1}).[204]

6.3.12 FT-IR Spectrometer

The FT-IR analyses were recorded using a Perkin Elmer Spectrum One spectrometer with a DTGS-detector (DTGS = deuterated triglycine sulphate). The polymer films on CaF_2 plates were characterized in transmission mode with 16 scans over a spectral range between 4000 cm^{-1} and 800 cm^{-1}.

6.3.13 Scratch Resistance Tests

The scratch resistance tests of polymer coatings on metal substrates were performed using a UMT2 Microtribometer from CETR (Bruker) equipped with a 5 N force cell and a diamond stylus with a tip diameter of 5 µm. 4 constant force runs (0.5, 1, 2, and 3 N) were performed and from these runs the coefficients of friction were calculated considering the ASTM G171 “Standard Test Method for Scratch Hardness of Materials Using a Diamond Stylus”. The scratch resistance tests were carried out in collaboration with the Polymer Competence Center Leoben GmbH.

7 Appendix

PHB Composite Materials

PHB/Herafill/ZrO_2 Composites

Table 7-1: Results of tensile testing of PHB and PHB composites with ZrO_2 and Herafill.

Material	Young's modulus [GPa]	Tensile strength [MPa]	Elongation at break [%]
PHB native (comm. grade)	2.55 ± 0.09	34.5 ± 1.7	19.5 ± 3.3
PHB + 3% ZrO_2	2.33 ± 0.08	24.5 ± 0.7	2.8 ± 0.2
PHB + 3% ZrO_2 + 10% Herafill	2.80 ± 0.10	31.0 ± 4.0	2.9 ± 0.2
PHB + 3% ZrO_2 + 30% Herafill	2.81 ± 0.05	25.3 ± 1.7	2.4 ± 0.1

PHB/Magnesium Powder Composites

Table 7-2: Results of tensile testing of PHB and PHB composites with magnesium powder (44 µm particle size).

Material	Young's modulus [GPa]	Tensile strength [MPa]	Elongation at break [%]
PHB native (Batch II)	3.19 ± 0.09	32.89 ± 0.3	2.77 ± 0.25
PHB + 10% Mg	3.42 ± 0.04	30.65 ± 4.6	1.96 ± 0.29
PHB + 20% Mg	3.46 ± 0.07	27.36 ± 1.8	1.44 ± 0.35
PHB + 30% Mg	3.59 ± 0.06	29.16 ± 2.2	1.08 ± 0.17
PHB + 40% Mg	3.79 ± 0.01	29.28 ± 4.2	1.27 ± 0.12
PHB + 50% Mg	4.29 ± 0.25	29.18 ± 6.4	0.87 ± 0.08

Polymer-Based Coatings on Metal Surfaces

Table 7-3: Scratch resistance tests of native PHB (batch III) coatings on copper-coated substrates.

Force [N]	Scratch width [µm]	Coefficient of friction
0.5	48.4	0.214
1.0	65.4	0.224
2.0	85.2	0.245
3.0	110	0.235

Table 7-4: Scratch resistance tests of PHB (batch III) coatings on copper-coated substrates crosslinked with 10 wt.-% TBA.

Force [N]	Scratch width [µm]	Coefficient of friction
0.5	57.3	0.164
1.0	75.2	0.184
2.0	93.8	0.200
3.0	119	0.121

Table 7-5: Scratch resistance tests of native PHB-HV (batch II) coatings on copper-coated substrates.

Force [N]	Scratch width [µm]	Coefficient of friction
0.5	50.6	0.214
1.0	65.1	0.276
2.0	89.8	0.295
3.0	99.5	0.170

Table 7-6: Scratch resistance tests of native PHB-HV (batch II) coatings on copper-coated substrates crosslinked with 10% TBA.

Force [N]	Scratch width [µm]	Coefficient of friction
0.5	41.6	0.158
1.0	65.4	0.178
2.0	87.3	0.196
3.0	103	0.206

Table 7-7: Surface roughness parameters and average coating masses of polymer-based coatings on magnesium LV-1 pins.

Coating	R_a [nm]	R_q [nm]	Average coating mass [mg]
None (native Mg pin)	168.6 ± 18.5	221.8 ± 22.8	n.a
PHB native	225.0 ± 13.3	290.4 ± 25.4	0.363 ± 0.033
PHB +10% TBA	264.4 ± 54.4	273.7 ± 17.4	0.370 ± 0.033
PDLLA	273.7 ± 54.4	354.6 ± 31.5	0.379 ± 0.055

UV-Induced Crosslinking of PHB-HV and PHB

Table 7-8: Gel fractions of PHB-HV crosslinked with 1 wt.-% BA after different irradiation times.

Time [s]	Gel fraction [%]	STD
0	3.92	0.44
5	12.5	1.51
10	44.7	7.70
15	49.6	0.12
20	63.5	7.17
25	61.5	2.16
30	69.1	4.32
45	67.7	4.13
60	70.4	2.74
75	65.7	1.44
90	64.2	4.08
120	60.2	4.96
180	60.4	7.79

Table 7-9: Gel fractions of PHB-HV crosslinked with 2 wt.-% BA after different irradiation times.

Time [s]	Gel fraction [%]	STD
0	2.28	-
3	2.52	2.52
7	1.19	1.20
10	2.45	2.45
13	2.46	2.46
17	1.65	1.65
20	2.38	2.38
30	1.22	1.22
60	4.02	4.02
180	3.38	3.38

Table 7-10: Gel fractions of PHB-HV crosslinked with 3 wt.-% BA after different irradiation times.

Time [s]	Gel fraction [%]	STD
0	3.54	-
3	34.96	0.97
7	66.01	1.84
10	67.73	0.36
13	83.30	2.51
17	83.71	3.82
20	86.88	1.30
30	78.58	2.38
60	81.24	4.02
180	85.72	2.99

Table 7-11: Gel fractions of PHB-HV crosslinked with 4 wt.-% BA after different irradiation times.

Time [s]	Gel fraction [%]	STD
0	4.35	-
5	53.68	7.01
10	71.39	5.10
15	77.97	2.95
20	84.64	7.05
30	86.69	3.16
45	88.48	2.19
60	87.74	1.78
90	84.99	0.76
180	82.26	1.80

Table 7-12: Gel fractions of PHB-HV crosslinked with 5 wt.-% BA after different irradiation times.

Time [s]	Gel fraction [%]	STD
0	3.44	-
5	78.64	3.38
10	78.45	0.73
15	86.40	2.28
20	88.17	2.45
30	87.50	5.04
45	83.06	1.75
60	83.83	2.45
90	80.85	1.32
180	80.91	1.59

Table 7-13: Gel fractions of PHB crosslinked with 3 wt.-% BA after different irradiation times.

Time [s]	Gel fraction [%]	STD
0	1.19	-
3	50.57	5.82
5	66.38	13.83
7	76.56	19.82
10	78.36	8.50
15	90.95	3.37
30	87.28	4.73
60	89.24	7.96

Charlesby-Pinner Analysis

Table 7-14: Calculated values for v_p and v_q from the Charlesby-Pinner plots.

v_p/v_q (y-axis intercept)	k	k^{-1}	$V_q = k^{-1} / P_0$	v_p
0.7569	0.08940	11.19	0.009321	0.007055
0.6333	0.06772	14.77	0.01231	0.007793
0.4011	0.05468	18.29	0.01524	0.006112
1.044	0.02784	35.92	0.02993	0.03125
1.085	0.01244	80.39	0.06698	0.07274

Temperature-Induced Crosslinking of PHB, PHB-HV and PLLA

Sol-Gel Analysis and Swelling Experiments

Table 7-15: Gel fractions of PHB crosslinked with different amounts of TBA.

Amount of TBA [wt.-%]	Gel fraction [%]	STD
0	-	-
10	2.69	1.74
20	23.80	1.49
30	26.78	6.53
40	39.40	2.80
50	40.24	2.52

Table 7-16: Gel fractions of PHB-HV crosslinked with different amounts of TBA.

Amount of TBA [wt.-%]	Gel fraction [%]	STD
0	-	-
10	22.27	0.96
20	55.01	2.51
30	56.1	6.16
40	71.73	1.92
50	77.6	1.86

Table 7-17: Gel fractions of PLLA crosslinked with different amounts of TBA.

Amount of TBA [wt.-%]	Gel fraction [%]	STD
0	-	-
10	-	-
20	22.93	3.00
30	27.45	2.41
40	41.00	0.65
50	47.13	2.69

Table 7-18: Swelling degrees of PHB/TBA networks in DCM and water.

Amount of TBA [wt.-%]	Swelling degree DCM	Swelling degree water
0	-	0.010 ± 0.07
10	-	0.050 ± 0.01
20	31.30 ± 4.13	0.060 ± 0.01
30	22.73 ± 6.26	0.077 ± 0.02
40	20.13 ± 1.97	0.080 ± 0.03
50	21.40 ± 0.93	0.140 ± 0.01

Table 7-19: Swelling degrees of PHB-HV/TBA networks in DCM and water.

Amount of TBA [wt.-%]	Swelling degree DCM	Swelling degree water
0	0	0.005 ± 0.001
10	0	0.039 ± 0.003
20	43.86 ± 6.35	0.042 ± 0.003
30	52.12 ± 3.21	0.078 ± 0.008
40	24.13 ± 0.38	0.089 ± 0.014
50	18.45 ± 2.09	0.194 ± 0.030

Table 7-20: Swelling degrees of PLLA/TBA networks in DCM and water.

Amount of TBA [wt.-%]	Swelling degree DCM	Swelling degree water
0	0	0.026 ± 0.011
10	0	0.031 ± 0.002
20	60.14 ± 5.68	0.056 ± 0.006
30	49.22 ± 12.82	0.089 ± 0.012
40	35.55 ± 8.04	0.095 ± 0.029
50	35.73 ± 14.25	0.081 ± 0.015

Tensile Testing of PHB, PHB-HV, and PLLA/TBA networks

Table 7-21: Tensile testing of dry samples of PHB (batch III) crosslinked with different amounts of TBA.

Amount of TBA [wt.-%]	Young's modulus [GPa]	Tensile strength [MPa]	Elongation at break [%]
0	0.61 ± 0.05	9.21 ± 0.88	2.157 ± 0.28
10	0.65 ± 0.04	10.48 ± 1.47	3.121 ± 0.56
20	0.62 ± 0.06	10.82 ± 0.64	3.697 ± 0.32
30	0.62 ± 0.06	10.72 ± 0.03	3.229 ± 0.14
40	0.66 ± 0.04	11.25 ± 0.64	4.814 ± 0.49
50	0.66 ± 0.13	14.42 ± 0.89	6.076 ± 0.49

Table 7-22: Tensile testing of water-swollen samples of PHB (batch III) crosslinked with different amounts of TBA.

Amount of TBA [wt.-%]	Young's modulus [GPa]	Tensile strength [MPa]	Elongation at break [%]
0	0.62 ± 0.02	7.85 ± 1.82	2.67 ± 0.51
10	0.55 ± 0.08	8.24 ± 2.22	2.97 ± 0.34
20	0.50 ± 0.06	9.51 ± 2.43	4.19 ± 0.79
30	0.50 ± 0.05	10.19 ± 0.59	3.50 ± 0.51
40	0.57 ± 0.06	9.79 ± 0.77	5.70 ± 0.51
50	0.47 ± 0.05	11.83 ± 0.31	6.67 ± 0.77

Table 7-23: Tensile testing of dry samples of PHB-HV (batch II) crosslinked with different amounts of TBA.

Amount of TBA [wt.-%]	Young's modulus [GPa]	Tensile strength [MPa]	Elongation at break [%]
0	1.28 ± 0.09	16.39 ± 0.99	2.67 ± 0.49
10	0.71 ± 0.04	18.29 ± 0.19	28.37 ± 15.27
20	0.58 ± 0.04	15.97 ± 0.78	55.00 ± 21.00
30	0.34 ± 0.01	11.92 ± 0.13	170.6 ± 56.8
40	0.31 ± 0.01	11.68 ± 0.45	175.81 ± 66.24
50	0.29 ± 0.01	10.93 ± 0.07	240.13 ± 28.46

Table 7-24: Tensile testing of water-swollen samples of PHB-HV (batch III) crosslinked with different amounts of TBA.

Amount of TBA [wt.-%]	Young's modulus [GPa]	Tensile strength [MPa]	Elongation at break [%]
0	1.23 ± 0.07	10.76 ± 0.79	2.08 ± 0.83
10	0.54 ± 0.06	16.48 ± 1.17	45.79 ± 0.13
20	0.48 ± 0.06	14.77 ± 1.04	29.88 ± 0.04
30	0.24 ± 0.03	10.20 ± 0.39	17.24 ± 0.01
40	0.29 ± 0.01	9.22 ± 1.03	19.95 ± 0.08
50	0.27 ± 0.01	9.42 ± 0.06	22.09 ± 0.03

Table 7-25: Tensile testing of dry samples of PLLA crosslinked with different amounts of TBA.

Amount of TBA [wt.-%]	Young's modulus [GPa]	Tensile strength [MPa]	Elongation at break [%]
0	1.39 ± 0.07	39.27 ± 1.22	4.30 ± 0.33
10	1.38 ± 0.04	39.38 ± 1.08	5.55 ± 0.53
20	1.37 ± 0.25	34.75 ± 6.96	23.34 ± 8.49
30	1.20 ± 0.08	35.08 ± 1.89	25.47 ± 15.43
40	1.09 ± 0.30	25.16 ± 1.98	21.48 ± 10.82
50	0.88 ± 0.88	22.24 ± 0.78	22.74 ± 7.48

Table 7-26: Tensile testing of water-swollen samples of PLLA crosslinked with different amounts of TBA.

Amount of TBA [wt.-%]	Young's modulus [GPa]	Tensile strength [MPa]	Elongation at break [%]
0	1.43 ± 0.18	40.14 ± 5.13	4.05 ± 0.28
10	1.51 ± 0.17	36.14 ± 2.03	4.68 ± 0.37
20	1.36 ± 0.26	32.13 ± 2.14	19.56 ± 7.74
30	1.21 ± 0.06	31.19 ± 2.55	22.78 ± 15.18
40	0.85 ± 0.20	21.72 ± 2.55	24.36 ± 1.40
50	0.81 ± 0.07	20.46 ± 1.18	31.48 ± 5.62

Recovery of TBA from Hydrolyzed PHB/TBA Networks

Table 7-27: Hydrolysis recovery rates of TBA and derivatives from purified and non-purified PHB/TBA networks (calculated from ^{1}H-NMR analyses).

Amount of TBA [wt.-%]	TBA recovered [%]	TBA recovered from purified samples [%]
0	-	-
10	8.3	8.8
20	17.8	15.3
30	26.3	19.3
40	32.4	24.1
50	45.2	28.3

Surface Modification of Injection-Molded PHB

Plasma Modification: Contact Angles and Surface Energy

Table 7-28: Contact angles for water and diiodomethane after O_2-plasma treatment for different times (measurement directly after plasma treatment).

Treatment time [min]	Contact angle water [°]	Contact angle CH_2I_2 [°]
0	71.9 ± 2.2	38.1 ± 1.6
2	38.6 ± 2.1	45.8 ± 1.7
3	37.2 ± 3.7	42.4 ± 3.7
4	20.7 ± 5.8	45.7 ± 2.3
6	19.8 ± 5.9	45.0 ± 4.6
8	31.7 ± 2.0	43.2 ± 1.5

Table 7-29: Surface energy, dispersed and polar contribution to surface energy calculated from the contact angles.

Treatment time [min]	Surface energy [mN·m^{-1}]	Polar part [mN·m^{-1}]	Disperse part [mN·m^{-1}]
0	47.61 ± 1.61	6.14 ± 1.85	41.47 ± 2.28
2	63.27 ± 2.36	25.73 ± 2.36	37.54 ± 1.51
3	64.44 ± 1.41	26.06 ± 1.41	38.38 ± 0.79
4	72.34 ± 1.22	33.55 ± 1.22	38.79 ± 0.41
6	72.11 ± 2.26	34.84 ± 2.26	37.27 ± 1.18
8	67.32 ± 2.64	29.00 ± 2.64	38.32 ± 1.66

Table 7-30: Surface energy, dispersed and polar contribution to surface energy calculated from the contact angles after 4 days of ageing.

Treatment time [min]	Surface energy [mN·m^{-1}]	Polar part [mN·m^{-1}]	Disperse part [mN·m^{-1}]
0	47.61 ± 1.85	6.14 ± 1.85	41.47 ± 2.28
2	46.7 ± 0.38	11.1 ± 0.19	35.60 ± 0.19
3	44.11 ± 1.26	6.72 ± 0.35	37.38 ± 0.91
4	48.88 ± 0.98	13.55 ± 0.48	35.33 ± 0.51
6	47.24 ± 1.09	10.04 ± 0.50	37.20 ± 0.59
8	47.18 ± 0.58	12.06 ± 0.32	35.12 ± 0.26

Table 7-31: Surface energy, dispersed and polar contribution to surface energy calculated from the contact angles after 12 days of ageing.

Treatment time [min]	Surface energy [mN·m^{-1}]	Polar part [mN·m^{-1}]	Disperse part [mN·m^{-1}]
0	47.61 ± 1.85	6.14 ± 1.85	41.47 ± 2.28
2	46.29 ± 0.69	7.43 ± 0.21	38.86 ± 0.47
3	43.07 ± 0.99	6.59 ± 0.28	36.48 ± 0.61
4	42.45 ± 1.91	9.41 ± 0.63	33.04 ± 1.28
6	42.22 ± 0.65	5.15 ± 0.23	37.06 ± 0.43
8	41.47 ± 1.05	7.89 ± 0.35	33.58 ± 0.70

Surface Roughness Parameters

Table 7-32: Surface roughness parameters of differently treated PHB surfaces determined by focus variation microscopy.

Treatment	R_q [µm]	R_a [µm]
none	0.352 ± 0.047	0.260± 0.051
Mg I (397 µm)	0.352 ± 0.058	0.262 ± 0.038
Mg II (44 µm)	0.400 ± 0.055	0.294 ± 0.041
O_2-plasma	0.522 ± 0.093	0.358 ± 0.041
HCl + Mg I (397 µm)	0.977 ± 0.393	0.432 ± 0.137
HCl + Mg II (44 µm)	1.533 ± 0.311	0.818 ± 0.002

8 Publications

Publications in Peer-reviewed Journals

C. Ebner, T. Bodner, F. Stelzer, F. Wiesbrock, *One Decade of Microwave-Assisted Polymerizations: Quo vadis?*. *Macromolecular Rapid Communications* **2011**, *32*, 254.

C. Ebner, T. Bodner, F. Stelzer, F. Wiesbrock, Cover Picture: *One Decade of Microwave-Assisted Polymerizations: Quo vadis?*. *Macromolecular Rapid Communications* **2011**, *32*.

B. Rupp, C. Ebner, E. Rossegger, C. Slugovc, F. Stelzer, F. Wiesbrock, UV-induced crosslinking of the biopolyester poly(3-hydroxybutyrate)-*co*-(3-hydroxyvalerate). *Green Chemistry* **2010**, *12*, 1796.

Patents

Hybrid polymeric materials for medical applications and preparation thereof, applicants: Technische Universität Graz, Medizinische Universität Graz, Heraeus Medical GmbH, AT&S Austria Technologie und Systemtechnik AG, invs.: F. Wiesbrock, C. Ebner, F. Stelzer, A.-M. Weinberg, K. D. Kühn. Application on 20.06.2011 at the European Patent Office.

Oral Presentations at International Conferences

C. Ebner, A. Schartner, A.-M. Weinberg, F. Stelzer, F. Wiesbrock. *Surface Roughness and Hydrophilicity of Bio-based Bone Fixation Materials: Plasma Techniques, Chemical and Mechanical Treatment.* BioNanoMed 2012. Krems, Austria on March 1, 2012.

C. Ebner, L. Olah, A.-M. Weinberg, F. Stelzer, F. Wiesbrock. *Novel PHA-based Polymer Networks as Potential Candidates for Biomedical Applications*. Health Care India 2012. New Delhi, India on Feb. 20, 2012.

C. Ebner, E. Rossegger, F. Stelzer, A.-M. Weinberg, F. Wiesbrock. *UV-Induced Crosslinking of Poly(hydroxyalkanoate)s.* European Polymer Conference EUPOC 2011. Gargnano, Italy on May 29, 2011.

E. Martinelli, S. Fischerauer, C. Ebner, M. Koller, S. Tauber, T. Kraus, A.-M. Weinberg. *PHAs as bioresorbable Implants? A Study in rat model.* 24th International Symposium on pediatric surgical research. Graz, Austria on Sept. 9, 2011.

C. Ebner, E. Rossegger, F. Stelzer, F. Wiesbrock. *Finishing of Polymer Coatings: Cross-linking of scl-Poly(hydroxyalkanoates).* Austrian-Slovenian Polymer Meeting ASPM 2010. Leoben, Austria on Sept. 8, 2010.

C. Ebner, E. Rossegger, B. Rupp, F. Stelzer, F. Wiesbrock. *Modification of short-chain-length poly(hydroxyalkanoate)s by UV-induced cross-linking.* Rolduc Polymer Meeting. Kerkrade, Netherlands on May 16, 2010.

Poster Presentations

C. Ebner, A. Schartner, A.-M. Weinberg, F. Stelzer, F. Wiesbrock. *Surface Manipulation for Tailor-Made Resorption Kinetics: Nanoscale-Roughness of Polymer-based Coatings for Fracture Correction Implants.* BioNanoMed 2012. Krems, Austria on March 1, 2012.

C. Ebner, L. Olah, A.-M. Weinberg, F. Stelzer, F. Wiesbrock. *PHB-PEG-based Polymer Networks as Novel Systems for Personalized Drug Delivery.* ICPE - 5th International Congress on Pharmaceutical Engineering. Graz, Austria on Sept. 29, 2011.

E. Rossegger, C. Ebner, F. Stelzer, F. Wiesbrock. *Influence of the Crosslinking Degree in scl-Poly(hydroxyalkanoate) Films on the Surface Structures.* Austrian-Slovenian Polymer Meeting ASPM 2010. Leoben, Austria on Sept. 8, 2010.

E. Rossegger, C. Ebner, F. Stelzer, F. Wiesbrock. *Injection Moulding of Short-Chain-Length Poly(hydroxyalkanoate)s.* Rolduc Polymer Meeting. Kerkrade on May 16, 2010.

C. Ebner, B. Rupp, H. Fasl, M. Koller, G. Braunegg, F. Stelzer, F. Wiesbrock. *Injection Moulding of Short-Chain-Length Poly(hydroxyalkanoate)s.* 11th Pacific Polymer Conference. Cairns, Australia on Dec. 6, 2009.

9 List of Abbreviations

1H-NMR	Proton nuclear magnetic resonance
BA	Bisazide [2,6-bis(4-azidobenzylidene)-4-methylcyclohexanone]
BRIC	Bioresorbable implants for children
CCD	Charge-coupled device
CoA	Co-enzyme A
DCM	Dichloromethane
DMSO	Dimethylsulfoxide
DSC	Differential scanning calorimetry
EPR	Ethylene-propylene rubber
EU	Endotoxin unit
FT-IR	Fourier-transformation infrared spectroscopy
GPC	Gel permeation chromatography
HA	Hydroxy apatite
ITO	Indium tin oxide
Mn	Number average molecular weight
PCL	Poly(caprolactone)
PDI	Polydispersity index
PDLLA	Poly-DL(lactic acid)
PE	Polyethylene
PEG	Poly(ethylene glycol)
PET	Poly(ethylene terephthalate)
PGA	Poly(glycolic acid)
PGLA	Poly(glycolic-*co*-lactic acid)
PHA	Poly(hydroxyalkanoate)
PHB	Poly(3-hydroxybutyrate)
PHHx	Poly(3-hydroxyhexanoate)
PHN	Poly(3-hydroxnonanoate)
PHO	Poly(3-hydroxyoctanoate)
PLA	Poly(lactic acid)
PLLA	Poly-L(lactic acid)
PMMA	Poly(methyl methacrylate)

PP	Polypropylene
PS	Polystyrene
PVA	Poly(vinyl alcohol)
R_a	Arithmetic mean roughness
R_q	Root mean squared roughness
TCP	Tricalcium phosphate

10 References

[1] C. J. Moore, *Environmental Research* **2008**, *108*, 131.

[2] J. Hopewell, R. Dvorak, E. Kosior, *Phil. Trans. R. Soc. B* **2009**, *364*, 2115.

[3] E. Chiellini, R. Salaro, *Adv. Mater.* **1996**, *8*, 305.

[4] C. K. S. Pillai, C. P. Sharma, *J. Biomater. Appl.* **2010**, *25*, 291.

[5] M. Lemoigne, *Bull. Soc. Chem. Biol*. **1926**, *8*, 770.

[6] R. W. Lenz, R. H. Marchessault, *Biomacromolecules* **2005**, *6, 1.*

[7] J. M. Luengo, B. Garcia, A. Sandoval, G. Naharro, E. R. Olivera, *Curr. Opin. Microbiol.* **2003**, *6*, 251.

[8] A. Steinbüchel, H. E. Valentin, *FEMS Microbiol. Lett.* **1995**, *128*, 219.

[9] E. Fernandez, M. P. Ginebra, M. G. Boltong, F. C. M. Driessens, J. Ginebra, E. A. P. De Maeyer, R. M. H. Verbeeck, J. A. Planell, *J. Biomed. Mater. Res. B* **1996**, *32*, 383.

[10] L. Claes, I. Hoellen, A. Ignatius, *Orthopädie* **1997**, *26*, 459.

[11] A. C. Hänzi, I. Gerber, M. Schinhammer, J. F. Löffler, P. J. Uggowitzer, *Acta Biomaterialia* **2010**, *6*, 1824.

[12] A. C. Hänzi, A. S. Sologubenko, P. J. Uggowitzer, *Int. J. Mat. Res.* **2009**, *100*, 1127.

[13] E. D. McBride, *J. Am. Med. Assoc.* **1938**, *111*, 2464.

[14] F. Witte, V. Kaese, H. Haferkamp, E. Switzer, A. Meyer-Lindenberg, C. J. Wirth, H. Windhagen, *Biomaterials* **2005**, *26*, 3557.

[15] S. C. Cifuentes, E. Frutos, J. L. Gonzelez-Carrasco, M. Munoz, M. Multinger, J. Chao, R. Benavente, M. Lieblich, *Materials Letters* **2012**, *74*, 239.

[16] Z. Qiu, T. Ikehara, T. Nishi, *Polymer* **2003**, *44*, 7519.

[17] O. Olea-Mejia, W. Brostow, E. Buchman, *J. Nanosci. Nanotechnol.* **2010**, *10*, 8254.

[18] Pictures taken at Medical University Graz, reproduced with permission of Stefan Fischerauer.

[19] S. Vogt, K.-D. Kühn, U. Gopp, M. Schnabelrauch, *Mat.-Wiss. u. Werkstofftech.* **2005**, *36*, 814.

[20] F. D. Matl, A. Obermeier, S. Repmann, W. Friess, A. Stemberger, K.-D. Kühn, *Antimicrob. Agents Ch.* **2009**, *52*, 1957.

[21] T. A. Holland, A. G. Mikos, *Adv. Biochem. Engin./Biotechnol.* **2006**, *102*, 161.

[22] *Biopolymers, Polyesters I, Biological Systems and Biotechnological Production, Volume 3a*, Y. Doi, A. Steinbüchel, Eds., Wiley-VCH Weinheim, **2002**.

[23] S. Taguchi, H. Matsusaki, K. Matsumoto, K. Takase, K. Taguchi, Y. Doi, *Polym. Int.* **2002**, *51*, 899.

[24] S. Philip, T. Keshavarz, I. Roy, *J. Chem. Technol. Bioechnol.* **2007**, *83*, 233.

[25] Y. B. Kim, R. W. Lenz, *Adv. Biochem. Eng./Biotechnol.* **2001**, *71*, 51.

[26] R. A. Gross, C. DeMello, R. W. Lenz, H. Brandle, R. C. Fuller, *Macromolecules* **1989**, *22*, 1106.

[27] M. Zenkiewicz, J. Richert, P. Rytlewski, K. Moraczewski, M. Stepczynska, T. Karasiewicz, *Polymer Testing* **2009**, *28*, 412.

[28] L. M. Matuana, *Bioresour. Biotechnol.* **2008**, *99*, 3643.

[29] M. Koller, P. Hesse, R. Bona, C. Kutschera, A. Atlic, G. Braunegg, *Macromol. Biosci.* **2007**, *7*, 218.

[30] R. V. Nonato, P. E. Mantelatto, C. E. V. Rossell, *Appl. Microbiol. Biotechnol.* **2001**, *57*, 1.

[31] M. Koller, R. Bona, E. Chiellini, E. G. Fernandes, P. Horvat, C. Kutschera, P. Hesse, G. Braunegg, *Bioresource Technol.* **2008**, *99*, 4854.

[32] J. M. R. H. Cornibert, *J. Mol. Biol.* **1972**, *71*, 735.

[33] M. C. Yokouchi, H. Tadokoro, K. Teranishi, H. Tani, *Polymer* **1973**, *14*, 267.

[34] T. L. Bluhm, G. K. Hamer, R. H. Marchessault, C. A. Fyfe, R. P. Veregin, *Macromolecules* **1986**, *19*, 2871.

[35] M. Kunioka, A. Tamaki, Y. Doi, *Macromolecules* **1989**, *22*, 694.

[36] I. Noda, P. R. Green, M. M. Satowski, L. A. Schechtman, *Biomacromolecules* **2005**, *6*, 580.

[37] H. Mitomo, W.-C. Hsieh, K. Nishiwaki, K. Kasuya, Y. Doi, *Polymer* **2001**, *42*, 3455.

[38] J. M. Merrick, in *Biopolymers, Polyesters I, Biological Systems and Biotechnological Production, Volume 3a*, Y. Doi, A. Steinbüchel, Eds., Wiley-VCH Weinheim, **2002**, chapter 4.

[39] J. M. Merrick, M. Doudoroff, *Nature* **1961**, *189*, 890.

[40] R. Griebel, Z. Smith, J. M. Merrick, *Biochemistry* **1968**, *7*, 3676.

[41] B. H. A. Rehm, A. Steinbüchel, *Int. J. Biol. Macromol.* **1999**, *25*, 3.

[42] U. Müh, A. J. Sinskey, D. P. Kirby, W. S. Lane, J. Stubbe, *Biochemistry* **1999**, *38*, 826.

[43] K. Sudesh, H. Abe, Y. Doi, *Prog. Polym. Sci.* **2000**, *25*, 1503.

[44] J. M. Luegno, B. Garcia, A. Sandoval, G. Naharro, E. R. Olivera, *Curr. Opin. Microbiol.* **2003**, *6*, 251.

[45] M. Zinn, B. Witholt, T. Egli, *Adv. Drug Rev.* **2001**, *53*, 5.

[46] J. M. Merrick, C. I. Yu, *Biochemistry* **1966**, *5*, 3563.

[47] J. M. Merrick, M. Doudoroff, *J. Bacteriol.* **1964**, *88*, 60.

[48] R. J. Griebel, J. M. Merrick, *J. Bacteriol.* **1971**, *108*, 782.

[49] J. M. Merrick, R. Steger, D. Dombroski, *Int. J. Biol. Macromol.* **1999**, *25*, 129.

[50] K. S. Anseth, C. N. Bowman, L. B. Brannon-Peppas, *Biomaterials* **1996**, *17*, 1647.

[51] S.-W. Ha, E. Wintermantel, G. Maier, *Medizintechnik Life Science Engineering, Part VI, Prozesstechnologien für medizintechnische Entwicklungen.* Springer Verlag Berlin, 5th edition, **2008**.

[52] J. Hao and X. Deng, *Polymer* **2001**, *42*, 4091.

[53] Y. Aoyagi, K. Yamashita, Y. Doi, *Polym. Degrad. Stab.* **2002**, *76*, 53.

[54] S. Y. Lee, *Trends Biotechnol.* **1996**, *14*, 431.

[55] S. Y. Lee, S. J. Park, in *Biopolymers, Polyesters I, Biological Systems and Biotechnological Production, Volume 3a*, Y. Doi., A. Steinbüchel, Eds., Wiley-VCH Weinheim **2002**, chapter 9.

[56] B. S. Kim, S. C. Lee, S. Y. Lee, H. N. Chang, Y. K. Chang, S. I. Woo, *Biotechnol. Bioeng.* **1994**, *43*, 892.

[57] B. S. Kim, S. C. Lee, S. Y. Lee, H. N. Chang, Y. K. Chang, S. I. Woo, *Enzyme Microbiol. Technol.* **1994**, *16*, 556.

[58] W. S. Ahn, S. J. Park, S. Y. Lee, *Appl. Environ. Microbiol.* **2000**, *66*, 3624.

[59] F. Wang, S. Y. Lee, *Biotechnol. Bioeng.* **1998**, *58*, 325.

[60] F. Wang, S. Y. Lee, *Appl. Environ. Microbiol.* **1997**, *63*, 3703.

[61] F. Wang, S. Y. Lee, *Appl. Environ. Microbiol.* **1997**, *63*, 4765.

[62] biomer.de, information retrieved on April 17, **2012**.

[63] P. A. Holmes, *Phys. Technol.* **1985**, *16*, 32.

[64] J. Asrar, K. J. Gruys, in *Biopolymers, Polyesters III, Application and Commercial Products, Volume 4*, Y. Doi, A. Steinbüchel, Eds., Wiley-VCH Weinheim, **2002**, chapter 3.

[65] S. Y. Lee, *Biotechnol. Bioeng.* **1995**, *49*, 1.

[66] Z.-J. Li, Z.-Y. Shi, J. Jian, Y.-Y. Guo, Q. Wu, G.-Q. Chen, *Metab. Eng.* **2010**, *12*, 352.

[67] Y. Saito, Y. Doi, *Int. J. Biol. Macromol.* **1994**, *16*, 99.

[68] resomer.evonik.com; information retrieved on May 2, **2012**.

[69] O. M. Böstman, *J. Bone Joint Surg. Am.* **1991**, *73*, 148.

[70] "Dissociation Constants of Organic Acids and Bases", in *CRC Handbook of Chemistry and Physics, Internet Version 2005,* David R. Lide, ed., <http://www.hbcpnetbase.com>, CRC Press, Boca Raton, FL **2005**.

[71] H. K. Makadia, S. J. Siegel, *Polymers* **2011**, *3*, 1377.

[72] S. M. Moghimi, A. C. Hunter, J. C. Murray, *Pharmacol. Rev.* **2001**, *53*, 283.

[73] F. von Burkersroda, L. Schedl, A. Göpferich, *Biomaterials* **2002**, *26*, 4221.

[74] H. Tsuji, *Polymer* **2000**, *41*, 3621.

[75] H. Tsuji, Y. Ikada, *Polymer* **1999**, *40*, 6699.

[76] K. Letchford, A. Södergard, D. Plackett, S. E. Gilchrist, H. M. Burt, in *Biodegradable Polymers in Clinical Use and Clinical Development, Part V: Synthetic Biodegradable Polymers*, A. J. Domb, N. Kumar, A. Ezra, Eds., John Wiley & Sons, Inc., Hoboken **2011**, chapter 9.

[77] N. J. Gunja, K. A. Athanasiou, *Sports Med. Rev. Arthro. Rev.* **2006**, *14*, 112.

[78] N. Ashammakhi, A. Ndreu, Y. Yang, H. Ylikauppila, L. Nikkola, *Eur. J. Plast. Surg.* **2012**, *35*, 135.

[79] P. Bansal, S. Verma, W. Khan, N. Kumar, in *Biodegradable Polymers in Clinical Use and Clinical Development, Part VIII: Synthetic Biodegradable Polymers*, A. J. Domb, N. Kumar, A. Ezra, Eds., John Wiley & Sons, Inc., Hoboken, **2011**, chapter 18, pp. 665.

[80] K. Bhubalan, W.-H. Lee, K. Sudesh, in *Biodegradable Polymers in Clinical Use and Clinical Development, Part IV: Biodegradable Polymers of Natural Origin: Polyesters*, A. J. Domb, N. Kumar, A. Ezra, Eds., John Wiley & Sons, Inc., Hoboken **2011**, chapter 8.

[81] Y.-W. Wang, F. Yang, Q. Wu, Y.-C. Cheng, P. H. F. Yu, J. Chen, G.-Q. Chen, *Biomaterials* **2005**, *26*, 755.

[82] X. Yang, K. Zhao, G.-Q. Chen, *Biomaterials* **2002**, *23*, 1391.

[83] G.-Q. Chen, Q. Wu, *Biomaterials* **2005**, *26*, 6565.

[84] C. W. Pouton, S. Akhtar, *Adv. Drug Deliver. Rev.* **1996**, *18*, 133

[85] C. Doyle, E. T. Tanner, W. Bonfield, *Biomaterials* **1991**, *12*, 841.

[86] E. Fukada, Y. Ando, *Int. J. Biol. Macromol.* **1986**, *8*, 361.

[87] J. Ni, M. Wang, *Mat. Sci. Eng. C-Bio. S.* **2002**, *20*, 101.

[88] Z. B. Luklinska, W. Bonfield, *J. Mater. Sci.-Mater. Med.* **1997**, *8*, 379.

[89] L. J. Chen, M. Wang, *Biomaterials* **2002**, *20*, 2631.

[90] K. A. Salihi, A. R. Samsudin, *Med. J. Malaysia* **2004**, *59 Suppl. B*, 202.

[91] O. Samsuria, A. S. Fadilah, A. B. Asiah, M. R. Rodiah, A. H. Suzina, A. R. Samsudin, *Med. J. Malaysia* **2004**, *59 Suppl. B*, 174.

[92] G. T. Köse, F. Korkusuz, P. Korkusuz, N. Purali, A. Özkul, V. Hasirci, *Biomaterials* **2003**, *24*, 4999.

[93] G. T. Köse, S. Ber, F. Korkusuz, V. Hasiriki, *J. Mater. Sci-Mater. M.* **2003**, *14*, 121.

[94] J. C. Knowles, G. W. Hastings, H. Ohta, S. Niwa, N. Boeree, *Biomaterials* **1992**, *13*, 491.

[95] Z.-W. Dai, X.-H. Zou, G.-Q. Chen, *Biomaterials* **2009**, *30*, 3075.

[96] E. Ruel-Gariepy, J.-C. Leroux, *Eur. J. Pharm. Biopharm.* **2004**, *58*, 409.

[97] A. Hafeti, B. Amsden, *J. Control. Release* **2002**, *80*, 9.

[98] Y.-C. Yao, X.-Y. Zhan, J. Zhang, X.-H. Zou, Z. H. Wang, Y.-C. Xiong, J. Chen, G.-Q. Chen, *Biomaterials* **2008**, *29*, 4823.

[99] Y. Wang, Y.-Z. Bian, Q. Wu, G.-Q. Chen, *Biomaterials* **2008**, *29*, 2858.

[100] G. Strobl, *The Physics of Polymers*, 2nd ed., Springer-Verlag Heidelberg **2007**, pp. 105.

[101] L. J. Chen, M. Wang, *Biomaterials* **2002**, *23*, 2631.

[102] N. Galego, C. Rozsa, R. Sanchez, J. Fung, A. Vazquez, J. S. Tomas, *Polym. Test.* **2000**, *19*, 485.

[103] N. R. Boeree, J. Dove, J. J. Cooper, J. Knowles, G. W. Hastings, *Biomaterials* **1993**, *14*, 793.

[104] I. D. Xynos, A. J. Edgar, L. D. K. Buttery, L. L. Hench, J. M. Polak, *J. Biomed. Mater. Res.* **2001**, *55*, 151.

[105] S. K. Misra, S. P. Valappil, I. Roy, A. R. Boccaccini, *Biomacromolecules* **2006**, *7*, 2249.

[106] J. Olsen-Claire, J. J. Blaker, J. A. Roether, A. R. Boccaccini, G. Schmack, K. Gliesche, *Mat.-wiss. U. Werkstofftech.* **2006**, *37*, 577.

[107] X. Ma, Y. Lv, Z. Gao, G. Cheng, *Advanced Materials Research* **2011**, *146*, 1170.

[108] Eric Wittchow, inventor; Biotronik VI Patent AG, assignee; *Implant Made of Biocorrodible Iron or Magnesium Alloy*. Patent Application US 2010/0106243 A1, **2010** Apr. 29.

[109] A. F. Galio, S. V. Lamaka, M. L. Zheludkevich, L. F. P. Dick, I. L. Müller, M. G. S. Ferreira, *Surf. Coat. Technol.* **2010**, *204*, 1479.

[110] S. Sathiyanarayanan, S. S. Azim, G. Venkatachari, *Prog. Org. Coat.* **2007**, *59*, 291.

[111] L. Sager, N. Adden, inventors; *Biocorrodible Implants Having a Functionalized Coating. Patent Application* US 2011/0153006 A1 **2011**, Jun. 23.

[112] M. Orlowski, A. Rübben, inventors; Eurocor GmbH, assignee; *Bioresorbable Metal Stent with Controlled Resorption*. Patent No. WO 2008/092436 A2 **2008**, Aug. 7.

[113] C. Strobel, N. Bormann, A. Kadow-Romacker, G. Schmidmaier, B. Wildemann, *J. Control. Release* **2011**, *156*, 37.

[114] C. Lorenz, A. Hoffmann, G. Gross, H. Windhagen, P. Dellinger, K. Möhwald, W. Dempwolf, H. Menzel, *Macromol. Biosci.* **2011**, *11*, 234.

[115] G. Schmidmair, B. Wildemann, A. Stemberger, N. P. Haas, M. Raschke, *J. Biomed. Mater. Res.* **2001**, *58*, 449.

[116] M. Avella, E. Martuscelli, M. Raimo, *J. Mater. Sci.* **2000**, *35*, 523.

[117] C.-S. Ha, W.-J. Cho, *Prog. Polym. Sci.* **2002**, *27*, 759.

[118] Y. Deng, K. Zhao, X.-F. Zhang, P. Hu, G.-Q. Chen, *Biomaterials* **2002**, *23*, 4049.

[119] Z. Kai, D. Ying, C. G.-Qiang, *Biochem. Eng. J.* **2003**, *16*, 115.

[120] E. Blümm, A. J. Owen, *Polymer* **1995**, *36*, 4077.

[121] L. Zhang, C. Xiong, X. Deng, *Polymer* **1996**, *37*, 235.

[122] B. Hazer, A. Steinbüchel, *Appl. Microbiol. Biotechnol.* **2007**, *74*, 1.

[123] B. Hazer, *Energy and Power Engineering* **2010**, *2*, 31.

[124] A. Göpferich, *Biomaterials* **1996**, *17*, 103.

[125] K. E. Uhrich, S. M. Cannizzaro, R. S. Langer, K. M. Shakesheff, *Chem. Rev.* **1999**, *99*, 3181.

[126] K. Knop, R. Hoogenboom, D. Fischer, U. S. Schubert, *Angew. Chem. Int. Ed.* **2010**, *49*, 6288.

[127] H. Kukula, H. Schlaad, M. Antonietti, S. Förstner, *J. Am. Chem. Soc.* **2002**, *124*, 1658.

[128] J. Li, X. Li, X. Ni, K. W. Leong, *Macromolecules* **2003**, *36*, 2661.

[129] J. Li, X. Ni, X. Li, N. K. Tan, C. T. Lim, S. Ramakrishna, K. W. Leong, *Langmuir* **2005**, *21*, 8681.

[130] F. Ravenette, R. H. Marchessault, *Biomacromolecules* **2003**, *4*, 856.

[131] J. Babinot, E. Renard, V. Langlois, *Macromol. Chem. Phys.* **2011**, *212*, 278.

[132] M. Yalpani, R. H. Marchessault, F. G. Morin, C. J. Monasterios, *Macromolecules* **1991**, *24*, 6046.

[133] X. Li, X. J. Loh, K. Wang, C. He, J. Li, *Biomacromolecules* **2005**, *6*, 2740.

[134] H. W. Kim, C. W. Chung, Y. H. Rhee, *Int. J. Biol. Macromol.* **2005**, *35*, 47.

[135] L. Grohndahl, A. Chandler-Temple, M. Trau, *Biomacromolecules* **2005**, *6*, 2197.

[136] S. Ilter, B. Hazer, M. Borcakli, O. Atici, *Macromol. Chem. Phys.* **2001**, *202*, 2281.

[137] T. Jiang, P. Hu, *Polymer J.* **2001**, *33*, 647.

[138] S. Domenek, V. Langlois, E. Renard, *Polym. Degrad. Stabil.* **2007**, *92*, 1384.

[139] S. Nguyen, R. H. Marchessault, *Macromol. Biosci.* **2004**, *4*, 262.

[140] X. M. Deng, J. Y. Hao, *Eur. Polym. J.* **2001**, *37*, 211.

[141] A. H. Arkin, B. Hazer, M. Borcakli, *Macromolecules* **2000**, *33*, 3219.

[142] M.-M. Bear, M.-A. Leboucher-Durand, V. Langlois, R. W. Lenz, S. Goodwin, P. Guerin, *React. Funct. Polym.* **1997**, *34*, 65.

[143] W. H. Park, R. W. Lenz, S. Goodwin, *J. Polym. Sci. A Polym. Chem.* **1998**, *36*, 2389.

[144] M. Y. Lee, W. H. Park, R. W. Lenz, *Polymer* **2000**, *41*, 1703.

[145] N. Kurth, E. Renard, F. Brachet, D. Robic, P. Guerin, R. Bourbouze, *Polymer* **2002**, *43*, 1095.

[146] D. J. Stigers, G. N. Tew, *Biomacromolecules* **2003**, *4*, 193.

[147] G. Tillet, B. Boutevin, B. Ameduri, *Adv. Polym. Sci.* **2011**, *36*, 191.

[148] V. K. Milinchuk, E. R. Klinshpont, V. P. Kiryukhin, *Int. J. Radiat. Appl. Instrum. Part C Radiat. Phys. Chem.* **1986**, *28*, 331.

[149] I. P. Shelukov, G. S. Zhdanov, E. R. Klinshpont, V. K. Milinchuk, *Int. J. Radiat. Appl. Instrum. Part C Radiat. Phys. Chem.* **1986**, *28*, 617.

[150] A. Dufresne, L. Reche, R. H. Marchessault, M. Lacroix, *Int. J. Biol. Macromol.* **2001**, *29*, 73.

[151] K. D. Gagnon, R. W. Lenz, R. J. Farris, R. C. Fuller, *Polymer* **1994**, *35*, 4358.

[152] G. J. M. Koning, H. M. M. van Bilsen, P. J. Lemstra, W. Hazenberg, B. Withold, H. Preusting, J. G. von der Galien, A. Schirmer, D. Jendrossek, *Polymer* **1994**, *35*, 2090.

[153] R. D. Ashby, A. M. Cromwick, T. A. Foglia, *Int. J. Biol. Macromol.* **1998**, *23*, 61.

[154] A. Bergmann, J. Teßmar, A. Owen, *J. Mater. Sci.* **2007**, *42*, 3732.

[155] A. J. Zielinska, J. W. M. Noordermeer, W. K. Dierkes, A. G. Dierkes, A. G. Talma, M. van Duin, *Elastomers and Plastics* **2010**, *63*, 308.

[156] M. G. Finn, V. V. Fokin, *Chem. Soc. Rev.* **2010**, *39*, 1231.

[157] L. Schlegel, W. Schnabel, in *Radiation Curing in Polymer Science and Technology, Volume 1: Fundamentals and Methods*, J. P. Fouassier, J. F. Rabek, Eds., Elsevier Science Publisher Ltd, New York **1993**.

[158] A. Bagno, C. di Bello, *J. Mater. Sci. - Mater. Med.* **2004**, *15*, 935.

[159] A. Wennerberg, Int. *J. Tools Manufact.* **1998**, *38*, 657.

[160] K. Tsougnei, N. Vourdas, A. Tserepi, E. Gogolides, *Langmuir* **2009**, *25*, 11748.

[161] T. Desmet, R. Morent, N. de Geyter, C. Leys, E. Schacht, P. Dubrel, *Biomacromolecules* **2009**, *10*, 2354.

[162] B. M. P. Ferreira, L. M. P. Pinheiro, P. A. P. Nascente, M. J. Ferreira, E. A. R. Duek, *Mat. Sci. Eng. C-Bio S* **2009**, *29*, 806.

[163] A. Charlesby, S. H. Pinner, *P. Roy. Soc. Lond. A Mat.* **1959**, *249*, 367.

[164] B. Ivan, T. T. Nagy, T. Kelen, B. Turcsanyi, F. Tüdös, *Polym. Bull.* **1980**, *2*, 83.

[165] R. Danzl, F. Helmi, S. Scherer, in *10th International Conference of the Slovenian Society for Non-Destrcutive Testing "Application of Contemporary Non-Destructive Testing in Engineering"* **2009**, Sept. 1-3, Ljublijana, Slovenia.

[166] X. Jiang, P. J. Scott, D. J. Whitehouse, L. Blunt, *Proc. R. Soc.* **2007**, *463*, 2071.

[167] H.-D. Dörfler, *Grenzflächen und kolloid-disperse Systeme: Physik und Chemie*, Springer, Heidelberg **2002**.

[168] T. Bodner, Dissertation, Graz University of Technology, **2012**.

[169] R. N. Wenzel, *Ind. Eng. Chem.* **1936**, *28*, 988.

[170] A. B. D. Cassie, S. Baxter, *Trans. Faraday Soc.* **1944**, *40*, 546.

[171] A. B. D. Cassie, S. Baxter, *J. Text. Inst.* **1945**, *36*, T67.

[172] D. K. Owens, R. C. Wendt, *J. Appl. Polym. Sci.* **1969**, *13*, 1741.

[173] W. Rabel, *Farbe und Lack* **1971**, 77, 997.

[174] D. H. Kaelble, *J. Adhes.* **1970**, *2*, 66.

[175] M. Müller, C. Oehr, *Plasma Process. Polym.* **2011**, *8*, 19.

[176] S. Wu, *J. Polym. Sci. C* **1971**, *34*, 19.

[177] J. Schultz, K. Tsutsumi, J.-B. Donnet, *J. Colloid Interf. Sci.* **1977**, *59*, 272.

[178] J. Schultz, K. Tsutsumi, J.-B. Donnet, *J. Colloid Interf. Sci.* **1977**, *59*, 277.

[179] C. J. van Oss, R. J. Good, M. K. Chaudhury, *Langmuir* **1988**, *8*, 884.

[180] W. Grellmann, S. Seidler, *Kunststoffprüfung* **2005,** Carl Hanser Verlag München, pp. 108.

[181] W. Grellmann, S. Seidler, *Kunststoffprüfung* **2005**, Carl Hanser Verlag München, pp. 15.

[182] A. J. Peacock, L. Mandelkern, *J. Polym. Sci. Pol. Phys.* **1990**, *28*, 1917.

[183] M. A. Kennedy, A. J. Peacock, L. Mandelkern, *Macromolecules* **1994**, *27*, 5297.

[184] W. C. J. Zuiderduin, C. Westzaan, J. Huetink, R. J. Gaymans, *Polymer* **2003**, *44*, 261.

[185] Z. Bartczak, A. S. Argon, R. E. Cohen, M. Weinberg, *Polymer* **1999**, *40*, 2347.

[186] G. M. Kim, G. H. Michler, *Polymer* **1998**, *39*, 5689.

[187] B. Rupp, C. Ebner, E. Rossegger, C. Slugovc, F. Stelzer, F. Wiesbrock, *Green Chem.* **2010**, *12*, 1796.

[188] T. Reicher, S. Löbbecke, in *Organic Azides Syntheses and Applications Part 1: Synthesis and Safety*, S. Bräse, K. Banert, Eds., John Wiley & Sons Ltd., Chichester **2010**, chapter 1.

[189] R. A. A. Upul Ranaweera, Y. Zhao, S. Muthukrishnan, C. Keller, A. D. Gudmundsdottir, *Aust. J. Chem.* **2010**, *63*, 1645.

[190] R. D. Goodridge, R. J. M. Hague, C. J. Tuck, *Polymer Testing* **2010**, *29*, 483.

[191] S. Bal, D. Mahesh, T. K. Sen, B. C. Ray, *Journal of Minerals & Materials Characterization & Engineering* **2007**, *6*, 1.

[192] E. E. Shafee, *Polymer* **2003**, *44*, 3727.

[193] J. L. Drury, R. G. Dennis, D. J. Mooney, *Biomaterials* **2004**, *25*, 3187.
[194] J. Yu, D. Plackett, L. X. L. Chen, *Polym. Degrad. Stab.* **2005**, *89*, 289.
[195] K. Tsougeni, N. Vourdas, A. Tserepi, E. Gogolides, *Langmuir* **2009**, *25*, 1174.
[196] D. T. Eddington, J. P. Puccinelli, D. J. Beebe, *Sensor Actuator B* **2006**, *114*, 170.
[197] L. Safinia, N. Daxtan, M. Höhse, A. Mantalaris, A. Bismarck, *Biomaterials* **2005**, *26*, 7537.
[198] M. M. Shalabi, A. Gortemaker, M. A. van't Hof, J. A. Jansen, N. H. J. Creugers, *J. Dent. Res.* **2006**, *85*, 496.
[199] N. J. Hallab, K. J. Bundy, K. O'Connor, R. L. Moses, J. J. Jacobs, *Tissue Eng.* **2001**, *7*, 55.
[200] A. J. Zielinska, J. W. M. Noordermeer, W. K. Dierkes, A. G. Talma, M. van Duin, *Elastomers and Plastics* **2010**, *42*, 308.
[201] Fa. Krüss, *Handbuch Drop Shape Analysis DSA1 v 1.92-02 für Kontaktwinkelmess-Systeme*, Hamburg **2001**.
[202] DIN EN ISO 527-1, **1996**, Plastics - Determination of tensile properties of plastics - Part 1: General principles for the determination of tensile properties.
[203] DIN EN ISO 527-2, **1996**, Plastics - Determination of tensile properties of plastics - Part 2: Test conditions for molding and extrusion plastics.
[204] P. J. Barham, A. Keller, E. L. Otun, E. L. Holmes, *J. Mater. Sci.* **1984**, *19*, 2781.